Die approbierte Originalversion dieser Diplom-/Masterarbeit ist in der Hauptbibliothek der Technischen Universität Wien aufgestellt und zugänglich.
http://www.ub.tuwien.ac.at

The approved original version of this diploma or master thesis is available at the main library of the Vienna University of Technology.
http://www.ub.tuwien.ac.at/eng

_____

Unterschrift des Betreuers

TECHNISCHE UNIVERSITÄT WIEN
Vienna University of Technology

DIPLOMARBEIT

Monitoring of cell-induced deformations in biocompatible hydrogels via 3D multiphoton grafting

Ausgeführt am Institut für

Angewandte Synthesechemie

der **Technischen Universität Wien**

unter der Anleitung von

Ao. Univ. Prof. Dipl.-Ing. Dr. techn. Robert **Liska**

und

Projektass. Ass. Prof. Dr.rer.nat. Aleksandr **Ovsianikov**,

durch

Ksenia **Sanchenkova**, BSc

Dr. Bruno-Buchwieser gasse 1, 2340 Mödling

Wien, 20. Juli 2016

_____

Unterschrift des Studenten

“О сколько нам открытий чудных
Готовят просвещенья дух
И Опыт, сын ошибок трудных,
И Гений, парадоксов друг,
И Случай, бог изобретатель…”

А.С. Пушкин

“How many blissful revelations
The spirit of enlightment hides!
And the Experience, son of lapses,
And Genius, the paradoxes` friend,
And Chance, the heavenly inventor... ”

A.S. Pushkin

This diploma thesis was a very important step in my career and also in my life. I want to thank Professor Robert Liska for giving me an opportunity to complete my thesis in his research group and also for his patient assistance during the whole time of my work. I also want to thank my second supervisor, Professor Aleksandr Ovsianikov, who played a big role in the process of my education. All my colleagues from the Institute of Applied Synthetic Chemistry, who always had time for me, if I needed any help deserve my heartfelt gratitude.

I want to thank Branislav Husar, who taught and supported me while working with Photorheometer, and always reminded me what means to be a scientist. A lot of thanks I should give to Peter Gruber, Marica Markovic and Katja Hölzl, for their assistance in multiphoton grafting experiments and working in a biology lab.

There is no way how I can express my gratitude to my family: Dmitry and Alexandra, my parents and Nikolay, my brother. I guess, I will never do enough to repay them for everything, that they have done for me: their support, their unbreakable faith, even when I refused to believe in my strength, they knew that I can. Their smiling faces in skype window, even in the hardest times, gave me the highest motivation.

Stefano, my second half. Being a pilot, he knows what means to ‘face with problems’. Calm and serious, without any shadow of trembling on his face, he was always there to show me the way, even if it was dark. My dear, my victory is because of you standing by my side. I would never make it without you.

I want to thank the parents of Stefano: Cecilia and Palmerindo and his brother Diego for their support and warm relationship.

I am gratefull to my friends, who never left me alone and always wished me the best.

Thank all of you very very much!

Abstract

Recent openings in regenerative medicine turned the site of tissue engineering science towards the new approaches of healing the damaged tissues: not replace, but repair and regenerate became the directional vectors. In this light, old artificial constructions gave way to the principally new 'vital-avital' compounds, which combine synthetic material and live cells, embedded in this material. Such compounds not only mimic the natural tissue in the best way, they also enable and accelerate a regeneration process in tissues and allow one to avoid the immune response of a host. For successful application of these systems, it is important to enable monitoring of live cells inside of material.

In this work live MC3T3 preosteoblast cells and their interactions with a 2D hydrogel substrate were monitored via fluorescent grid, produced by multiphoton grafting (MPG) on the surface of the substrate. A proposed model should allow one to see cell-induced deformations in hydrogel layer, via deformations of a grid.

Hydrogel substrates were produced from mixtures of biocompatible, enzymatically degradable and photosensitive chemically modified gelatin (GelMOD) with photoinitiators (PIs). Photorheology was utilized for cross-linking of initial reaction mixtures and also for determination of an optimal type and concentration of PI - factors, which influence on mixture reactivity and mechanical properties of produced hydrogels. Two PIs were compared in this work: a commercially used IG2959 and Li-TPO-L, concerning their cytotoxicity, reactivity and influence on stiffness of produced substrates.

Produced hydrogel was then decorated with fluorescent molecules in a particular pattern of a square grid, which could be visible if observed with laser scanning microscopy (LSM). The main benefit of MPG process, rising from a group of technologies, utilizing multi-photon absorption (MPA) chemistry, over commonly used stereolithografic techniques is possibility to create precise computer-designed patterns with high resolution. For our studies water-soluble grafting agents (GAs) were preferential, therefore, a commonly used insoluble in water BAC-M was compared with a new water-soluble GA. Toxicity studies were performed in order to determine cell-friendly concentration of a new grafting agent (GA). Finally, processing window for MPG of selected hydrogel substrates was also determined.

Presented system should not only enable an *in vivo* monitoring of cell-induced deformations in 2D substrates. Ability to change and control matrix stiffness, which is one of key factors, influencing differentiation process of stem cells, makes it potentially applicable for studying the influence of environment on differentiation process of stem cells, which is a distant motivation of our work. Later, the same method can be applied for 3D matrices, which better represent a natural cell environment – extracellular matrix (ECM). Better understanding of the mechanisms and processes, taking place in the cell, more precise study of cell-cell and cell-environment interactions becomes possible, if this method succeeds.

Zusammenfassung

Aktuelle Forschung in der regenerativen Medizin haben für die Gewebekonstruktion neue Wege geöffnet, um geschädigtes Gewebe heilen zu können: nicht ersetzen, sondern regenerieren ist das Ziel. Aus diesem Grund haben klassische künstliche Rekonstruktionen den neuen 'vital-avital' Ansätze, die synthetisches Material mit lebendigen Zellen kombinieren, den Weg frei gegeben. Solche Ansätze reproduzieren das natürlichen Gewebe, ermöglichen Regenerationsprozesse und beschleunigen diese. Die Immunantwort des Körpers wird ebenso vermieden. Damit solche Systeme erfolgreich verwendet werden können, ist es wichtig lebendige Zellen im Material beobachten zu können.

Diese Arbeit beschreibt wie man mit Hilfe von fluoreszierendem Gitter MC3T3 preosteoblast Zellen und seine Wechselwirkungen mit 2D hydrogel basierten Substraten beobachtet. Fluoreszierende Gitter wurde durch die Mehrphotonenpropfung (MPG) auf der Oberfläche des Substrates produziert. Das vorgeschlagene Modell soll die Zellen-induzierte Deformationen im hydrogel basierten Substrat durch Deformationen im Gitter sichtbar machen.

Das Hydrogel wurde aus eine Mischung aus biokompatibler, enzymatisch abbaubarer und lichtempfindlich chemisch modifizierter Gelatine (GelMOD) und Photoinitiatoren (PIs) produziert. Zur Quervernetzung der primären Reaktionsmischung wurde Photorheologie verwendet. Der optimale PI und seine Konzentration wurden durch Photorheologie festgestellt. Zwei PI: IG2959 und Li-TPO, wurden in dieser Arbeit, in der Abhängigkeit vom ihren Zytotoxizität und Beeinflussung der Eigenschaft der hergestellten Hydrogele, verglichen.

Die so hergestellten Hydrogele wurden durch MPG mit einem Gitter aus fluoreszierenden Molekülen dekoriert. Das Gitter kann mit Raster-Laser Mikroskopie (LSM) beobachtet sein. Der Vorteil des MPG gegen üblich verwendbare Methoden ist dass man sehr präzise Computer-gesteuerte Muster mit hohe Auflösung herstellen kann. Für unsere Arbeit war wichtig, dass Propfreagentien (GAs) wasserlöslich sind. Deswegen, wurden die üblicher nicht wasserlöslicher GA, BAC-M, mit einem wasserlöslichen GA, Li-TPO, verglichen. Um die Zell-freundliche Konzentration den beiden GA zu bestimmen, wurden Toxizität Teste durchgeführt.

Das vorgeschlagene System soll nicht nur *in vivo* Beobachtung der Zellen-induzierten Deformationen in 2D Substraten erlauben. Schlüsselfaktor der Stammzellendifferenzierung ist die Steifigkeit der Matrix. Diese Eigenschaft des Hydrogels kann man leicht durch Typ und Konzentration des PI ändern. Auf diese Weise kann man den Einfluss der Umgebung an Stammzellendifferenzierung untersuchen. Später kann die gleiche Methode auch für 3D Matrizen, die am besten die natürliche Umgebung der Zellen imitieren, verwendet werden. Wenn die vorgeschlagene Methode Erfolg hat, ist es leicht Mechanismen und Prozesse in Zellen zu erfassen und akkurate Forschung der Zell-Zell und Zell-Umgebung Wechselwirkungen zu möglich.

Contents

		Gen.	Exp.
Introduction		**8**	
Objective		**26**	
General		**27**	
Experimental		**93**	
Summary		**118**	
Material and methods		**124**	
Abbreviations		**126**	
Bibliography		**128**	
1	**State of the art**	**27**	
2	**Evaluation of monomer formulation**	**33**	**93**
2.1	Hydrogel matrix	33	
2.2	Support for hydrogel	38	
3	**Photoinitiator for hydrogel**	**42**	**95**
3.1	Selection of photoinitiator	42	
3.2	Cytotoxicity of photoinitiator	44	
4	**Rheology**	**47**	**96**
4.1	Optimum setup	47	
4.1.1	Protection of hydrogel from drying	48	97
4.1.2	Influence of glass-supporter	51	98
4.2	Storage stability of formulations	53	100
4.3	Evaluation of optimal photoinitiator	55	102
4.4	Determination of an optimal photoinitiator concentration	57	104
4.5	Influence of macromere concentration	63	108
4.6	Selection of the optimal formulation	64	
4.7	Double-bonds conversion	64	
4.8	Swellability	72	111
5	**Multiphoton grafting**	**74**	**113**
5.1	Selection of a water-soluble grafting agent	75	
5.2	Evaluation of cytotoxicity of grafting agent	77	
5.3	Determination of processing window	80	114
5.4	Changing the hatch distance in a fluorescent grid	84	115
5.5	Changing the distance from the surface of hydrogel	85	
6	**Cell seeding**	**88**	**116**
6.1	Cell seeding procedure	88	

6.2 Life-dead staining procedure 88
6.3 Integration of cells into the hydrogel layer 89
6.4 Stability of the samples 92 117

Introduction

Tissue Engineering

Tissue Engineering is a field of science, which aims to replace damaged tissues or even the whole organs and parts of the human body with appropriate artificial analogues. Many efforts have been made in order to produce an artificial analog of living materia, which would resemble its natural prototype in the best ways: artificial blood vessels, heart and aortic valves, stents, joints replacement prosthesis, corneal transplants. Nowadays the progress and the advances made in the machinery to replace the damaged tissues and organs are gigantic. However, no matter how good these devices are, there are limitations to all of them. For a better understanding of the drawbacks of all artificial materials and constructions let us compare them with their natural prototypes: our own tissues.

First, when implanted into the body, any artificial construct faces with many destructive factors: acidic pH level, evaluated temperatures, presence of water, body fluids, reactive biomolecules like proteins, amino acids, dissolved oxygen, microorganisms and ions. All these factors build a very aggressive biological environment, causing a failure of even the most stable of materials. Materials, used in automotive and airplane engineering like ceramics, metals and metal alloys, which are thousands times stronger than a bone, possessing enormous stability under the evaluated temperatures, pressures, and friction, fail when applied for tissue engineering applications. As an example, one can give a hip-joint implant, which is typically made of inert metals, like titanium and its alloys. Such implants are able to remain stable for a certain period of time: not undergoing degradation reactions, nor influence a metabolism of surrounding tissues. However, even those materials could not serve forever. On the Fig. 1 below, one can see that at the taper interface between femoral head (cobalt-chrome alloy) and neck (titanium alloy), the direct traces of corrosion were detected.

Fig.1: Images of parts of a hip-joint implant, which was affected by a corrosion process.

Because of the constant friction at the taper interface between two parts of the implant, crevice and fretting corrosion destroyed the head-neck junction. Femoral head, made of ceramic material supposed to be entirely immune to corrosion process. However, ceramic materials undergo another destructive process under aggressive environment – dissolution, which can initiate a fretting corrosion process on the metallic parts of an implant, like it was reported in work of Bonnaig and Bal, see Fig.2.

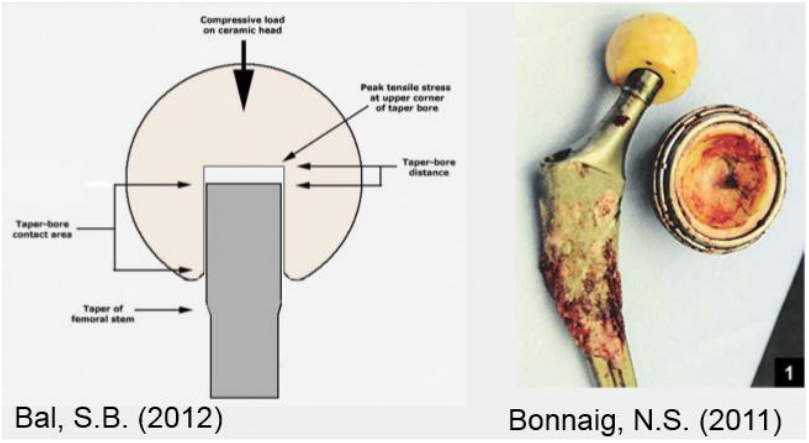

Fig.2: Induced fretting corrosion of a metallic part of a hip-joint implant.

Polymeric materials are known to be very inert and stable, but even they may undergo degradation and aging processes under the influence of physical, chemical and microbial agents, presenting in a living organism. Instability of artificial materials, which causes a release of toxic degradation products in surrounding tissues, results in inflammation reactions and rejection of an implant.

Beside the aggressive environment, there is another reason for a hip-joint implant failure. An implant, when placed into the body, constantly experiences the same loads and stresses as a natural bone does: weight of the body, friction, torsion. As it can be seen from the Figure 3, which demonstrates the strain fields in a metallic hip-joint replacement implant, the most probable failure points are developed in the areas of the highest stresses, and the arrangement of these stresses depends on the form of an implant.

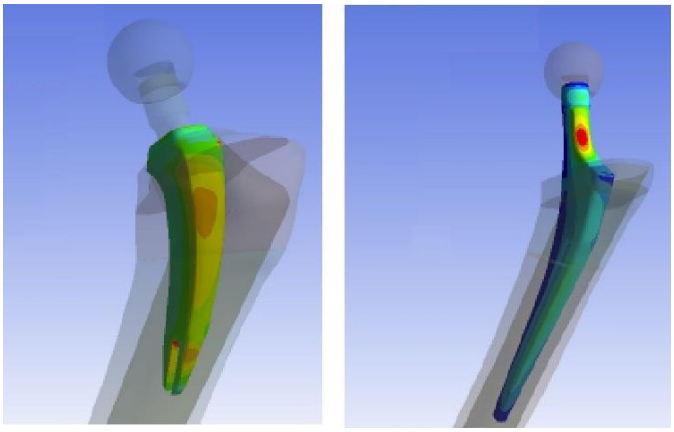

Fig.3: Image of the strain fields within a metallic hip-joint implant. The points, marked with orange and red colours are the potential failure points of an implant.

From the Figure 3 it can be seen, that the most probable failure point, marked with red colour, is situated on the femoral neck of the implant. The same does not happen with the bone, because the bone has an ability to adapt to the loads very successive. On the Figure 4 one can see the lines of the strain field in the femur bone. It is not by a coincidence, that the femur bone has such a special form, this is because the bone adapts to the loads in order not to allow an

appearance of any failure points. This is a unique property of vital systems, which no man-made material would possess.

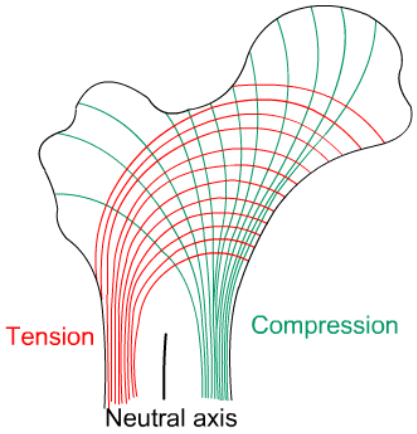

Fig.4: Schematic image of the strain field lines within a femur bone.

Another important property, which only a vital tissue possesses, is an ability of self-reconstruction. Principally, it is nothing else as, again, an adaptation of an organism to the new conditions: cells renewing in a wound-healing process, or in case of a bone, it is a bone remodeling process. In this process special types of bone cells constantly destroy an old and build a new bone material. The main advantage is, that due to remodeling process, our skeleton can adapt to the new conditions, i.e. excessive loads, like overweight by producing more bone material: the bones will become thicker.

Natural tissues are able to integrate: together with ligaments, muscles and tendons, bone creates a very functional system. No matter how strong an artificial material is one can never achieve a full functional integration of an artificial material with muscles, tendons and ligaments, which again, speaks in favor of natural tissues.

For all above described reasons, it can be concluded, that artificial materials will never be as good as the natural tissues. An alternative to the usage of artificial implants would be transplantation operation. However, a very limited number of donor organs restricts this approach. A problem, which also assists transplantation operation is immune response of a host organism, which may recognize the donor cells as foreign and reject them. The only way to transplant donor tissues is to suppress the immune system of a patient by giving the immunosuppressive drugs. Unfortunately, these drugs a patient will probably have to take for the whole life, which elevates the risk of cancer formation.

Therefore, basic tissue engineering approaches have their drawbacks. Another principally new approach have been invented relatively recent, when the stem cells technology researches gave rise to the new ideas for tissue engineering, which are based on tissue regeneration.

Tissue Regeneration

One of the most remarkable and life-necessary properties of each living organism is an ability to regenerate. Regeneration process is nothing else as a 'self-healing' ability, which is natural for all living organisms and aims to recapitulate the damaged tissue, organ or its function, or even the whole part of the body. It is already well-known, that such species as reptiles, starfishes or worms are able to regenerate their bodies, even if the biggest part of them is lost. For example, zebra-fish can completely regenerate its heart if 2/3 of it is cut. Numerous amphibian species regenerate not only their limbs, but also eyes and other sensing organs. For humans, unfortunately, regeneration ability is strictly limited. Understanding and control over regeneration process in humans could open a new perspective for tissue engineering, where no artificial constructs are needed.

Regeneration process is governed by stem cells. Stem cells possess two unique features, which the other cells do not: firstly, they are pluripotent, which means that they can give rise to all known cell types, and secondly, they are self-renewal, which means that each stem cell can give birth to the same stem cell again. A mature differentiated cell of any tissue type can only give rise to two daughter cells of the same phenotype, but it is not able to recapitulate itself. However, humans, firstly, do not possess as many stem cells as animals, and, secondly, those few stem cells, which present in human tissues, unfortunately, lose their properties with aging. Therefore regeneration ability in humans is significantly lower.

Another problem, restricting a regeneration process is a scar tissue formation or repair process. It is very important to identify the difference between these two processes: regeneration means recapitulation, in whole or in part, of the same program that directed initial tissue formation. Repair is nothing else, as replacement of damaged or diseased tissues with more tissue (scar tissue). Scar tissue, however, has totally different properties, than the origin tissue: it has different functionality and elasticity and it lacks of blood supply, therefore, the stem cells, even if being activated, have no chance to be directed into this area in order to start the regeneration process. A good example, confirming this phenomenon is the possibility to observe the old bone fractures on the X-ray pictures even after many years. Because of the lack of blood supply in rupture areas, the mechanism of repair and bone remodeling is disrupted in this area. In other words, once being broken, this area of skeleton will never be remodeled. Why our organism instead of starting regeneration process creates a scar tissue still remains a question. However, when the answer will be found, many diseases and injuries, which were considered to be incurable till this time, will become curable.

Stem cell technology opens a very perspective and wide way for tissue engineering science. If one could culture stem cells and force them to differentiate into a desirable phenotype *ex vivo*, and then implant them into a recipient organism, a fast and controlled regeneration process in humans could be possible. However, stem cells are very sensitive in handling and difficult to culture and grow: they are very reactive and may undergo chaotic differentiation even if touched each other, creating a teratoma– very specific tumor, which consists of all possible tissues. Therefore, there is a need of special structures, which could embody stem cells and make them transportable for further implantation procedure. Such structures are scaffolds for tissue engineering.

Scaffolds in regenerative medicine

Tissue engineering scaffold (TES) is, typically, a biodegradable 3D construct, which represents a temporal mechanical, physical and biological support for embedded live cells [1-4]. Advantages of TES over classical tissue engineering approaches are: TES does not restrict natural cell processes, i.e. being placed inside of TES cells are able to migrate, proliferate, divide and differentiate; being made of biodegradable substance, TES will serve only as a temporary support, till cells create a new tissue, which will completely substitute the artificial one [5], moreover, an undesirable negative immune response of the host organism can be avoided, if the cells of the host are used. According to the recent researches, stem cells respond to mechanical, topographical and biochemical stimuli [6-8], therefore control over differentiation can be gained via control over mechanical, architectural, chemical and biochemical characteristics of scaffolds. That is why physical and biochemical designs of TESs are very important. Physical design concerns architecture, mechanical properties and degradation properties of a scaffold, while biochemical design determines chemical composition and biological properties of the scaffold [9].

Scaffolds should ideally represent a natural cell environment, which is an extracellular matrix (ECM). ECM is a structure of very high complexity, which carries a lot of different functions and governs many important processes in tissue. A simplified structure of ECM is represented on Fig. 5.

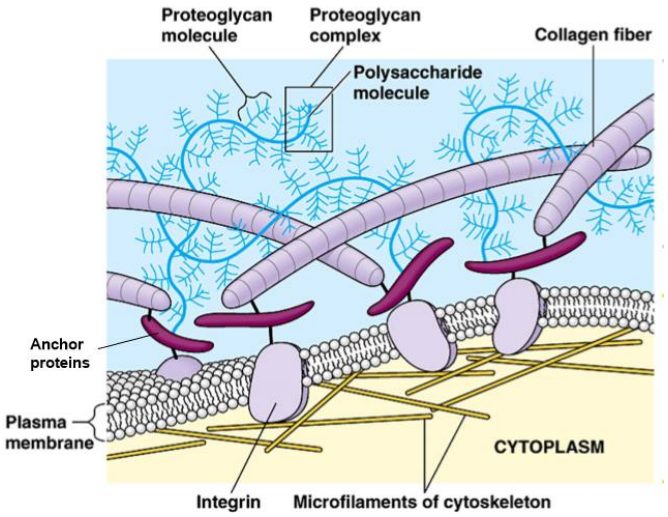

Fig.5: Simplified image of the ECM structure.

As it can be seen from the Figure 5, ECM consists of collagen fibers, which are extended through the interstitial tissue and provide durability, coiled proteoglycan filaments, with protein chain in the centre and covalently bonded glucoseaminoglycanes, or hyaluronic acid. ECM is directly linked to the cell membrane and interstitial space, interconnecting them both, and therefore providing a bidirectional dynamic dialog between cell and its environment and between cells. By sending special biological signals, cell can communicate via ECM with the other cells. Signals identification occurs via bonding of cell surface proteins and proteoglycans on ECM-linked proteins.

The role of ECM cannot be over-estimated. Together with the interstitial space and cell membrane, ECM builds the mechanical framework of natural tissue. In other words, it is a natural scaffold, which supports and protects cells in almost every tissue of an organism. Mechanical properties of ECM differ for each specific tissue, e.g. elasticity, and ultimate tensile strength. It holds tissue together, gives shape to the organs, constitutes water content of tissues, regulates the dynamic behavior of the cells, transport nutrients and contains cellular growth factors and necessary biomolecules, like cytokines - signaling molecules, helping cells signaling at nano- to pico-molar concentrations. ECM is no static structure: cells can synthesize and degrade components of ECM on demand. Whereas, ECM governs the degree of cell division and cell differentiation, and by that determines the inner architecture and outer shape of the tissue. Formation of ECM is essential for processes like growth, wound healing and fibrosis. Expression of genes, which results in composition, conversion, and degradation of tissue, is also regulated by ECM.

Accurately-designed micro-architecture of ECM with multi-scaled features and chemical complexity on a single cell level have to be mimicked in order to make TESs as similar to the natural ECM as possible.3D-constructions are more preferable than 2D. It was demonstrated by the recent findings, that cells tend to behave totally different if grown on flat 2D substrates: breast epithelial cells exhibited a tumoral trend when assayed in 2D and only returned to the normal state after transferring into 3D models [10], embryonic stem cells cultured in 3D exhibited an increased chondrogenesis, than those on the flat 2D substrates [11]. Better maintenance of chondrocyte morphology and differentiation [12, 13] and higher expression of genes, regulating cell activities [14, 15] was also detected in 3D environments. Such difference in behavior is mainly because any tissue originally develops in a 3D environment, where cells are surrounded by neighboring cells. In contra, cells, cultivated on flat 2D substrates have one side attached to the substrate and only some other edges in contact with other cells, whereas the main surface is exposed to the culture media [16]. One should also mention the differences in mass transport physics: in 2D systems growth factors, cytokines, morphogens etc. being dissolved in culture media reach the cells quick and uniformly, while in native tissue there are chemical and biological diffusion gradients, which play a key role in signaling and tissue development [17].

It was also shown that presence of pores in 3D scaffolds is preferable: high degrees of porosity and pore interconnectivity allow better impregnation of cells or cell-carrier substance into and through the scaffold, better cell-cell and cell-matrix interactions, mass transfer of nutrients and metabolites, tissue growth [18-20], and also more efficient blood vessel ingrowth, which results in enhanced oxygen and nutrient supply and waste diffusion [9]. HepG2 cells demonstrated a better proliferation and albumin production values in porous alginate hydrogels [21]. On the example of neocartilage tissue formation, it was demonstrated, that geometry, size [22-24], distribution, accessibility, and tortuosity of pores, determine morphology, composition, mechanical properties and functionality of formed tissue [18, 25-27]. Macropores (>50 μm) promote cell migration [28] and micropores cell-cell interaction and mass transport [29]. In general, high degrees of porosity and pore interconnectivity allow better impregnation of cells or cell-carrier substance into and through the scaffold [18].For a better structural mimicry to ECM, scaffolds can be also decorated with appropriate bioactive molecules (e.g., growth factor

proteins (GFs)) [30, 31], which induce and govern cells differentiation and many other processes. It was demonstrated, that in such constructs live cells can grow *ex vivo*, develop the desired phenotype [32-35] and the whole construct is capable to integrate slowly into the recipient organism [36, 37].

Biomaterials and Hydrogels

Material for scaffold is one of the main design components. A proper TES material should be biocompatible, have a good cell affinity, adjustable biodegradability and provide a suitable environment for cell attachment, proliferation, differentiation, and cell-cell interaction [18, 38, 39]. Structural stability of material is required during fabrication, clinical handling, and fixation at the implant site [39]. It should possess a necessary mechanical strength to protect the embedded cells from harmful mechanical stresses and to withstand the*in vivo* loading environment until the newly formed tissue will take over the load-bearing function.

Synthetic polymers are widely used as materials for scaffolds creation in tissue engineering, e. g. polyester-based solid scaffolds, firstly, have outstanding biomechanical properties, because they are made from biocompatible synthetic materials [40, 38], secondly, structure and internal architecture of such scaffolds can be easily designed. Typically used synthetic polymers are poly(glycolic acid) (PGA), poly(lactic acid) (PLA), poly(lactic-co-glycolic acid) (PLGA), poly-caprolactone (PCL), and poly(ethyl glycol) (PEG). Via chemical synthesis, mechanical and degradation properties of synthetic polymers can be well-controlled [9]. A good example is a new biomaterial poly(glycerol sebacate) (PGS), which mechanical modulus can be increased to the range of native articular cartilage simply by changing the molar ratios of glycerol:sebacic acid and increasing the polymer curing time [41]. However, solid scaffolds, made from synthetic polymers often do not allow gradual hydrolytic attack, possess lower degradation ability [12], cell adhesion affinity, and bioactivity than hydrogels [42] and not sufficient replacement by newly formed tissue [9].

Hydrogels are ideal materials for scaffolds, in spite of the fact that their mechanical properties are weaker, then those of synthetic polymers [9], which restricts their application in regeneration of hard tissues, like articular cartilage or bone tissue [43]. High water content and porosity, which provides diffusion of oxygen, nutrients and growth factors [11, 44] are the beneficial characteristics of hydrogels, which make them similar to many tissues. Moreover, cells can be efficiently encapsulated and uniformly distributed within a hydrogel under gentle and cytocompatible conditions [45]. Chondrocytes were shown to retain their phenotype and morphology [46, 47] if impregnated into a supportive hydrogel matrix, which provided also a cartilage ECM secretion both *in vitro* and *in vivo* [48-51].

Structurally, hydrogels are insoluble in water three-dimensional networks of cross-linked hydrophilic polymers. Hydrogels are easy to prepare and can be made from a very wide range of materials. Biomaterials, including carbohydrate-based (e.g., alginate, agarose, chitosan, hyaluronic acid (HA)) and protein-based (e.g., fibrin glue, collagen type I and II, silk) [38, 42] natural materials, also in combinations with synthetic materials, such as poly(hydroxyethyl methacrylate), polyethylene glycol and its derivatives, or poly(vinyl alcohol) (PVA) [42] are used for hydrogels creation. A drawback of hydrogels is a limited control over shape and

internal structure of produced scaffolds [9] and, as it was demonstrated, stability of the hydrogel constructs without an internal pore collapse is also difficult to achieve [52-54].

The final cross-linked structure of hydrogel can be yielded via several methods. First one is the cross-linking of hydrophilic monomers (e.g. acrylamide, acrylic acid and its salts, N-vinylpyrrolidone) or polymers (e.g. PVA, polyacrylamide, polyethylene oxide) in the presence of different cross-linking agents, like ethylene glycol dimethacrylate (EGDMA) or methylenebis(acrylamide) (MBAA), where cross-linking proceeds either via reaction of side groups in polymer chains, or via ionizing irradiation, which is called photopolymerization. Second method is insertion of above discussed monomers into the natural polymer chains, like starch, cellulose and its esters, dextran, gelatin, which again leads to formation of a network; chemical reactions of polymers, e.g. hydrolysis of polyacrylonitrile [55].

Photopolymerization:

Photopolymerization is a subcase of radical polymerization, which is initiated by a photoinitiator (PI) molecule:

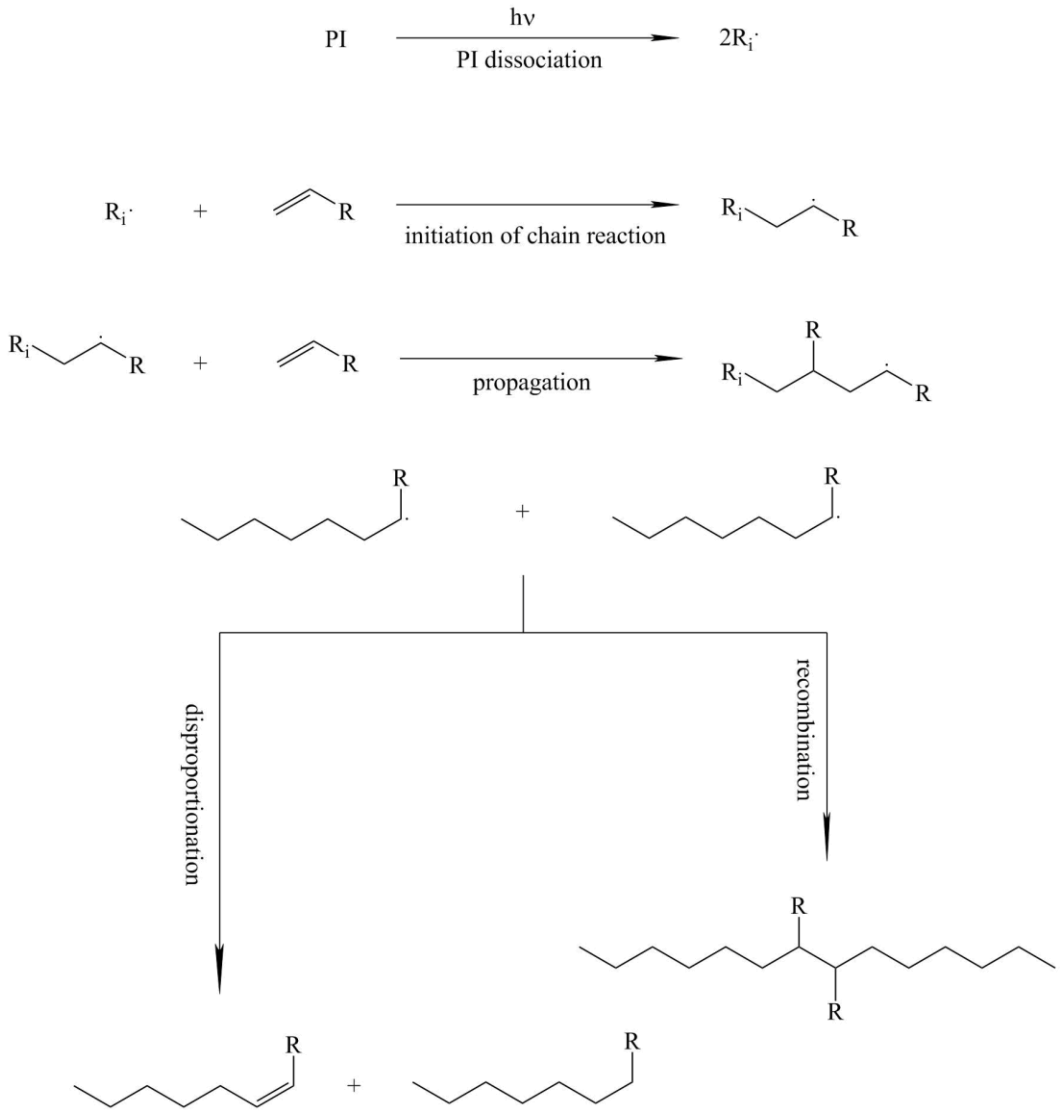

Fig.6: Mechanism of photopolymerization.

As it is shown on the Figure 6 above, a photopolymerization reaction starts with radiation-initiated cleavage of a PI molecule, resulting in two radicals. After, the radicals start radical polymerization, which is a type of chain polymerization, where each monomer molecule is stepwise attached to the propagating polymer chain. Reaction ends with termination of propagating polymer chain: by recombination or disproportionation of two reactive species. Radicals can theoretically react with every component of a system: monomer, PI, solvent, and polymer itself. Such reactions are also known as chain transfer reactions and in all cases they lead to deactivation of a macroradical and formation of polymer, or to formation of a new radical, which is also able to start polymerization. Therefore, material chain is terminated, but kinetic chain is preserved.

PIs, like monomers, are the important constituents of photopolymerizable reaction mixtures. PIs have an influence on curing speed, double bonds conversion (DBC), and final properties of hydrogel. A properly chosen PI contributes development of the optimal formulation. The main difficulties, which should be considered by choosing a PI, are the rests of unreacted PI, and the products of its photolysis, which are, as a rule, toxic [56-60]. Therefore, an ideal PI should possess:

- no or, at least, very low toxicity
- good solubility
- high initiation efficiency
- a proper shelf-life in ready-to-use formulations

As it was already discussed above, photopolymerization process begins when a PI molecule absorbs the light from the light-source. On this stage the match of emission bands of the UV lamp (light source) with the absorption maxima of PI is crucial, because it strongly influences the efficiency of energy absorption by PI. A PI absorbs light through chromophores with conjugated double or triple bonds, often in combinations with carbonyl groups, which cause electronic transitions of π- π^* or n- π^* orbitals [61]. As it can be good seen from the simplified Jablonski diagram on the Figure 7, at first, one electron is excited from the ground state (S_0) to the excited singlet state (S_1^*) by absorption of light with the energy hν. After, an electron either loses the energy by fluorescence or radiationless deactivation, or the transition into an excited triplet state (T_1^*) by 'intersystem crossing' (ISC) takes place. Therefore, the molecule can relaxate to T_1.

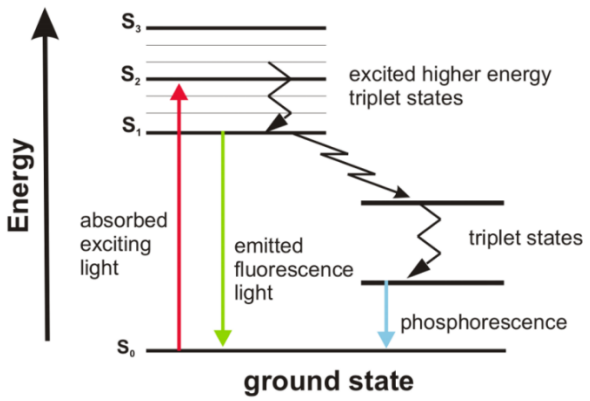

Fig. 7: Simplified Jablonski diagram.

From the triplet states, which are characterized by a longer life-time, the radical formation can be induced. However, radical formation process is concurring with radiationless deactivation, phosphorescence or bimolecular extinction processes, which became more probable with higher stability of a triplet state [62].

The following formation of initiating radicals from the excited state can proceed by:

- Photofragmentation (α- or β-cleavage) [63]
- Hydrogen abstraction from a H-donor [64]
- Electron transfer followed by proton transfer [65]

The radical generating PIs often contain the benzoyl chromophore, which displays a good photoreactivity and absorption in the UV-range (200-400 nm). Radical PIs are divided into cleavable or hydrogen abstracting systems, Type I or Type II respectively. Type I refers to a monomolecular and Type II to a bimolecular reactivity. The operation modes for such PIs are: cleavage, which proceeds normally at the α- or β-position of a carbonyl group (Type I), abstraction of a hydrogen atom with a hydrogen donor, or electron transfer via an amine (Type II), [66].

The principle of the α-cleavage is the hemolytic scission of the bond next to the carbonyl group. It is based on the presence of a C-X (X=heteroatom), as for example in thioacid esters and acylated phosphineoxides, see Fig. 8 below.

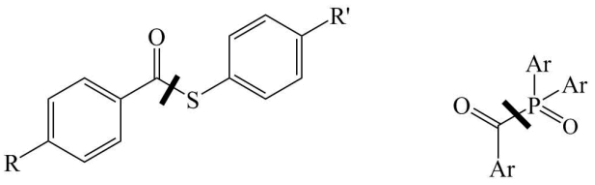

Fig.8: C-X bond of an α-cleaving PI.

Next to a keto group (at an activated C-C bond), an α-cleavage can also take place. The efficiency can be enhanced by stabilization of the ion pair, generated by a heteroatom (oxygen or nitrogen at the α-carbon atom), see Figure 9 below.

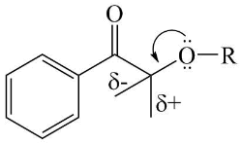

Fig.9: C-C bond in a PI with α-cleavage.

A good example, demonstrating the mechanism of decomposition of a Type I PI, that undergoes α-cleavage is Darocur 1173 ®Ciba, see Figure 10 below.

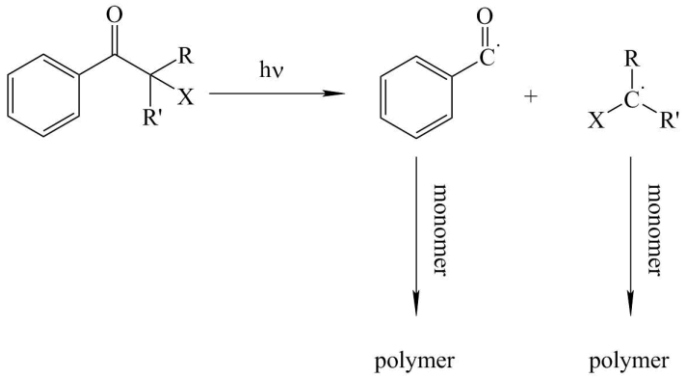

Fig. 10: α-Cleavage of a Type I PI (Darocur 1173 ®Ciba; R=R'=CH_3, X=OH).

The α-cleaving Type I PIs are depicted on the Figure 11 below [67].

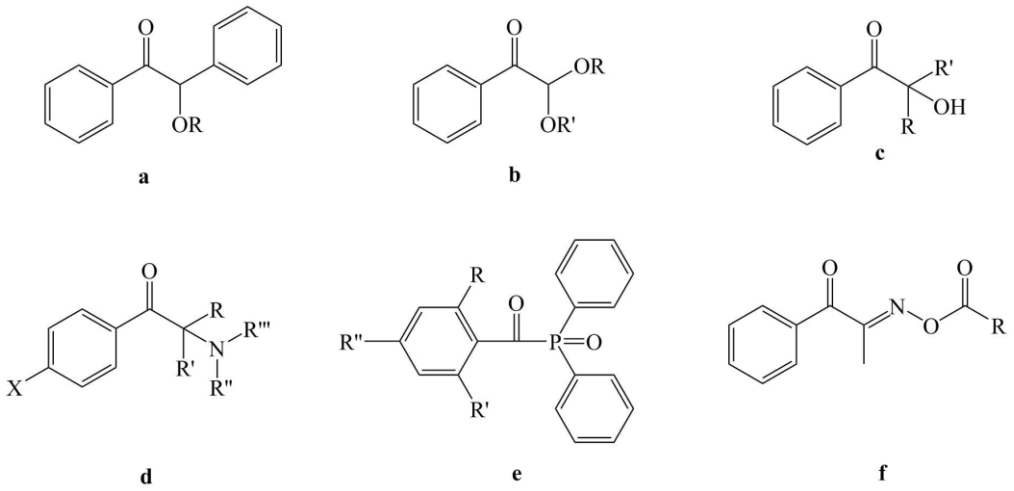

Fig.11: Type I PIs: (a) benzoin ethers, (b) dialkoxyacetophenones, (c) hydroxyalkylphenones, (d) aminoketones, (e) benzoylphosphineoxides, (f) benzoyloxime esters.

PIs which undergo β-cleavage contain α-haloketones and ketosulfides. As an example, the decomposition of α-chloroacetophenone is shown on the Figure 12 below.

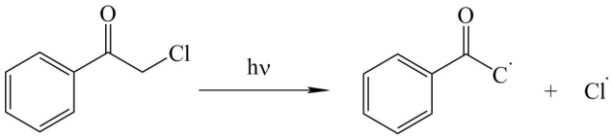

Fig.12: Mechanism of β-cleavage of α-chloroacetophenone, a Type I PI.

Type II PIs operate by hydrogen abstraction in a bimolecular process. The common Type II PIs consist primarily of benzophenone (g), thioxanthone (h), anthrachinone (i), xanthone (j), fluorenone (k), benzyl (l), ketocoumarine (m) and camphorquinone [68], as it is demonstrated on the Figure 13. Type II PIs absorb in the visible light range, therefore, they can also be used for applications in this diapason [67].

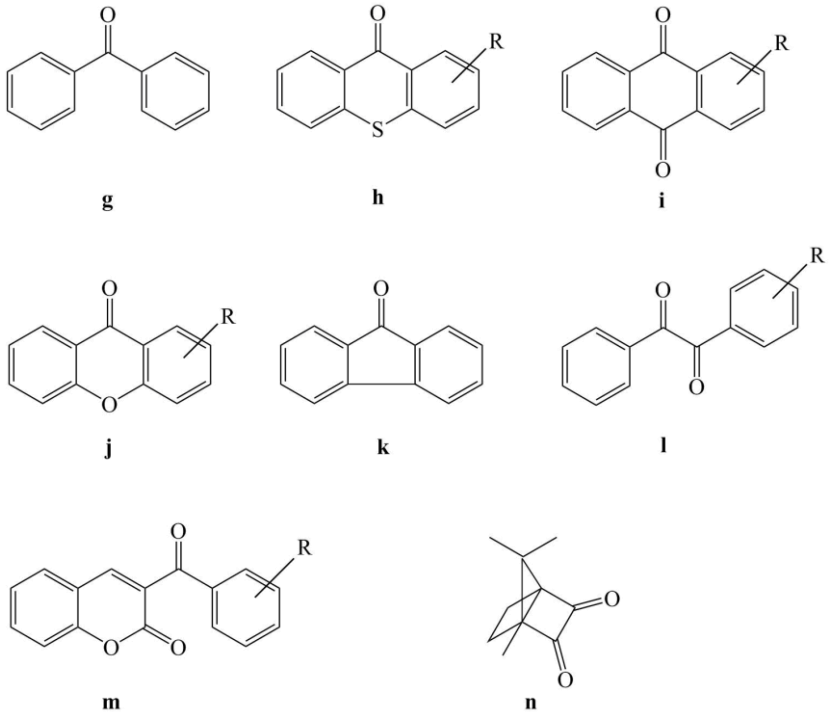

Fig.13: Examples of Type II PIs.

Alcohols and ethers are able to generate radicals via direct hydrogen abstraction (see Figure 14), which can only occur from the n-π* triplet.

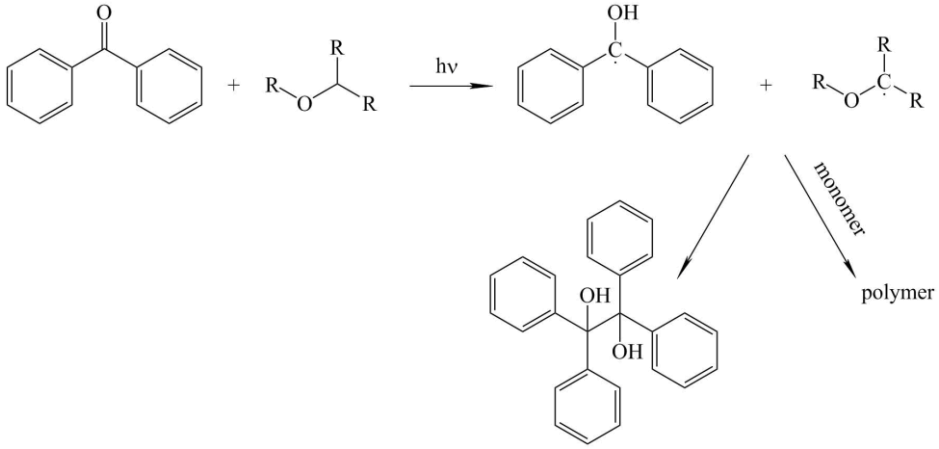

Fig.14: Proton transfer on ether to benzophenone.

Electron and proton transfer, however, might originate either from the n-π* triplet or the more intensive π-π* transition. Therefore, in a first step, an electron is transferred to the excited PI via electron-donors (such as secondary or tertiary amines and thiols [69]), resulting in generation of two radical ions at the same time. The radicals are formed by proton transfer in a second step [70, 71], as it is shown on the example of mechanism for benzophenone (BP) and tertiary amine on the Figure 15, leading to polymer formation.

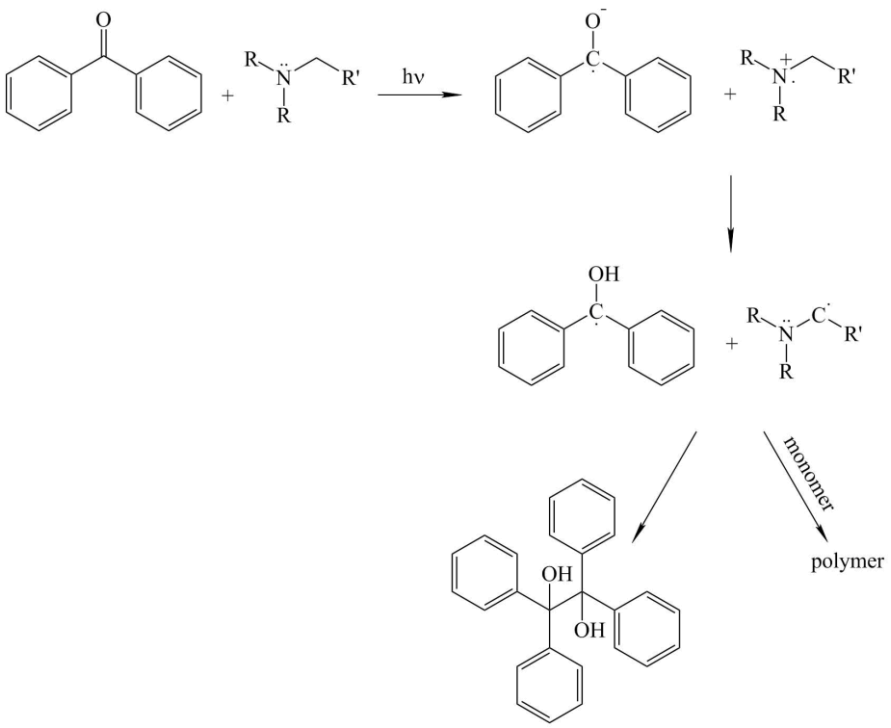

Fig.15: Electron and proton transfer by tertiary amines to benzophenone.

First, the tertiary amine is oxidized by benzophenone via an electron transfer from the amine to the BP-triplet [71, 72]. When an ion pair is generated, a deprotonation takes place in the α-position of the amino radical cation. The induction of electron/proton transfer can proceed by excitation of both the n-π* and the more intensive π-π* transition. A competing process is a quenching reaction, induced by the back electron transfer (BET), which strongly reduces the initiation reactivity of PI [73].

A life time of the excited state is very important for the process of radical formation. It was demonstrated, that Type II initiators, in comparison with Type I, require a longer life time of the excited state, resulting in a lower excitation rate and lower curing speed [74].

For a photocurable formulation the factors influenced by a PI, such as radical reactivity, rate of radical generation and sterical factors are of a high importance [75, 76]. Nevertheless, not only a PI determines the final properties of a formulation. A monomer, being a second constituent, also plays a key role.

The synthesized macromers for production of photopolymerisable hydrogels are typically poly (ethylene glycol) diacrylate (PEGDA), poly (ethylene glycol) dimethacrylate (PEGDMA), acrylic modified PVA with glycerin spacer and methacrylic modified dextran [77], depicted on the Figure 16 below.

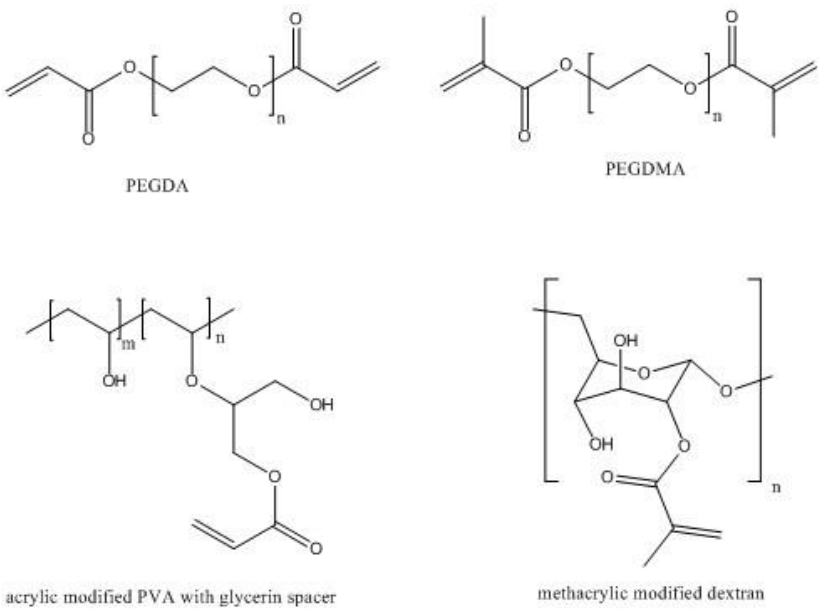

Fig.16: Chemical structures of macromers modified with acrylic and methacrylic acids.

Many techniques for production of hydrogel scaffolds were already performed. Via conventional scaffold fabrication techniques, such as particulate leaching and gas foaming, one can produce 3D porous structures, but unfortunately, pore distribution cannot be controlled [78, 79]. Electrospinning enables production of similar to ECM nano-scaled architecture, but it may impact on mechanical stability of the construct [80]. Phase separation and particulate leaching are not capable of fine-tuning the scaffold geometry [81, 82]. A group of rapid prototyping techniques [83, 84], which include stereolithography [85-87], selective laser sintering [88, 89], fused deposition modeling [90-92], and inkjet fabrication [93-95] is remarkable, because all named methods utilize computer-governed modeling of TES structure, which gives an exact control over scaffolds architecture and reproducibility. However, spatial resolution is not sufficient for mimicking of multi-scaled architecture of natural ECM.

As long as single methods failed, combination of them should have overcome their drawbacks [96, 97], but results also in an increased complexity of the whole processing procedure and, therefore, bad reproducibility of obtained results [98].

The single versatile platform is needed, which could not only mimic the architectural complexity of natural ECM, but also allow to study all known cell and tissue types (which requires a big diapason of variable experimental parameters), providing an independent control over all scaffold parameters, and produce scaffolds in a reproducible manner according to a defined design [98].

Multiphoton processing methods for creation of structures for tissue engineering

All methods related to the multiphoton processing (MPP) group allow production of very complex multi-scaled 3D structures with a high resolution utilizing a multiphoton absorption (MPA) of laser irradiation, resulting in a highly localized photochemical reaction in material.

For MPP one needs a high-energetic radiation source, like laser, a proper photoinitiator (PI) and a cross-linkable compound. At first, a PI molecule absorbs two (two-photon absorption [2PA]) or more photons (MPA), in both cases higher laser intensity is required, because probability of such processes is very low [99]. Typically, a PI for MPA processes is planar π-conjugated system, containing strong donor and/or acceptor groups [100-102].Energy of combined photons is then enough to bridge an energy gap, which is larger than the energies of each photon individually. This process can be good seen on the example of 2PA on the Figure 17 below.

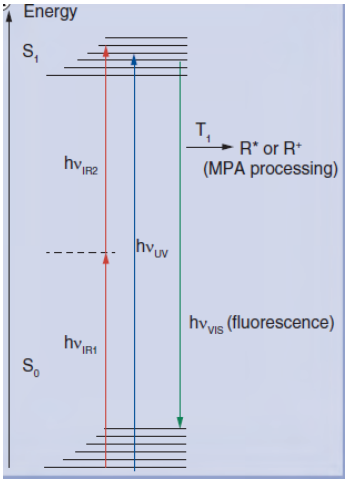

Fig.17: Jablonski diagram of the 2PA and possible radicals (R*) formation, resulting in initiation of a photochemical reaction, and fluorescence, reducing initiation of photochemical reaction.

The dashed line on the diagram on the Figure 17 is a short-lived virtual state, which results from the absorption of a first photon ($h\nu_{IR1}$). The excited S_1 state is reached if the second photon, ($h\nu_{IR2}$), is absorbed within this short time. Then, from an excited state a PI molecule can release a photon (via fluorescence) and fall back into a ground state, or initiate highly-reactive species, which trigger a photochemical reaction, resulting in three different processes:

- Initiation of a cross-linking/ polymerization reaction of the material, or two-photon polymerization (2PP);
- Immobilization of activated molecules in structure of matrix compound, or multiphoton grafting (MPG);
- Photo-cleavage of material, or photodegradation.

In contra to the single-photon absorption, MPA is a nonlinear absorption process. This results in a most exciting characteristic feature of MPA: by adjusting the laser-beam power, it is possible to achieve a state when the light-material interaction is limited to the focus spot, see Fig.18.

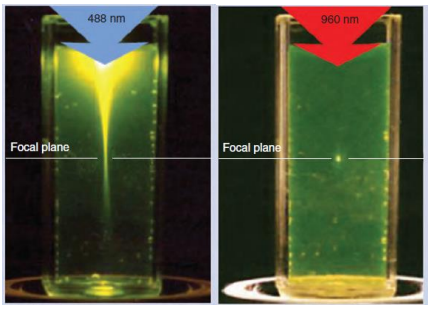

Fig.18: Image demonstrating the difference between one-photon (left) and two-photon (right) excitation.

It can be good seen from the Figure 18, that in case of a simple one-photon excitation the whole volume of material is irradiated, while in case of a highly-localized two-photon excitation, only a single spot in a focus of a laser beam is irradiated. Therefore a photochemical reaction is strictly limited by this irradiated volume of material. If one moves a laser beam in a desired manner, a highly-defined structures can be produced, see Figure 19 [98].

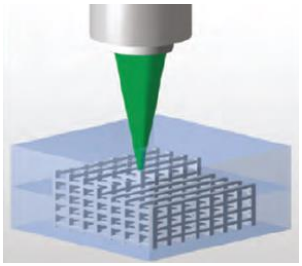

Fig.19: Direct writing of a structure in a photoactive material via MPP method.

Dependently on the type of induced multiphoton reaction, MPP enables:

- a single-step direct writing of complex 3D structures containing features on multiple length scales with a high spatial resolution (up to nanometer scale), which is essential for ECM mimicking via 2PP;
- spatially resolved functionalization of cell-culture matrices with bioactive molecules via MPG;
- modification of matrices via photodegradation or photocleavage.

It must be clarified, that MPG, in contrast to 2PP, is not capable to produce volumetric structures, like scaffolds, however, the aim of MPG is different. MPG is a method, which allows one to decorate an already created structure or cross-linked hydrogel matrix with desirable molecules in a precise computer-aided pattern. Immobilization of the molecules will proceed only in the focal spot of the laser beam, enabling, therefore, a direct 'writing' of any pattern. Even a single-molecule insertion becomes possible with utilization of MPG.

All three approaches can be realized by using essentially the same experimental setup. Moreover, MPP enables computer-designed modeling, which results in a very good reproducibility of produced structures [103]. Another important issue is that MPP can be applied to varieties of different biomaterials: natural and synthetic polymers and also hydrogels

and thermosensitive materials, which are known to be problematic for structuring. The main requirement is photosensitivity of material for MPP.

A first 2D structure, produced via MPP was made from bovine serum albumin (BSA) and Rose Bengal as a PI, for entrapping the enzymes by Pitts JD et.al [59]. First porous 3D scaffolds were produced via 2PPfrom commercially available synthetic resins, such as Ormocomp (micro resist technology GmbH), SU8 (MicroChem) and demonstrated no cytotoxicity [104].After, acrylate- and methacrylate-based nondegradablephotoresins PEGDA, SR368, SR499 (Sartomer), Accura SI10 (3D Systems Corporation), ORMOCER (The Fraunhofer ISC) were also structured via 2PP [104]. Further improvement came with utilization of biodegradable photoprocessable biopolymers, which allowed production of temporal supportive structures: hydrolytically degradable polycaprolactone-based material with photopolymerizable methacrylate groups [105] able to degrade in accordance to new tissue formation [106] and poly(lactic acid)-, oligolactones- and urethane-based photopolymers [107, 108]. 2PP was used for cross-linking of BSA in the presence of live cells [109], for investigation of cell migration [110], at last for cells differentiation in a work of Kiyan *et al.*, resulting in discovery of a new differentiation mechanism [111].

An important advance in 2PP-processing of biocompatible hydrogels was introduction of methacrylamide-modified gelatin (GelMOD). In comparison to others, GelMOD has even more outstanding properties: firstly, it is derived from collagen, which is one of the main structural and load-bearing proteins in natural ECM, and secondly, GelMOD is enzymatically degradable [103]. GelMOD, as a modified natural polymer, combines benefits of hydrogels and synthetic polymers and addresses their drawbacks: stiffness of produced hydrogel can be controlled by concentrations of polymer or/and PI in the initial liquid mixture. Scaffolds, produced from GelMOD mimic the natural ECM in the best ways [112]. GelMOD was firstly used for creation of 3D CAD (computer aided design) scaffolds via 2PP in a work of A. Ovsianikov *et al.* Produced scaffolds shown stability in culture medium and ability to support porcine mesenchymal stem cells and adipose-derived stem cells adhesion, proliferation and differentiation [103].

With introduction of tissue-mimicking constructs, the influence of environment on differentiation of stem cells has been studied on 2D substrates as well as in 3D models. An ability of cells to sense not only their molecular, but also mechanical microenvironment was demonstrated in works of Adam J. Engler *et al.* [113]. Working group cultured myoblasts on collagen strips attached to glass or polymer gels of varied elasticity and found, that cells transform in myotubes in all cases, but typical myosin/actin striations could be achieved only on gels with normal muscle stiffness. In the other work, the same group demonstrated, that matrix elasticity directs specification of stem cell lineage: naive mesenchymal stem cells (MSCs) exhibited neurogenesis when placed into soft brain-mimicking matrices, myogenesis if placed in stiffer matrices mimicking muscle tissue, and osteogenesis in stiffer bone-mimicking matrices [114].On 2D substrates, thecell function dependence from mechanical signals was also demonstrated [115]. Human mesenchymal stem cells (hMSCs) differentiated accordingly to mechanical stiffness of 2D culture platform in a work of Disher and his

colleagues [116, 117]. Degree of mechanical cell extension by adhesive ligands on 2D scaffold governs the rates of grow and apoptosis, as it was shown by Ingber et al. [118–121].

In spite of success and great contribution of these experiments, tissue-mimicking approach faces with several difficulties. Bryant *et al*. studied the response of chondrocytes, incapsulated in non-degradable PEG gels to dynamic loads [122] and found out, that in spite of applying homogeneous (on macroscopic scale) loads, cells responded in a non-homogeneous fashion on microscopic scale. The study shown, that microscopic cells deformation varied from cell to cell, due to individuality of each cell and non-uniform gel properties on microscopic scale. Experiment was conducted with static, non-degrading material system. In ECM-mimicking hydrogels which degrade in response to cell-secreted proteases observed situation is even more complicated. Cells, in order to move or divide, secrete enzymes to degrade the local matrix [123, 124]. Such processes are local, and it is still unclear how the cells become information about their environment and, how material responds to cell-induced changes. In order to understand complex biological processes, taking place in such systems and to improve the design of cell-bearing constructs, one has to be able to monitor cells inside of artificial constructs [125].

Objective

Possibility to observe living cells inside of synthetic materials would allow one to study cell-cell and cell-matrix interactions, understand the origins, stimulation and consequences of cellular processes. These factors would lead to improvement and perfection of cell-bearing materials and constructs. Whereas the methods for monitoring local changes in the network structure already exist, still there is a need of convenient methods, enabling the measurment of cell-induced deformations in real-time, in order to understand more completely the processes and mechanisms, proceeding between cells and hydrogel matrix.

The aim of this work was to create such a system for monitoring cell-induced deformation in a 2D hydrogel substrate. The substrate, made of chemically modified gelatin (GelMOD) fulfills all criteria of biocompatibility, moreover being photoactive, it can be cross-linked via photorheometry into a hydrogel with controllable stiffness. This opportunity is of high importance for studying stem cells differentiation in dependence from stiffness of a substrate material.Via multiphoton grafting (MPG) a fluorescent pattern should be created on the substrate material, which will allow to visualize cell-induced deformations of hydrogel, if observed with laser scanning microscopy (LSM).

If this method will be successful on 2D substrates, one can use grafted hydrogels for monitoring the cells already in 3D, which still remains more challenging.

Firstly, the optimal formulation, considering hydrogel stiffness and type and concentration of photoinitiator (PI) for photo-curing process should be chosen. Afterwards, produced hydrogels should be characterized by their photorheological and toxicological properties. Also the most suitable grafting agent (GA) for MPG should be selected and optimal concentration of GA should be chosen and verified by toxicological tests. Finally, the storage stability, transportability and applicability for the cell-culture of the whole system should be tested.

General

1 State of the Art

Real-time monitoring of cells allows one to observe and study cells behavior in synthetic materials. This leads to a better understanding of cell-material interactions, and therefore, to a further improvement of ECM-mimicking materials. Many methods have already been developed in this field. For monitoring dynamic cell functions, like cells migration, motility and morphology, and also to quantify their speed, real-time cell tracking is widely used [126, 127]. Reporter-based systems and intracellular mechanical measurement techniques can provide molecular-level information, like changes in cell function and cytoskeletal organization in real-time. A non-invasive monitoring of processes in cell is achieved via labeling of cell-secreted proteins with fluorescent reporter proteins, which can be then fluorescent-imaged [128-132].

Micromechanical measurements, such as microrheology and atomic force microscopy (AFM) allow to monitor microscopic changes in intracellular mechanics [133, 134]. Via particle tracking, or traction force microscopy (TFM), one can distinguish and measure forces, which cells exert on their microenvironment [135,136].

For visualization of local changes in material on micro-level, like in case of cell-induced matrix degradation, localized gel degradation methods are applied. A good example is given in a work of Lee *et al*.: they incorporated a fluorescence resonance energy transfer (FRET)-based dye into a collagenase degradable linker within a PEG-based gel. When encapsulated fibroblasts started locally degrade a gel in order to migrate, increased fluorescence was observed, allowing visualization of these degradation tracks [137]. AFRET-based reporter system was also developed by a working group of Kong: towards real-time measurement of alginate-based gel degradation polymer chain conformation was monitored as a function of gel crosslinking density [138].

Hydrogels derived from GelMOD containing well-designed geometrical fluorescence patterns produced by multiphoton grafting (MPG) would be an elegant method to monitor deformation of hydrogels, induced by cells, and to characterize them both quantitatively and qualitatively. However before performing in 3D, this system should be tested on 2D substrates.

The main benefit of MPG over common material modification methods is that MPG utilizes a covalent binding of grafted species, while non-covalent modification techniques [139, 140-142], typically based on physiosorption and surface adsorption, suffer from low surface density or heavily desorption of attached molecules. Another popular methods for surface modification also utilizing covalent attachment are self-assembled monolayers (SAMs) [143, 144-146] and direct covalent binding to surface activated groups [147-149]. However, they lack of temporal and spatial control, are too time-consuming and not applicable for wide range of substrates [150]. MPG is a single-step direct writing process, which can be applied to many substrates, producing computer-designed patterns with high resolution and accuracy, even in 3D volume, as it was shown in a work of A. Ovsianikov et al. [151], where MPG was performed within a PEG-based matrix. Moreover, the density of immobilized molecules can be controlled via

changing laser exposure time or intensity [152, 153]. Even patterns, composed of different species can be made, using molecules, absorbing in different wavelength diapasons [154].
Modification of cell substrates and scaffolds via MPG would allow to closely mimic the structure of natural ECM, where cells known to recognize and attach to specific molecules [152, 155]. Hahn et al. used 3D MPG [156] and demonstrated in their work, that tubulogenesis of endothelial cells can be accelerated if biologically inert 3D hydrogel structure is complemented with integrin ligands and signaling factors [157]. Cell-guiding capability was demonstrated by JL West et al. by utilizing 2PP for production of 3D patterns within PEGDA- and PEG-based hydrogels [158, 159]. Localized cross-linking of BSA proteins within hyaluronic acid-based hydrogels was demonstrated by Seidlits et al. [160]. Two-photon uncaging, as alternative to MPG was utilized for spatially resolved photochemical modification of 3D matrices [161-163]. Finally, MPG-induced incorporation of aromatic azide molecules into a PEG-based matrix was demonstrated by A. Ovsianikov et al. [154]. Resulting patterns with resolution down to 4 μm can undergo further modification via click-chemistry.

MPG rises from a group of MPA processes, already described above. It utilizes the same highly-localized photochemical reaction, but, unlike 2PP, MPG does not initiate a chain-growth reaction, it only immobilizes single molecules into material. Therefore, instead of PIs, typically used for photoprocessing techniques, MPG utilizes special molecules – grafting agents (GAs). For GA only specially designed molecules can be used: they typically include planar π - conjugated systems containing strong donor and/or acceptor groups [164, 165, 166], like reactive aromatic azides. The mechanism of MPG is as following: the focused laser beam induces MPA by a GA molecule, resulting in photolysis of the azide, followed by dissociation of N-N bond, and generation of nitrogen and highly reactive nitrene intermediate [167]. Nitrene intermediate can undergo various reactions, but the major pathway is expected to be an insertion into C-H bond of a matrix compound, like it was demonstrated in works of R. Liska *et al.* [168] and A. Ovsianikov *et al.* [153]. On the Figure 20 an MPG of PEG-based matrix with BAC-M as a GA is depicted, which was performed in a work of A. Ovsianikov *et al.* [153].

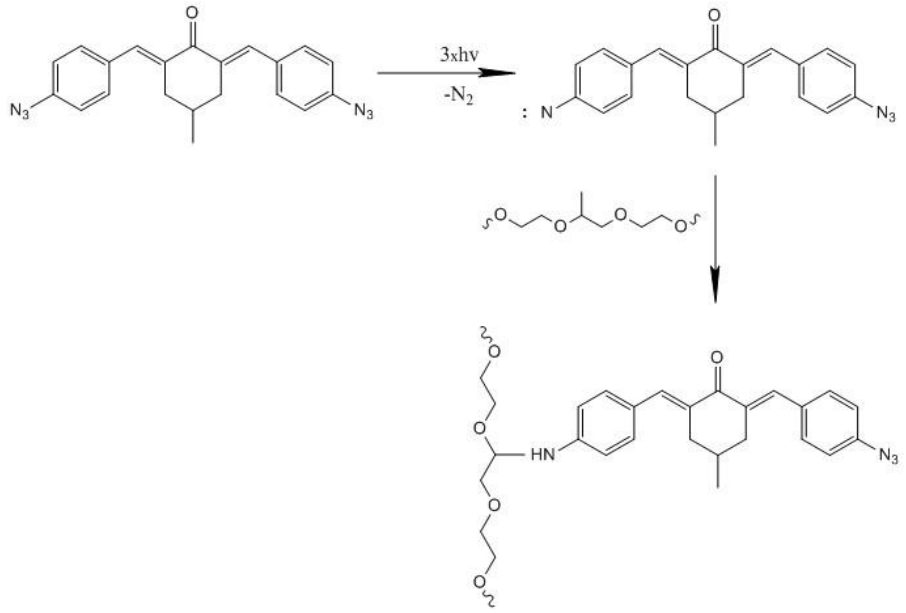

Fig.20: Mechanism of MPG with use of BAC-M GA.

However, there are also several possible side-reactions. As it was demonstrated in a work of M. F. Budyka *et al.* [151], among the by-products, which a highly-reactive nitrene species can form are: polymers, azobenzene, small quantities of azoxybenzene and aniline. High yields (≥ 70%) formation of azepines was established in works of Charles J. Shields *et al.*[169] and Doering and Odum [170] during photolysis of 4-(dimethylamido)phenyl azide and phenyl azide, respectively, in the presence of nucleophiles (such as diethylamine (DEA)). The simplified scheme of azepine formation is depicted on the Figure 21 below.

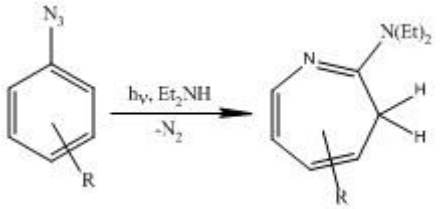

Fig. 21: Schema of azepine formation uponphotolysis of phenyl azide in the presence of DEA.

Upon photolysis of phenyl azide in ethanethiol, formation of ortho-substituted aniline (in a yield of 39%) was discovered, see Figure 22, [171]. Both reactions are of relevance for our matrix as gelatin contains free amino and thiol groups.

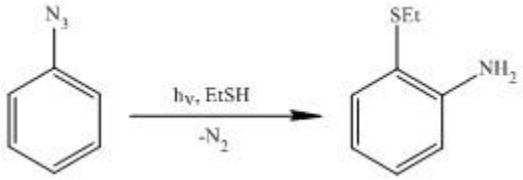

Fig. 22: Schema of ortho-substituted aniline formation upon photolysis of phenyl azide in the presence of ethanethiol.

If photolysis reaction is carried out in highly diluted solutions of phenyl azide, polymer formation can be suppressed and the resulting product will be azobenzene [172, 173]. A simplified scheme of azobenzene formation can be seen on the Figure 23 below: formed nitrene species reacts with another molecule of GA to yield a final product.

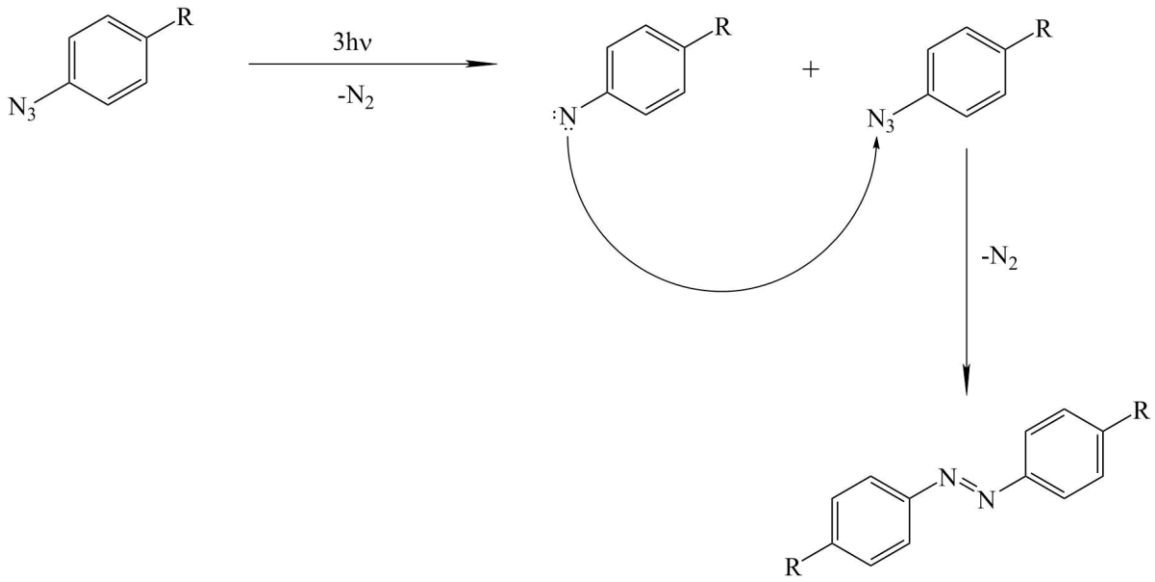

Fig.23: Azobenzene formation mechanism.

Strictly speaking, solution phase photochemistry of phenyl azides is not that easy. It was shown, that the mechanisms of either azobenzene or azepine formation proceed in several stages with formation of short-living singlet intermediates, which play a role of 'reservoir' for triplet phenylnitrenes, which in turn either undergo dimerization or react with a primer phenyl azide molecule to yield azobenzene [172], as it can be seen from the mechanism depicted below on the Figure 24.

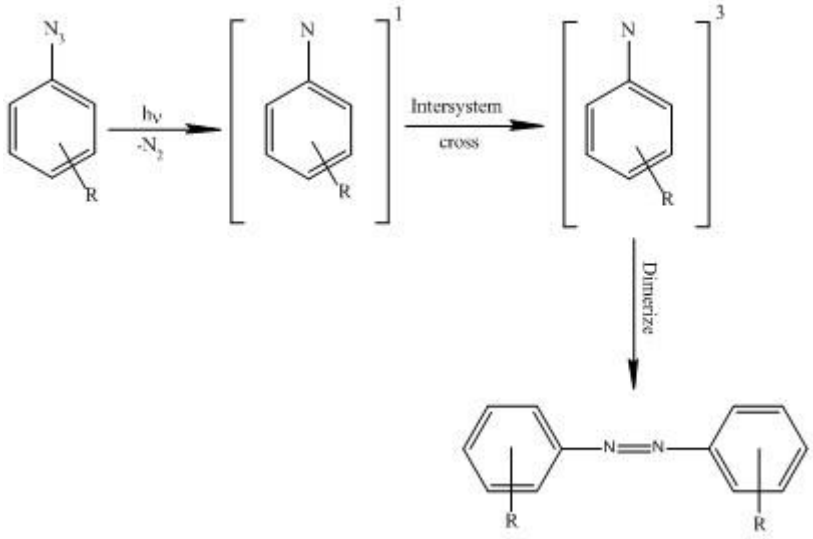

Fig.24: Mechanism of azobenzene formation via formation of singlet and triplet intermediates.

Accordingly to the work of Smith P. A. S., [174], there are two competitive processes in solution phase photolysis of phenyl azides: reversible isomerization of the singlet-state nitrene to a ground-state intermediate and formation and dimerization of the triplet nitrene (see Figure 15 above). It was demonstrated by Doering *et al*. [170], that the valence tautomer, formed from the singlet intermediates, can be trapped by added nucleophiles (such as diethylamine, DEA) to give eventually 2-substituted-3H-azepines, see Figure 25 below.

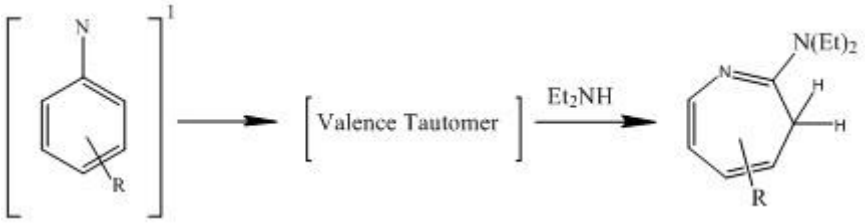

Fig.25: Formation of tautomer from the singlet-state intermediate with the following formation of azepine.

The structure of the valence tautomer (see Figure 16 below), formed from a singlet-state intermediate has long been questionable. Bicyclic azirines were firstly proposed by Huisgen et al. [175], later, dehydroazepine structures by Sunberg [176], Wentrup [177], and Chapman and LeRoux [178]. Azirine and/or ketenimine (1, 2-didehydroazepine) were also suggested as the trappable reactive intermediates (see Figure 26) [170, 171, 175, 179].

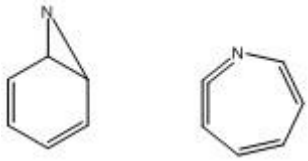

Fig.26: Chemical structures of azirine and ketenimine.

Formation of ketenimine, as the species trapped by nucleophiles in solution, was registered by laser flash photolysis techniques (broad band at ~ 350 nm) [180, 181] and also proved by time-resolved IR spectroscopy (TRIR) [169, 182]. Formation of a primary trapping product, 1H-azepine from ketenimine and its tautomerization, yielding the final 3H-azipine was also studied [176, 183] and schematic representation of this process can be seen on the Figure 27.

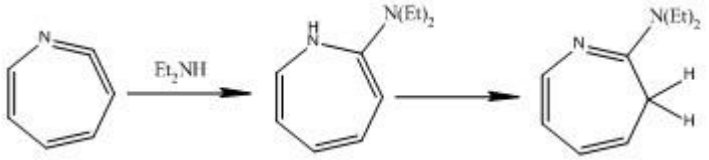

Fig.27: Formation of 1H – azepine from ketenimine with the following tautomerization, yielding the final 3H-azipine.

Interestingly, Dunkin and co-workers demonstrated a possibility to convert azirines into dehydroazepines [184, 185]. Eventually, formation of a valence tautomer was proved to be temperature-dependent: photolysis of phenylazide in the presence of diethylamine at ambient temperature yields azepine (the product of reaction of singlet intermadiate), while lowering the temperature suppresses its formation and below 160 K azobenzene is formed (the product of triplet nitrene dimerization) [180]. In a work of Platz and Wirz [180, 186] irradiation of phenyl azide at 77 K gave a triplet nitrene. Shields and Turner [169] established the presence of 5-(dimethylamido)-l,2-dehydroazepine as a trapped by nucleophiles intermediate in photolysis reaction of 4-(dimethylamido)phenyl azide at room temperature in solution. From all above discussed facts, it can be concluded that high temperatures favor reactions of singlet state

intermediates, whereas low-temperature reactions favor reactions of a triplet phenylnitrene [187].

In the presence of oxygen, photolysis of the dilute hydrocarbon solutions (< 10^{-4} M) of simple phenyl azide derivatives yields the corresponding nitro - and nitrosobenzenes [188, 189, 190].Theoretically, even more by-products can be formed, because nitrene intermediate is capable of immobilization in any C-H or N-H bond, which it finds, but the main reaction mechanism proceeds as discussed[154, 168]. Even if the by-products are formed, their yields are very low [125]. As it was also demonstrated on example of BAC-M [154] after grafting procedure, either one or both azide groups of a GA molecule can be covalently linked to the matrix and both products will exhibit strong fluorescence [191].

It can be concluded that there are several side reactions present and therefore a detailed quantification of the grafting process will not be possible. Nevertheless, it is a good model system to wright the desired fluorescent grid in a 2D or 3D hydrogel matrix.

2 Evaluation of Monomer Formulation

2.1 Hydrogel Matrix

Among all biomaterials used in tissue engineering, hydrogels occupy a certain niche. Their attractivity is mainly due to a natural 3D porous structure, which in a best way replicates the natural cells environment, extracellular matrix (ECM). Improved cell-cell contact, cell-matrix interactions and even more efficient blood vessel ingrowth and enhanced oxygen, nutrient and waste diffusion makes hydrogel matrices for cell culture a very promising approach. It has been reported that one of the advantages of 3D porous scaffolds is, for example, an enhancement of both cell proliferation and albumin production of HepG2 cells in porous alginate hydrogels [192]. A number of synthetic and natural hydrogels has been developed and used as 3D scaffold for studies of cell behavior and tissue formation [193].

The recent advances in multiphoton absorption (MPA)-based processing methods shown, that hydrogels can also be used as starting materials for production of three-dimentional (3D) scaffolds and matrices for cell cultures with precise and very complex architecture, characteristic to all MPA-based methods. In a recent study Torgersen *et al.* have shown that two-photon polymerization (2PP) is capable of producing 3D scaffolds from hydrogels [194], see Fig. 28.

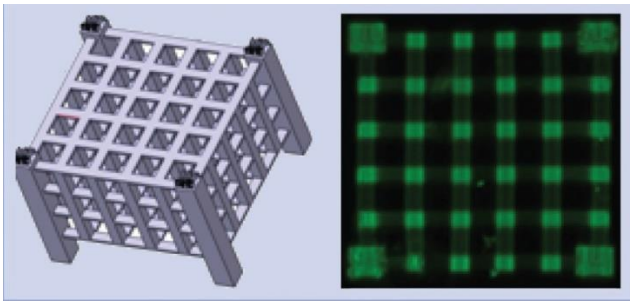

Fig.28: 3D scaffolds produced from a poly(ethylene glycol)-based hydrogel with a 50% water content.

A highly sensitive two-photon photoinitiator (PI) was synthesized and verified for biocompatibility using nematode *Caenorhabditis elegans*as, a multicellular test organism. The utilization of this water-soluble PI allowed fast 2PP processing of poly(ethylene glycol) diacrylate (PEGDA)-based hydrogels with up to 80% water content. Furthermore, 2PP scaffolds were successfully produced around and in direct contact with living *C. elegans*. Recent study of Ovsianikov A *et al.*, showed that encapsulation of live cells within hydrogels is also possible by 2PP [195], see Fig.29. These studies demonstrate that in addition to conventional photopolymers, 2PP can also make use of hydrogels, which present a highly relevant and well-established biomimetic material platform. Utilization of hydrogels for 2PP will facilitate development of systems for live-cell encapsulation within 3D scaffolds in a spatially defined manner [113].

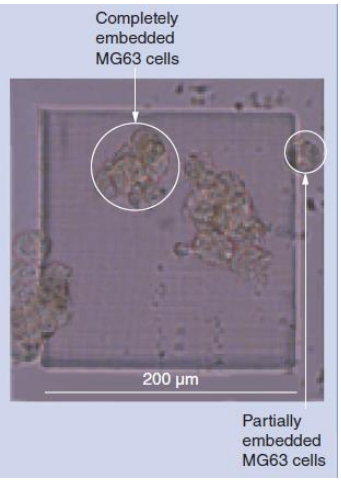

Fig.29: Image of the living cells, completely and partially embedded into the hydrogel material.

Generally, the tissue engineering scaffolds are expected to provide only temporary support. This is because the mechanism of ECM remodeling *in vivo* relies on the capability of cells to degrade the matrix via enzymes. The latest option is in fact one of the critical components of a natural tissue regeneration process: a dynamic dialogue between cells and ECM. Therefore, the scaffolds, which can be enzymatically degraded by the cells are of a great interest. An important advance in the direction of 2PP processable biopolymers came with the development of hydrolytically degradable polycaprolactone-based material containing photopolymerizable methacrylate groups [105]. Previous studies on this triblock co-polymer have shown that it is not only biocompatible and biodegradable, but it also degrades on a similar time-scale as tissue formation [106]. Recently, 2PP processing of hydrolytically degradable poly(lactic acid)-, oligolactones- and urethane-based photopolymers [107, 108] was demonstrated.

A further important advance came with utilization of enzymatically degradable methacrylamide-modified gelatin, GelMOD. The first enzymatically degradable biomimetic 3D scaffold produced by means of 2PP was reported by Ovsianikov A. et al. [196, 197], see Fig. 30. The gelatin is derived from collagen, which is one of the main structural adhesive and load-bearing proteins of the native ECM. Thus, from a chemical point of view, scaffolds, produced from GelMOD closely mimic the natural cellular microenvironment. It was shown that the enzymatic degradation capability of gelatin is preserved for the methacrylamide-modified derivative [196].Chemical modification of gelatin with methacrylamide groups makes the resulting substance photoactive, which makes GelMOD applicable for production of photocross-linkable hydrogels via different photoprocessing techniques. Additionally, by applying 2PP technique, structural properties of the cellular microenvironment can also be mimicked. In a work of Ovsianikov A., the GelMOD was cross-linked employing a femtosecond laser emitting at 515 nm and the water-soluble PI Irgacure2959 (IG2959), known to be highly biocompatible[198, 199]. Produced 3D scaffolds showed an excellent stability in culture medium and were shown to support adhesion, subsequent proliferation and differentiation of both mesenchymal and adipose-derived stem cells [196, 197].

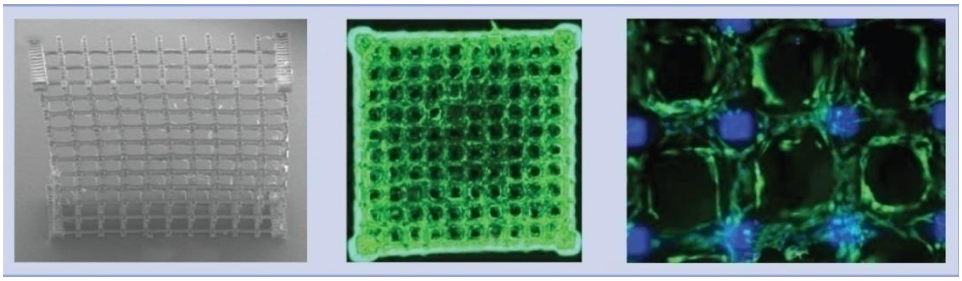

Fig.30: Images of a 3D scaffold from enzymatically degradable gelatin-based photopolymer, seeded with adipose-derived stem cells, created in a work of Ovsianikov A. et al.

Upon applying osteogenic stimulation, the seeded cells differentiated into the anticipated lineage. Energy dispersive X-ray (EDX) analysis showed the induced calcification of the scaffolds. The results indicated that photopolymerized GelMOD preserves its enzymatic (in vitro) degradation capability. By adjusting the physical versus chemical cross-linking of GelMOD, and by altering the synthesis protocol, it is theoretically possible to control the degradation rate and the stiffness of resulting materials. These parameters are known to be important for control over cell phenotype and proliferation [200].

From all above discussed facts, it can be concluded, that GelMOD combines biomimetic properties of natural gelatin with the advantages of synthetic materials, like tunable mechanical properties [79, 201, 202]. In the same work of Ovsianikov A. *et al.* the photosensitive gelatin was prepared starting from gelatin type B (Rousselot, Ghent, Belgium) isolated from bovine skin. To obtain a photopolymerizable material, they chemically modified gelatin by substituting lysine and hydroxylysine amino-side groups with methacrylamide moieties [201]. Figure 31 demonstrates a schematic representation of the GelMOD synthesis.

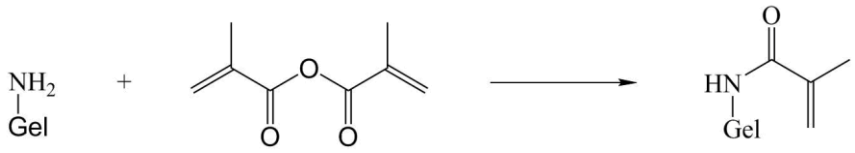

Fig.31: Schematic representation of photosensitive gelatin synthesis by substitution of amine groups with methacrylamides.

The amount of incorporated cross-linkable side groups or degree of substitution (DS), defines the mechanical properties of resulting GelMOD-based hydrogel [201, 203] and, subsequently, can be adjusted by varying the amount of methacrylic anhydride (Aldrich, Bornem, Belgium) added during the synthesis. The selected DS of 65% was recently verified using ^{1}H NMR spectroscopy at elevated temperature (40 °C), see Fig.32, [104]. This method allows accurate determination of the methacrylamide substituents on the gelatin in D_2O.

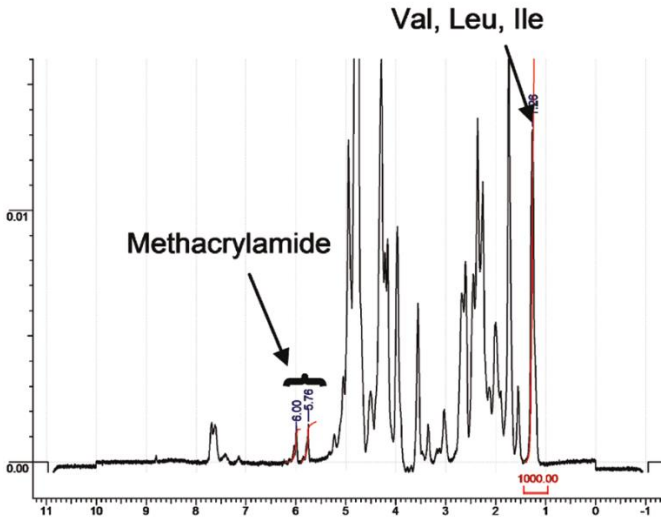

Fig.32: ^{1}H NMR spectrum of gelatin derivative used to verify the incorporated amount of cross-linkable side groups.

The NMR spectrum of gelatin is extremely complex, because gelatin is composed of more than 20 different amino acids [204]. The structure of these amino acid building blocks is –NH—CHR—CO--, in which the side chain (R) varies and possesses different functional groups. The method used in this work defines the DS relative to the total amount of available amine groups in gelatin (0.0385 mol/100 g) by attributing only one peak to a component, which cannot be modified. The signal at 1.26 ppm is ascribed to the resonance in the valine (Val), leucine (Leu), and isoleucine (Ile) hydrophobic alkyl side chains, which considered to be chemically inert. On the basis of the known composition (0.023 mol Val + 0.026 mol Leu + 0.015 mol Ile in 100 g gelatin), it can be calculated that the integration of this peak (18 protons) corresponds to 0.3836 mol/100 g, [205]. The DS is then defined as a function of the initial amount of free amine groups in gelatin:

$$DS\ (\%) = 0.3836\text{mol} \times (I_{5.7\text{ppm}}/I_{1.2\text{ppm}}) \times (100/0.0385\text{mol})$$

The integration at 1.2 ppm ($I_{1.2\text{ppm}}$) was 1000, and that at 5.7 ppm ($I_{5.7\text{ppm}}$) was 65.23. The DS was thus calculated as 65%, which corresponds to 6.5 double bounds per 10 amine-groups (lysine and hydroxylysine) [201]. Interestingly, the remaining amine groups could still be applied after scaffold fabrication to realize modification of the gelatin backbone with biomolecules including RGD peptide.

As it has been confirmed by A. Ovsianikov *et al.*, GelMOD also preserved its enzymatic degradation ability. In order to evaluate this fact, photopolymerized material pellets were incubated in a collagenase solution. Collagenase binds and unwinds triple helices prior to peptide bond hydrolysis [206]. As a result, the molecular weight of the gelatin chains decreases and the in vitro degradation finally results in the presence of peptides. Increasing collagenase

concentrations substantially accelerated the degradation process, as it can be good seen on the Figure 33.

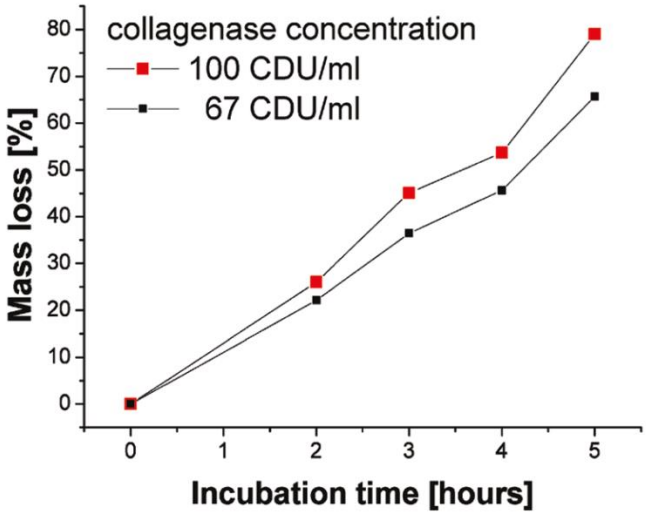

Fig.33: In vitro degradation behavior of photopolymerized gelatin using different collagenase concentrations.

Around 80% of the material was degraded after 5 h of incubation in a collagenase solution of 100 CDU/mL (collagenase digestion units). Immersing the samples into a solution corresponding to 67 CDU/mL led to a mass decrease of 65% after 5 h. Both the appearance of the degraded samples as well as the degradation progression indicated that the bulk degradation occurred. Therefore, an enzymatic degradation capability of the methacrylamide-modified gelatin is preserved after its photopolymerization, which means, that the degradation via cell-secreted enzymes should also be possible with GelMOD [207].

In our work, the GelMOD with DS of 70%, verified by the same method, was used as purchased. GelMOD was used as the initial material for creation of a substrate for cell culture. From all above discussed facts, the main priorities of GelMOD can be highlighted. GelMOD successfully combines the biomimetic properties of natural gelatin: a good in vitro cytocompatibility of photosensitive gelatin methacrylamides for the incapsulation of fibroblasts, myoblasts, chondrocytes endothelial cells, and cardiac cells has been shown [208, 209-211], and also ability of synthetic materials to modulate their mechanical properties. Modification degree of gelatin determines to a large extent the mechanical properties of substrate material, and the amount of incorporated methacrylamide groups can be controlled by varying the amount of methacrylic acid added during the synthesis of GelMOD [212]. GelMOD is a hydrogel-forming material. Hydrogel materials present a big advantage for tissue engineering applications, because of their porous structure. Porosity of hydrogels helps to achieve a required three-dimentionality of the structure, which is necessary requirement for mimicking ECM. GelMOD is enzymatically degradable material, which means that the cells, incorporated in it will be able to rebuild it on their own desire. The last important fact is that GelMOD is photoactive substance, which means, that if being mixed with an appropriate PI, it can be used in modern and precise techniques, based on MPA processes. GelMOD has already

shown good results being cross-linked via 2PP process. In our work GelMOD was cross-linked simply via UV-light in order to obtain the hydrogel, which will be later used in a multiphoton grafting process (MPG), which also relates to the group of MPA techniques. Via MPG a fluorescent pattern of the square grid was grafted on the surface of the hydrogel. This pattern should serve as an indicator of cells viability and proliferation on the surface of the hydrogel.

2.2. Support for Hydrogel

Gel-layers, used as the substrates for cells in this work, are not transportable without an external support and can be easily damaged during the experiments. For this reason, usage of glass slides as a support material, on which the gel samples were produced and transported present a certain advance.

The glass slides were functionalized in order to provide a better adhesion of the hydrogel layer to the surface of the sample. This is achieved by the following procedure, in which the surface of a glass plate was chemically modified with trimethoxysilyl propyl methacrylate.

Trimethoxysilyl propyl methacrylate is a transparent, flammable, and very reactive with water fluid. Because of its high heat and moisture sensitivity, it has to be kept cold and stored under the inert gas. Chemical reaction of trimethoxysilyl propyl methacrylate with a glass surface, also known as silanization reaction, which is carried out in a presence of water and acidic acid, can be seen on Fig. 34.

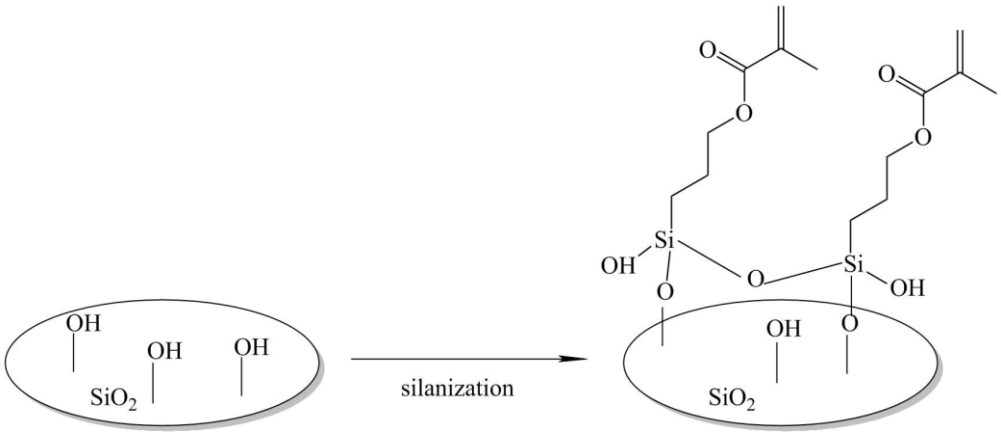

Fig.34: Silanization reaction on the surface of glass coverslips.

As it can be seen from the Fig. 34, the surface hydroxy-groups of the glass coverslips react with methoxy-groups of trimethoxysilyl propyl methacrylate with formation of covalent bonds between the glass surface of the glass slides and reagent. The mechanism of this reaction can be seen on the Fig. 35.

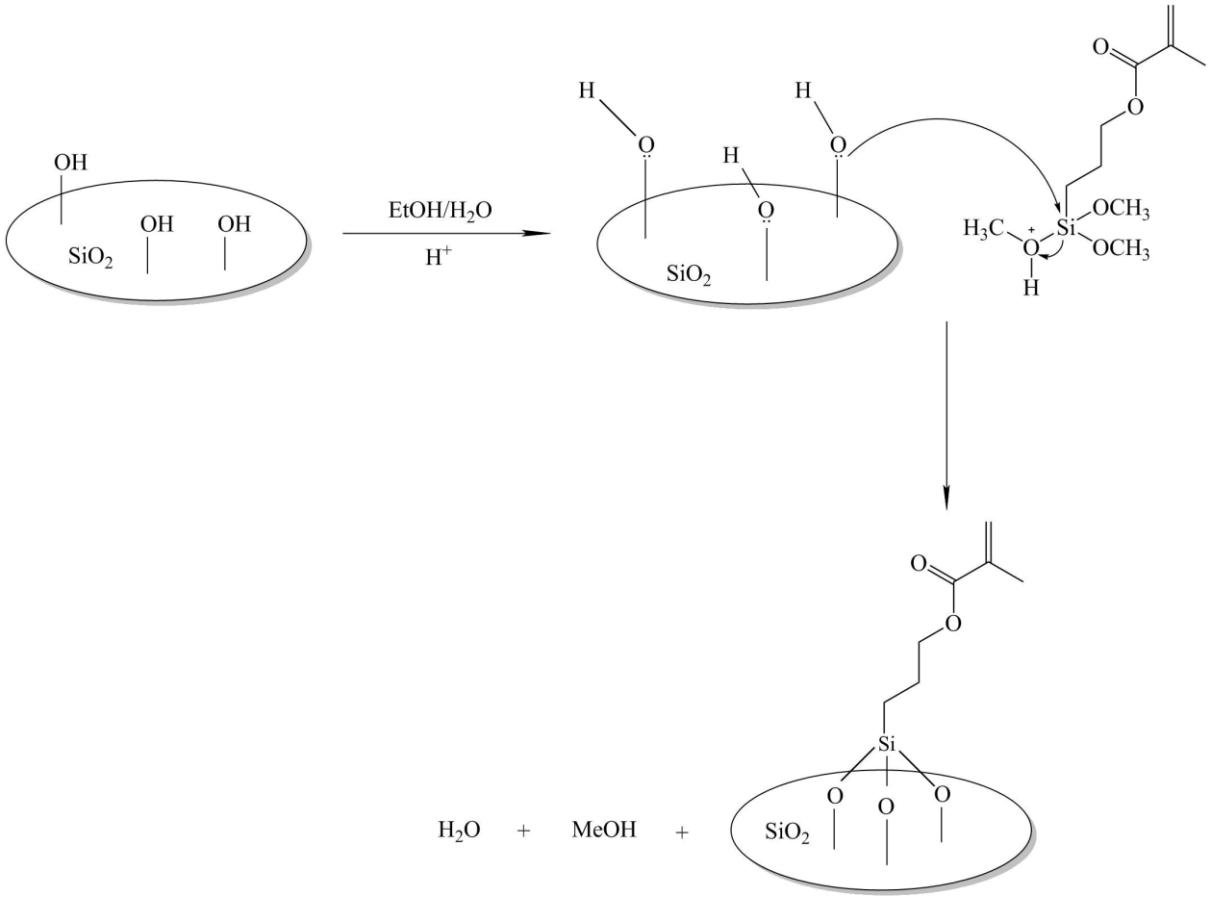

Fig.35: Schematic illustration of the reaction mechanism.

When the glass slides are put into reaction mixture, containing ethanol, water and acidic acid, the surface hydroxy-groups are protonated and attack negative-polarized oxygen in methoxy-groups of trimethoxysilyl propyl methacrylate, which is added in a drop-wise manner to the reaction mixture. The formed bond is hydrolytically transformed into a covalent bond and methanol and water are formed as by-products.

Before covering the glass slides with a hydrophobic layer of trimethoxysilyl propyl methacrylate, they must be cleaned from any foreign substances, which present on the surface of the glass slides. There are two common methods of cleaning the glass surfaces. First one is chemical method, where the substrates are immersed in a Piranha solution, which is a very strong oxidizing agent. The second method is physical, plasma cleaning procedure. In our work plasma cleaning method was chosen, because in spite of the fact, that both methods are activating glass surfaces, plasma cleaning has its benefits, namely:

- eliminating the use of chemical solvents as well as storage and disposal of solvent waste;
- rendering most surfaces hydrophilic (decrease water droplet contact angle and increase surface wettability);
- promoting adhesion and enhance bonding to other surfaces, prepare surface for subsequent processing (e.g. film deposition or adsorption of molecules and also promote attachment and adhesion of functional biological species or coatings);

- sterilizing and remove microbial contaminants on the surface, which is beneficial for biomedical applications and biomaterials;
- providing clean substrates in order to reduce background autofluorescence originating from organic contaminants for fluorescence microscopy.

Plasma cleaning procedure was already successfully applied in many works, not only in biomedical engineering [213-216], but also in such fields as surface patterning [217-219], self-assembly [220-223], surface modification [224-226] and surface adhesion [227-229]. After finishing the cleaning procedure, coverslips are prepared for silanization procedure. The full procedure is described in an experimental section more precisely. The glass coverslips were immersed in a mixture of trimethoxysilyl propyl methacrylate with ethanol, acetic acid and water. After 30 min, glass slides were removed from the reaction mixture and washed with deionized water several times. Post-baking of the coverslips in an oven by 110°C is necessary to achieve stable and uniform hydrophilic layer.
In order to confirm the changes in surface properties of the glass slides made by applying the surface modification procedure, the contact angle of modified glass slides was measured and compared with the contact angle of the non-modified glass slides. The experiment was made with 8 modified and 8 unmodified glass slides. All modified samples were treated via the same procedure, described before. The unmodified samples were only cleaned via Plasma cleaning procedure, also described before. In this experiment a droplet of deionized water was put in the centre on the surface of each glass slide and then a contact angle was measured via a camera. The results of the experiments are given in the Table 1 below.

Table 1: Results of contact angle measurements

Contact Angle of modified glass slide, °	Contact Angle of unmodified glass slide, °
45	18
51	17
49	12
45	16
48	15
47	18
50	14
52	16
The average value	
48	16

As one can see from the Table 1, the contact angle measurement is not a very exact method, because the obtained data vary in a quite broad range. This typically happens because water in a droplet begins soon to evaporate, changing therefore the volume of the droplet and the contact angle. For that reason it was necessary to test several samples in order to calculate the statistical average value. Two average values calculated for modified and unmodified glass slides confirm, that modification of the surface of the glass slides led to the hydrophobization of the

surface: the contact angle of the modified glass slides is much higher, then the contact angle of non-modified glass slides. The hydrophobization tendency can be also good seen on the pictures of the droplets of water on the glass slides, given below, see Figure 36.

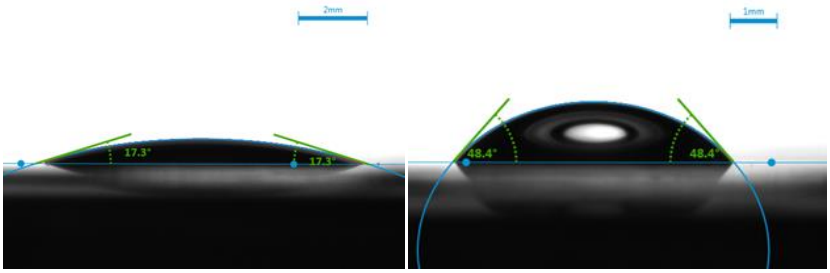

Fig.36: Images of the water droplets on the surface of the unmodified glass (left) and modified glass (right).

It can be clearly seen from the image above, that the surface of the unmodified glass slide has a higher water affinity than the surface of the modified glass slide. Therefore, based on this experiment, we can conclude, that the examined surface modification procedure of the glass slides can be successfully applied in order to achieve the desirable surface properties of the glass slides, which will be used as a support for hydrogel layers.

After accomplishing the surface modification procedure, glass slides are ready for being covered with the gel layers for the following experiments.

3 Photoinitiator for hydrogel

3.1 Selection of photoinitiator

Hydrogels are insoluble in water three-dimentional networks, made from cross-linked hydrophilic polymer chains. In case of photoactive polymeric substances, such as GelMOD, cross-linking process can be performed in a form of photopolymerization reaction. Photopolymerization is triggered by ionizing irradiation. Irradiation acts at first on the special type of molecule – photoinitiator (PI), which in its turn, initiates formation of radicals, starting the radical polymerization. The selection of a most suitable PI was for us an essential task for two reasons. First of all, as it was already discussed in this work, the materials biocompatibility is critically important for successful application of our system in tissue engineering. The problem is that residuals of monomer and PI, not consumed during the UV-curing process, are potentially cytotoxic. A recent report on systematic studies of cytotoxicity of commercially available photopolymers, using standard ISO10993-5 material extract protocol, demonstrated that the significant contribution to toxicity of materials comes from PIs [230]. Therefore, it was important for us to indicate a PI with the lowest cytotoxicity. It is obvious, that the relative cytotoxicity level differs for each single PI, but the general trend is that the higher PI concentrations are more toxic to the cells. However, the automatically rising problem is that low concentrations of PI, in its turn, result in a less efficiency of a PI. As a matter of fact, the efficiency of a PI is a second important criterion for selection of a PI in this work. Therefore, in order to minimize the toxic effects and at the same time not to lose an efficiency of PI, one of the aims in this work was to distinguish a PI, which will be still effective with reduction of its necessary content in the reaction mixture.

There are two potential PIs, which could be used for hydrogel samples preparation in our work. The first one is an already well-known commercially used water-soluble UV-photoinitiator IG2959, see Figure 28 for a chemical structure. This PI was successfully used in works of Ovsianikov *et al.*, where a photosensitive material was structured via 2PP technique [173], where it was demonstrated, that IG2959 being used in concentrations, which do not exceed the established limit, is not harmful to the cell culture. According to Bryant *et al*. and Williams *et al*., IG2959 has a very low cytotoxicity in the dark and also during UV-curing. However, the main draw-back of IG2959 is that it has a very poor solubility in water. In the present work, we decided to test another PI: Lithium benzoyl phenyl phosphonat (Li-TPO), which is a water-soluble salt, see Fig.37.

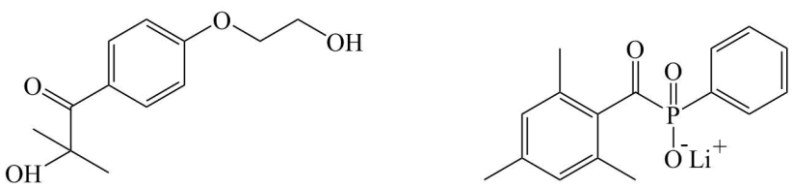

Fig.37: Chemical structures of IG2959 (left) and Li-TPO (right).

Moreover, from the UV-VIS absorption spectra of IG2959 and Li-TPO, measured with the same concentrations of both PIs, which were taken from the work of S. Benedikt [231], see

Figure 38 below, it can be clearly seen, that IG2959 and Li-TPO absorb differently in the interval of wavelengths between 300 nm and 420 nm.

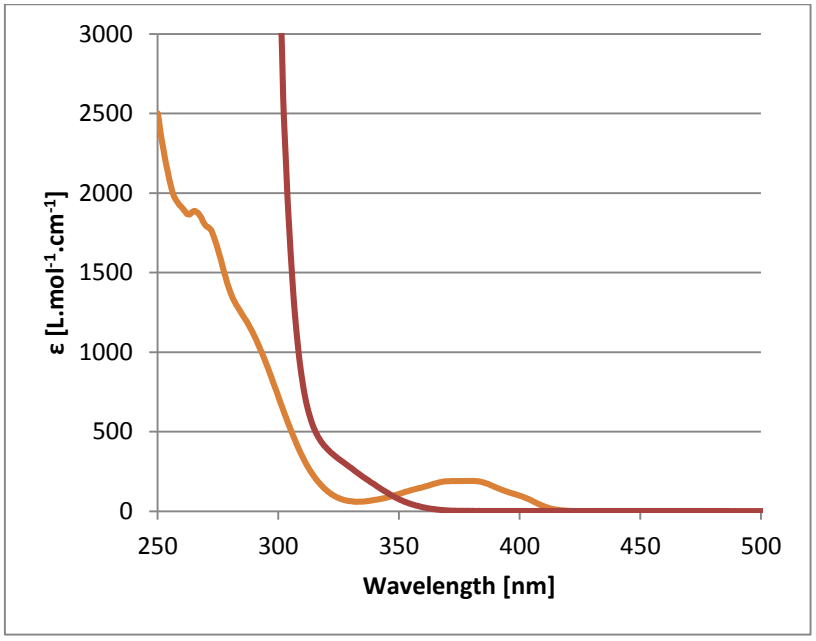

Fig.38: UV-VIS spectra of Li-TPO (orange line) and IG2959 (red line), concentrations of both PIs were 10^{-3} mol/L in methanol.

According to the spectra, depicted on Figure 38, IG2959 only absorbs in the UV-region and have its maxima of the n–π* transitions between 328 and 347 nm, which is behind the emission region (340-370 nm) of the UV-lamp used in our experiments. Another spectra line on the Figure 38, which refers to the second PI, Li-TPO, on the contrary, has strong absorption bands well above 350 nm, which is exactly in the emission region of this UV-Vis-lamp.

It is possible to shift the board-line of the absorption spectrum of IG2959 to the higher wave-lengths region, but only when the concentration of PI is increased, which, firstly, will be very difficult to achieve, because according to S. Benedikt [231], the solubility of IG2959 is only 5 g/L (see Table 2 below) and, secondly, will have a negative effect in terms of cytotoxicity. This means, that there is no way for further improvement of IG2959.

Being a water-soluble salt, Li-TPO overcomes the problems, related with IG2959 and could combine a less required concentration with low cytotoxicity and high absorption in the emission region of a UV-lamp utilized. In this work we compared IG2959 and Li-TPO in terms of their efficiency, concentrations required for formation of good hydrogels and also cytotoxicity.

The data, demonstrated in the Table 2 below show the difference between IG2959 and Li-TPO, according to S. Benedikt [231].

Table 2: Data, demonstrating the difference between IG2959 and Li-TPO

PI	Solubility [g/L]	λ_{max} [nm]	Ɛ [L/mol/cm]
Li-TPO-L	47	380.5	191
IG2959	5	328.0	296

3.2 Cytotoxicity of photoinitiator

The toxicity of Li-TPO, used for UV-curing of the reaction mixture, was tested with MC3T3-E1 cells according to the Presto Blue cell viability reagent protocol. All cytotoxicity tests and the results obtained were provided by biological department of our group. It was necessary to evaluate the cytotoxicity of Li-TPO and also to estimate the optimal concentration, which will not be toxic for the cells. For this purpose different concentrations of Li-TPO were dissolved in Alpha Minimum Essential Medium (α-MEM, Thermo Fisher Scientific) with serum proteins. In the previous works of A. Ovsianikov a common concentration of IG2959 used for UV-encapsulation of cells was 2.23 mM/L, which considered to be optimal in terms of cytotoxicity and efficiency. Therefore, this value was selected as the highest possible concentration of Li-TPO for testing its effect on metabolic activity of the cells and its cytotoxicity. The concentrations range of Li-TPO was, therefore, 2.23 mM/L and the following dilutions of 1.12, 0.6, 0.3, 0.15 and 0.075 mM/L. Observed values were compared to the corresponding control samples, which were cells untreated with PIs. The metabolic activity of the control samples not exposed to PI or UV light was assumed to be 100%.

A detailed explanation of the assay is described in Experimental Section. The sample solutions were put on the cells and left for 24h. Then the medium was exchanged and the fluorescence dye Presto Blue (PB) reagent was added and left for 1h. After 1 hour of incubation the fluorescence was measured in order to count the living cells. All substances were analyzed with 8 repetitions.

The cell counting is based on the metabolic reduction of the Presto Blue dye by living cells. When cells are viable, they maintain a reducing environment within their cytosol. Upon entering a living cell, Presto Blue reagent is reduced from resazurin, a blue compound with no intrinsic fluorescent value, to resorufin which is red in colour and highly fluorescent. The reduced dye exhibits fluorescence, which is measured by a plate reader and gives quantitative information proportional to the number of living cells.

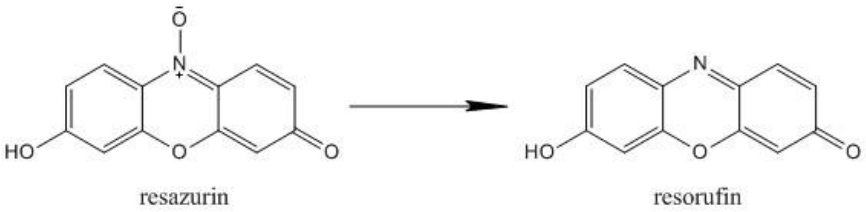

Fig.39: Reduction of the dye in the Presto Blue assay by the reducing environment of the viable cell.

Figure 39 demonstrates the reaction of resazurin (the dye in the Presto Blue assay) to the fluorescence dye resorufin. Resazurin is a blue dye with no intrinsic fluorescence value, while resorufin is red coloured and exhibits strong fluorescence at 586 nm, as it can be seen from the Figure 40, given below.

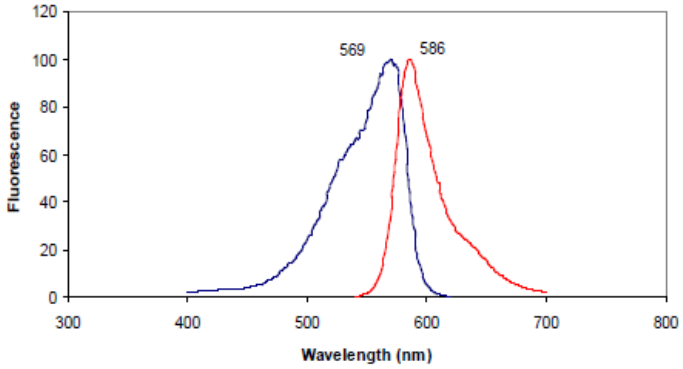

Fig.40: Reduction of Presto blue reagent: Excitation (blue line) and emission (red line) peaks for resorufin to measure fluorescence values.

The cytotoxicity tests, described before gave the following results. Observed values were compared to the control samples, which were cells untreated with PI: a positive control (10% Presto Blue and 90% medium) and a negative control (50% DMSO [Sigma Aldrich] and 50% medium). Metabolic activity of cells was measured before and after exposure to UV-light with a wavelength 365 nm and intensity 4 mW/cm^2 for 10 min. The results of the test can be seen from the Figure 41 below.

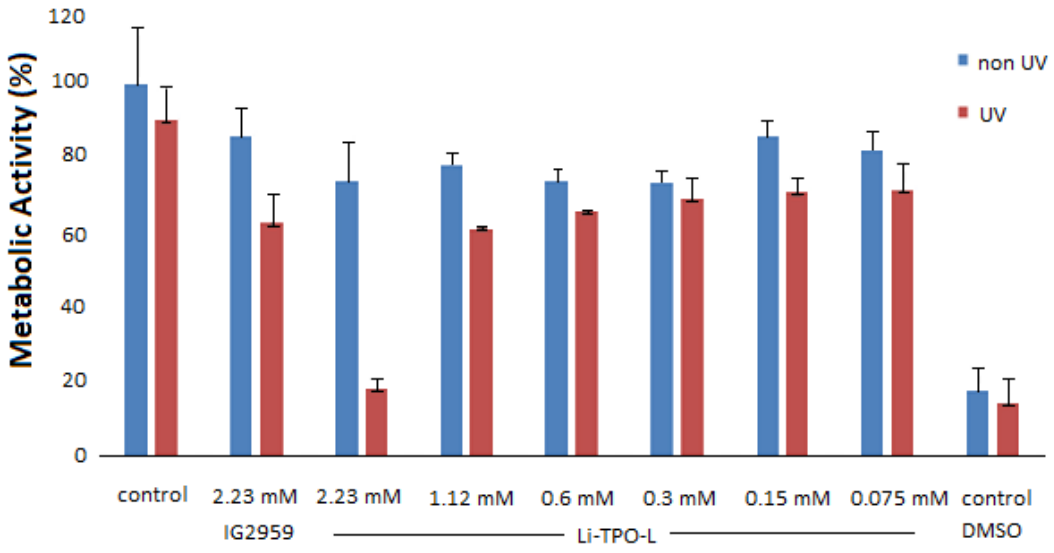

Fig. 41: Influence of IG2959 and different concentrations of Li-TPO on metabolic activity of MC3T3-E1 after 24 h and exposed/not exposed to UV light (Presto Blue Cell Viability assay). All values are presented as % of positive untreated control.

The metabolic activity of cells treated with IG2959 and exposed to UV was 61% compared to untreated control. It showed no significant difference to the samples treated with 1.12mmol Li-TPO and its lower concentrations, which confirms that cytotoxicity of Li-TPO in the observed range of concentrations does not exceed the cytotoxicity of IG2959 in its optimal concentration. The metabolic activity of cells treated with 2.23mmol Li-TPO and UV was significantly decreased and dropped to only 17%, which is similar to the DMSO control (dead cells control). Concentrations of Li-TPO lower than 0.6 mM/L showed less cytotoxicity, but these

concentrations of PI are not sufficient for UV polymerization of GelMOD in practical work: obtained hydrogels are too soft and breakable. The results of these preliminary tests allow one to conclude that the concentration of 0.6 mM/L Li-TPO is most appropriate for our investigations, as the resulting cell viability level is similar to that observed in controls.

In conclusion it can be said, that Li-TPO demonstrated not only the lower cell-toxicity, but also a higher absorption-efficiency by far fewer concentration, than IG2959. However, before the final choice of PI, further rheological measurements have to be done in order to achieve the data about mechanical properties of the hydrogels, produced with both Li-TPO and IG2959. Using different concentrations of Li-TPO will allow us to observe a dependence of hydrogel stiffness from concentration of PI. It is necessary to point out that the hydrogels, used for this purpose will be created only for rheological experiments and estimation of mechanical properties of hydrogels, and not for further cell seeding procedure.

4 Rheology

4.1 Optimum setup

The aim of our work was to study the possibility of controlling and monitoring the growth of cells via deformations of the fluorescent grid, grafted on the hydrogel substrate. Deformation of the grid should clearly demonstrate how the cell changes with time and with variable stiffness of the hydrogel, two main parameters, which have been chosen for our investigation. Therefore, our first aim was to evaluate the optimal stiffness of the hydrogel, which would be high enough to maintain the hydrogel mechanical stability and low enough to allow the cells to integrate into the hydrogel and adjust this environment to their own preference. The distant aim, related to this approach and placed beyond the frames of the present work is application of the hydrogel substrates for facilitation of the preosteoblast cells differentiation into the osteoblast cells.

For definition of the hydrogel optimal stiffness photorheometry was used. Photorheometry is a technique, which allows one to measure an increasing storage modulus (G') of a photoactive compound during its irradiation with a UV light. Storage modulus is a good indicator of material stiffness, because it increases with increasing stiffness of material. In case of photoactive compounds, the hardening is determined by a crosslinking reaction, initiated by light irradiation.

Generally, viscoelastic characteristics of a sample are characterized with two main curves, which appear on the monitor of experimental set-up in a 'real-time' when the measurement proceeds. These curves are time dependences of storage (G') and loss (G'') moduli, which will be two most important parameters, obtained via photorheology technique in this work.

Working principle of a photorheometer is not complicated. As it can be seen from the Fig. 42, a measuring system of a photorheometer is driven down till it contacts with a surface of a liquid reaction mixture. The distance between a sample and a measuring system can be programmed, though enabling creation of hydrogel layers with desirable thickness. After, measuring system oscillates and a measurement of mechanical characteristics of a sample starts. After a certain period of time, which is also determined in the experimental parameters, the UV-light source is switched on, starting a cross-linking process of an initial polymeric substance. Cross-linking process propagates with time and results in an evaluation of stiffness of a sample. Storage and loss moduli curves are registered and showed on the monitor in a real time.

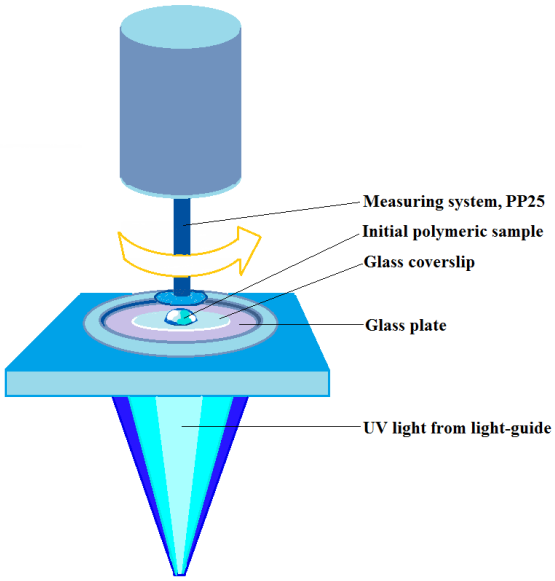

Fig.42: Schematic image of photorheometer.

Calibration of the light source of the experimental set-up results in performance of UV-light with a well-defined wave-lengths interval, which better overlaps with an absorption diapason of a PI. This leads to a higher light absorption efficiency, and therefore to a higher quality of hydrogel samples.

4.1.1 Protection of hydrogel from drying

A common problem, occurred during the measurements was drying of the hydrogel samples due to evaporation of water. This phenomenon can be easily registered by the experimental set-up. Drying of a hydrogel layer is characterized by as a sudden appearance of uncharacteristic artefacts, sharp peaks on the straight plateau-part of the rheometrical curves or by an abnormal increase of G'. Drying of the hydrogel layer not only complicates obtaining of appropriate data from experimental set-up, but also makes impossible to use the hydrogel sample after photorheology for further experiments. Dried hydrogel layer is easily destroyed if one tries to remove it from the measuring system.

In order to overcome this complexity, the edge of the measuring system was coated with mineral oil, which should protect the hydrogel from drying. In order to demonstrate the benefits of using mineral oil in our experiments, and also to show, that the presence of oil does not have any influence on the experimental data, the series of measurements were performed.

In the given case the measurements were done for mixtures between GelMOD (DS: 70%) as a polymeric component and IG2959 as a PI component. The hydrogel mixtures were calculated to a polymer-content of 20% with a PI content 2.23 mM/L based on the whole formulation. The high concentration of polymeric component results in a more obvious and fast drying process. All percentage specifications in this section are weight/weight percent, if not otherwise stated. All measurements were done twice: without mineral oil at first and after with mineral oil. The

measurements were made with 7 repetitions in order to demonstrate good reproducibility of the results (See Table 13; Experimental part 4.1.1).

On the Figure 43 one can see the typical curves obtained from photorheometry. The curves represent time-dependence of G'. An ideal curve rises in a predictable manner without any steps and discrepancies, demonstrating the stiffness increase of the examined sample. When the maximum stiffness is achieved, the curve reaches a plateau, which means, that a photochemical reaction is completed with a full conversion of initial reagents.

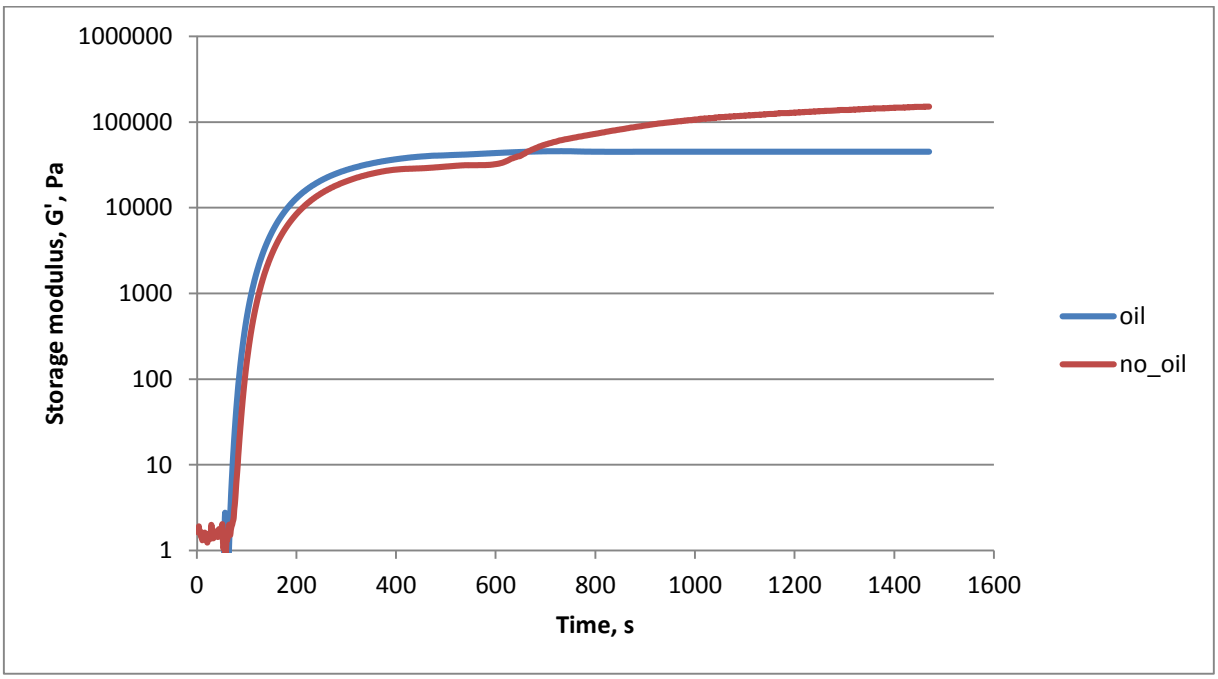

Fig.43: Image of typical photorheometry curves, obtained by measuring a hydrogel mixture of the following content: GelMOD 20%, IG2959 2.23 mM/L. Blue line represents the sample measured with mineral oil, red line represents the sample measured without mineral oil.

From the Figure 43 one can see, that drying of the hydrogel layer of the sample, measured without mineral oil, took place already after 600 s of measuring, where an abnormal increase of a storage modulus, G', can be observed. By comparison, the sample measured with mineral oil demonstrated that the drying of the hydrogel layer was prevented: the obtained curve does not have any irregularities.

Eventually, the first data, obtained from photorheometry experiment are the maximum G' values, from which can be clearly seen which hydrogel sample possesses a higher cross-linking density. By calculating time after which 95% of the maximum value of G' are reached, one speaks about how fast 95% of conversion were reached in each case, in other words how fast the cross-linking reaction propagates.

For analysis of the slope, which indicates the reactivity of a given system, a regression line was fit through the linear region of the measuring curve so that the correlation coefficient R^2 exceeded 0.99.

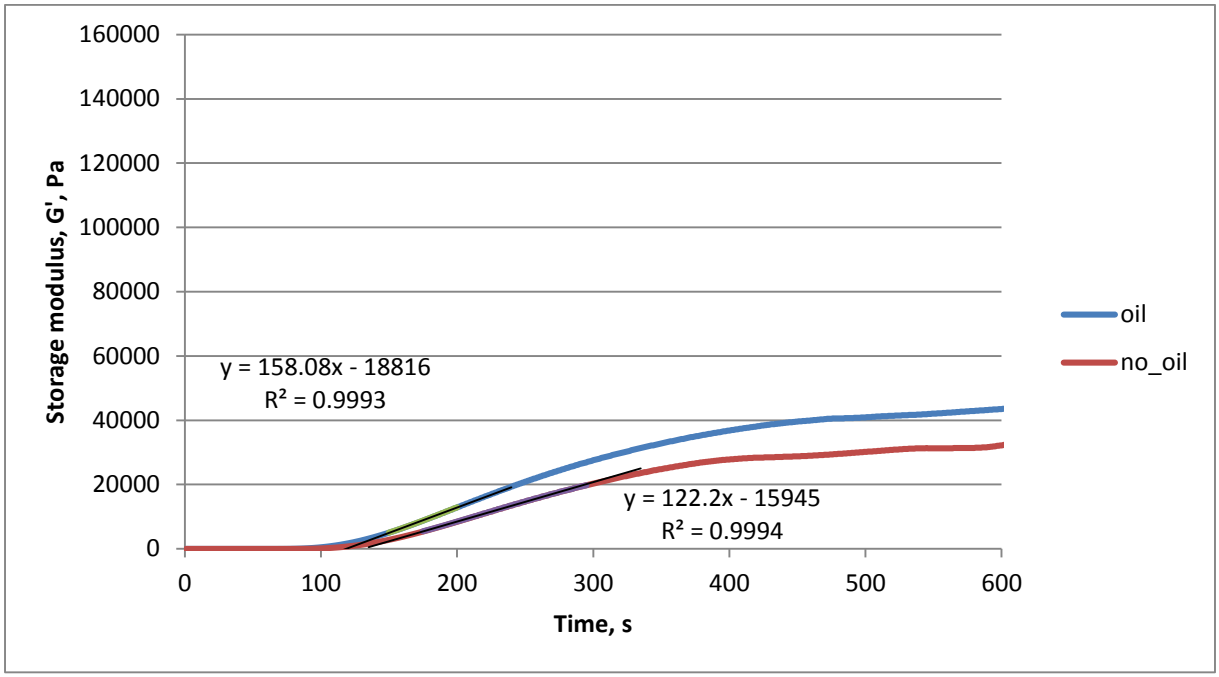

Fig.44: Example of how the slope and the delay of initiation were determined.

Figure 44 demonstrates how the regression line is laid through the curve in order to calculate and compare the slope of both curves.

Another important parameter, which can also be calculated, is the delay of initiation. At the beginning of each measurement the measuring system starts with oscillation, but without radiation. After 20 s the shutter of the UV-lamp gets opened and from this moment the initiation should start. But in some cases initiation does not start at once, but after a certain time, which corresponds to the time of delay of initiation, specific for each reaction mixture. In order to analyze the point where an increase of viscosity was visible, the point of intersection of the regression line with the abscissa is calculated and the time, where no irradiation occurs (20 s in this case) was subtracted. Figure 44 demonstrates also how each curve is intersected with the abscissa to calculate the delay of initiation.

The maximum value of storage modulus G'max, the time after 95% of G'max are reached, the slope of G' in the linear region, and the delay of initiation, which were determined for the samples are given in the Table 3.

Table 3: Data, obtained by photorheometry measurements of mixtures for determination of the influence of mineral oil on the formation of the hydrogel layers

Sample	Delay, s	Slope, $Pa*s^{-1}$	Time of 95%G'max, s	G' max, kPa
GelMOD20%_IG2959_2.23_oil	99±1.9	158±15	570±25	45±5
GelMOD20%_IG2959_2.23_no_oil	110±1.4	122±13.8	1362±29.5	153±12.4

As it can be seen from the Table 3, in terms of reactivity both samples have the similar results: the values of slope and delay in both cases are nearly equal. However, time of 95% G'max of the sample measured without oil exceeds this value of the sample measured with oil more than at twice. Also the value of G'max of the sample measured without oil is more than three times greater than the same value of the sample with oil, which is an incontestable evidence of drying phenomena.

Therefore, according to obtained data, the fact, that mineral oil prevents the drying of the hydrogel layer and does not influence on reproducibility and accuracy of the experimental data can be proved. This experiment confirms, that mineral oil is a good tool for protection of a hydrogel layer, which means, that all further rheological experiments in this work will be done in presence of mineral oil.

4.1.2 Influence of glass-supporter

It was necessary for our work to be able to use the hydrogel layers, produced on the photorheometer, for cells seeding. In other words, the produced samples need to be mechanically stable for further transportation and numerous manipulations in the cell-culture laboratory.

Unfortunately, it was impossible to detach the hydrogel layers from the measuring system of photorheometer after the measurements without destroying them. For this reason, it was decided to use special thin glass slides as a support for soft hydrogel layers.

The glass slides, before being used in experiments were functionalized. For a detailed description of a functionalization procedure, see a correspondent experimental section. Functionalization results in hydrophobization of the surface of the glass slides. This and the copolymerizable methacrylic groups, result in a better adhesion of a hydrogel layer to the surface of the glass slide.

The functionalized glass slide was then placed on the glass plate of the photorheometer and well-fixed on it by putting a drop of water between the glass slide and glass plate. After that the measurements were performed as usual.

It was important to demonstrate, that the presence of functionalized glass slide as a support does not have any influence on the accuracy of the experimental data and that the results of experiments performed on the glass slides are reproducible. Again, the maximum value of storage modulus G', the time to reach 95% of the maximum value of G', the slope of the storage modulus in the linear region, and the delay of initiation were determined from these samples.

The measurements were done for mixtures between GelMOD (DS: 70%) as a polymeric component and Li-TPO as a PI component. The hydrogel mixtures were calculated to a polymer-content of 20% with a PI content of 2.23 mM/L based on the whole formulation. All percentage specifications in this section are weight/weight percent, if not otherwise stated. All measurements were done twice: without support of a glass slide at first and after with support of a glass slide.

After this series of measurements two average curves were obtained: for the samples without a support and for those with support. Both curves are depicted on the Figure 45.

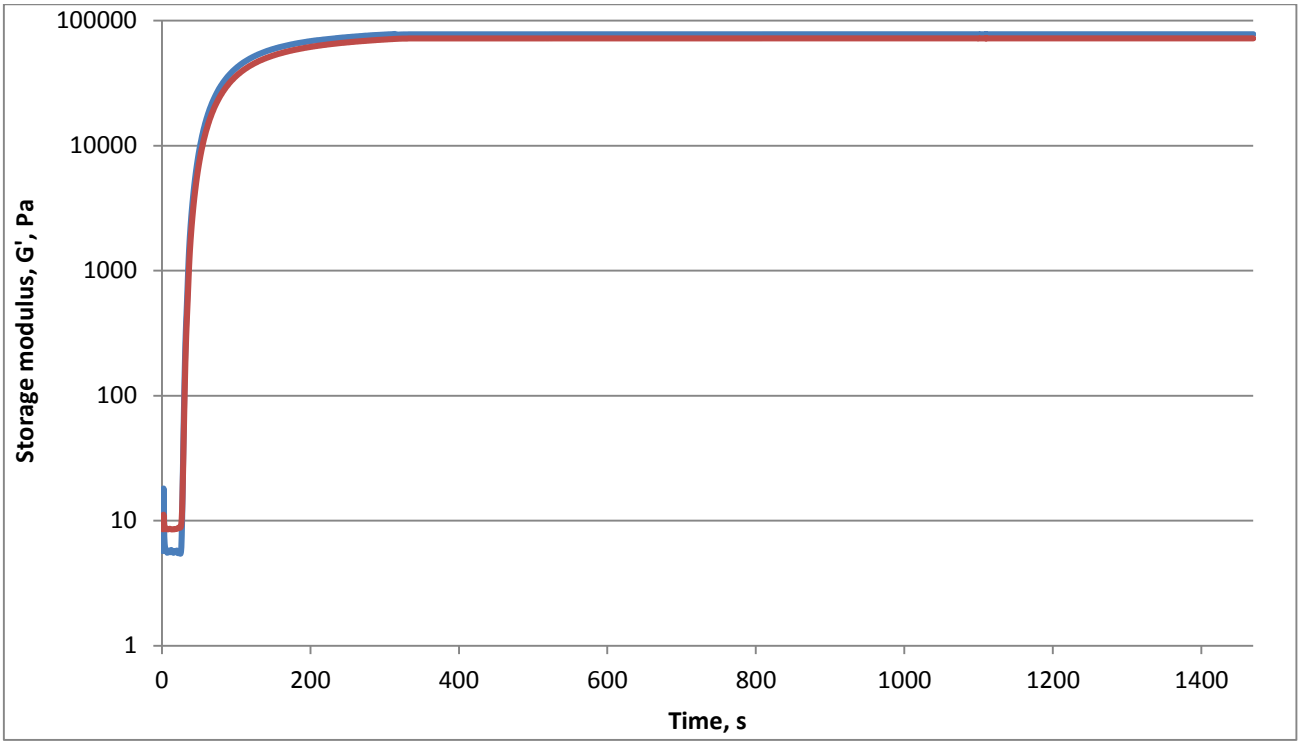

Fig.45: Image of photorheometry curves, obtained by measuring a hydrogel mixture of the following content: GelMOD 20%, Li-TPO 2.23 mM/L. Blue line represents the sample measured with an external support of a glass slide, red line represents the sample measured without a support of a glass slide.

As it can be seen from Figure 45, the obtained curves look quite identical, which proves that the presence of glass slides do not influence on the experimental data. Table 4 below shows the resulting maximum value of storage modulus G', the time to reach 95% of the maximum value of G', the slope of the storage modulus in the linear region, and the delay of initiation.

Table 4: Data, obtained by photorheometry measurements of mixtures for determination of the influence of glass support

Sample	Delay, s	Slope, $Pa*s^{-1}$	Time of 95%G'max, s	G'max, kPa
GelMOD20%_LiTPO2.23_glass	17±0.7	733±51	252±31.5	78±2.8
GelMOD20%_LiTPO2.23_no_glass	18±1	630±46	267±32.5	72±3.3

From the Table 4 it can be seen, that delay of initiation and slope of the storage modulus in the linear region of both curves have the same values. Time to reach 95% of the maximum value of G' (95% G'max) and resulting maximum value of storage modulus G'max in both cases are nearly equal. Therefore, it can be concluded, that using of glass slides does not change the values of experimental data.

During the experiment all samples could be easily detached from the measuring system and glass table of photorheometer. A good stability of the hydrogels on the glass slides was also proved: none of the samples was damaged during this experiment and after it - when the samples were transferred into the petri dishes for being used in further experiments.

Therefore, relying on the data achieved from the above described experiment, it can be concluded, that the idea of using functionalized glass slides as a support for hydrogel layers was successful. This approach will allow not only to obtain the undamaged samples from photorheometry, but also it will allow us to produce a more stable system, where the soft hydrogel layer can be easily transported and manipulated without destruction. According to the conducted experiment, all hydrogel samples in this work will be produced on the functionalized glass slides.

4.2 Storage stability of formulations

As it was already discussed in Introduction, GelMOD is an enzymatically degradable biocompatible compound. Theoretically, this means, that GelMOD could also degrade and loose its properties with time. If this hypothesis is true, and degradation of GelMOD with time really takes place, it could have a big influence on the relevance of obtained experimental data and on the results of our work, as long as GelMOD is one of the main compounds for reaction mixtures in this work.

In order to find out if degradation of GelMOD happens, several measurements were performed, which aim to compare mechanical properties of the hydrogel layers, obtained from the fresh-made reaction mixtures and reaction mixtures, which were prepared for a week before the experiment started.

The series of standard photorheological measurements were done for two reaction mixtures with the following content: GelMOD (DS: 70%) with concentration of 20% as a polymeric component and Li-TPO-L 2.23 mM solution as a PI component, and also GelMOD (DS: 70%) 20% concentrated as a polymeric component and IG2959 2.23 mM/L solution as a PI component. The measurements were performed for both types of PIs in order to see if there will be any difference in aging behavior, related to the PI type. Two reaction mixtures were made right before performing the photorheological measurements, and two reaction mixtures were prepared one week before the measurements and hold in two test tubes with caps, wrapped into the aluminium foil and stored in darkness by room temperature. Measurements with each reaction mixture were performed with 7 repetitions as usual in order to obtain four average curves, shown on Figure 46.

As before, the maximum value of storage modulus G'max, time after which 95% of the maximum value of G'max are reached, slope and delay of initiation were measured and compared.

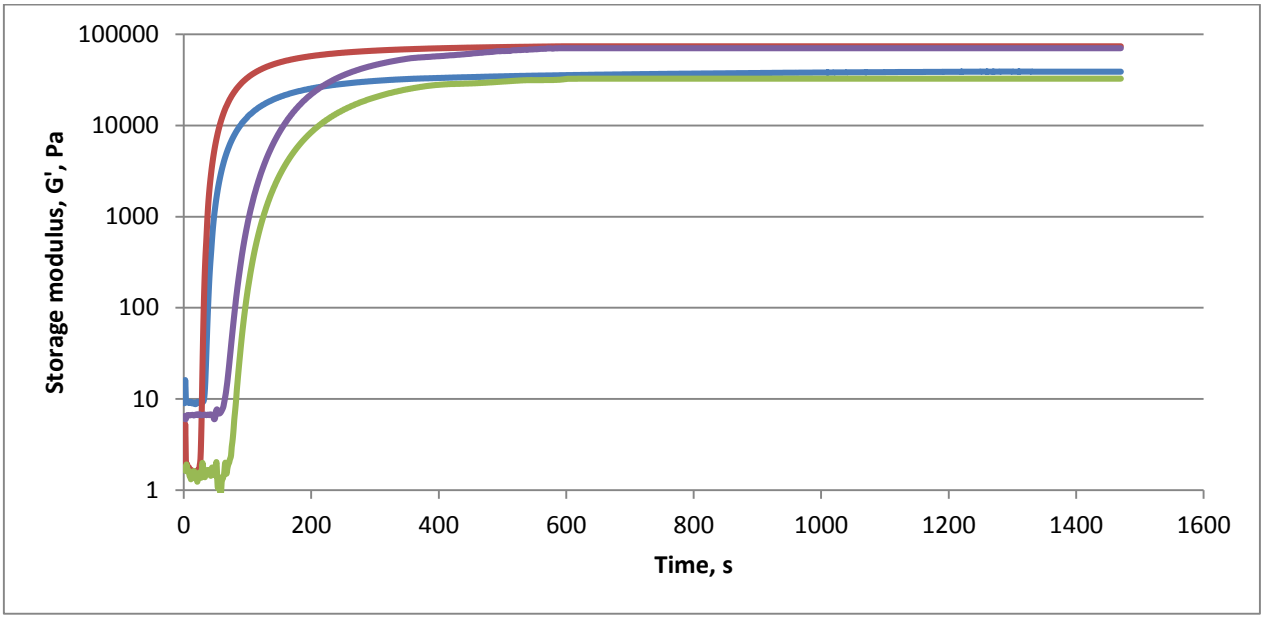

Fig.46: Image of photorheometry curves, obtained by measuring four reaction mixtures: GelMOD 20%, IG2959 2.23 mM/L (violet line) and GelMOD 20%, Li-TPO-L 2.23 mM/L (red line), which were new-made; and GelMOD 20%, IG2959 2.23 mM/L (green line) and GelMOD 20%, Li-TPO-L 2.23 mM/L (blue line), which were made for a week before the experiment.

The aging process of reaction mixtures is clearly seen from the obtained curves, depicted on Figure 46: there is a big difference between the same reaction mixtures already after a week. In order to analyze this difference in mechanical properties of produced hydrogel layers, like described in the previous sections, maximum value of storage modulus G'max, the time to reach 95% of the maximum value of G'max, the slope of the storage modulus in the linear region, and the delay of initiation were calculated. The results are given in Table 5 below.

Table 5: Data, obtained from photorheological measurements of reaction mixtures for determination of the aging process of the hydrogel layers

Sample	**Delay, s**	**Slope, $Pa*s^{-1}$**	**Time of 95%G'max, s**	**G'max, kPa**
GelMOD20%_IG2959_2.23_new	101±1.4	278±12.3	517±15.5	70±1.7
GelMOD20%_IG2959_2.23_old	111±2.2	123±13	520±15	32±2
GelMOD20%_LiTPO_2.23_new	19±1.5	581±27.4	395±29	74±1.4
GelMOD20%_LiTPO_2.23_old	25±2	232±15.2	415±31	39±1.8

It can be seen from Table 5 that the value of delay of initiation for reaction mixtures with the same type of PI differs, although not drastically: initiation of cross-linking reaction in the old mixtures begins approximately 10 s later, than in the fresh-made mixtures. The slope of the curves differs more than twice for each mixture type: fresh-made reaction mixtures with both PIs types possess the higher slope values of 278 $Pa*s^{-1}$for mixture with IG2959 and 581 $Pa*s^{-1}$ with Li-TPO-L, whereas the old reaction mixtures have only 123 and 232 $Pa*s^{-1}$ for mixtures with IG2959 and Li-TPO-L respectively. Such difference in slope values speaks about the less reactivity of the old reaction mixtures in comparison with the new reaction mixtures. Time to reach 95% of the maximum value of G' for mixture with IG2959 as PI is quite the same for both new and old samples, while for the mixtures with Li-TPO-L as a PI this value is two time higher for the old reaction mixture. Another important result gave the calculation of maximum storage modulus of the samples. G'max of the new-made reaction mixtures exceeds this value of old reaction mixtures at twice.

Therefore, regarding to the data obtained from this experiment, one can conclude, that the degradation process of GelMOD in reaction mixtures really takes place and results in a loss of reactivity of the mixture and also decrease of mechanical strength and quality of produced hydrogel layers.

4.3 Evaluation of optimal PI

Two potential PIs for our work: IG2959 and Li-TPO were already compared in terms of cytotoxicity and UV-light absorbance in Section 2. Next, it was interesting to compare the reactivity of these PIs by photoreometry.

For determination of the best-suited PI for our investigations the measurements were done for mixtures between GelMOD (DS: 70%) 5% as a polymeric content and IG2959 and Li-TPO as PI compounds. Concentrations of both PIs were taken the same 2.23 mM/L. In order to obtain two average curves, depicted on the Figure 47, the measurements for each reaction mixture were done with 7 repetitions as usually.

As before, the maximum value of storage modulus G'max, time after which 95% of the maximum value of G'max are reached, slope and delay of initiation were measured and compared. The results are shown in the Table 9.

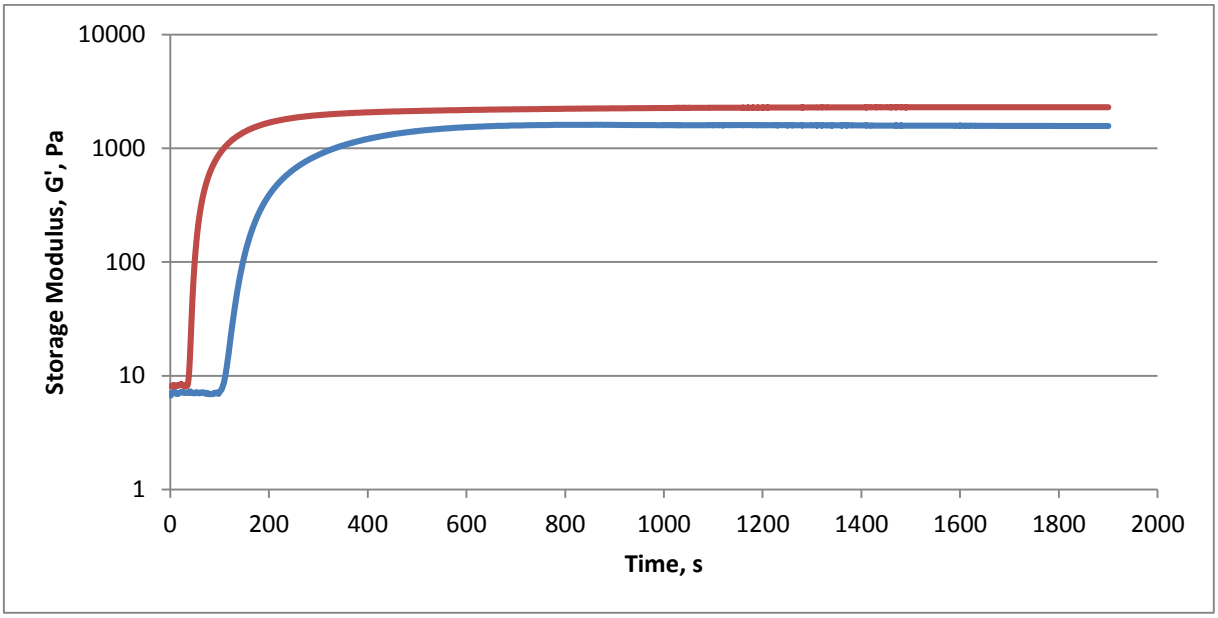

Fig.47: Image of photorheometry curves, obtained by measuring two reaction mixtures: GelMOD 5%, IG2959 2.23 mM/L (blue line) and GelMOD 5%, Li-TPO-L 2.23 mM/L (red line).

It can be good seen from the Figure 47 that the curve obtained from the reaction mixture with Li-TPO as a PI is positioned definitely higher above the curve obtained from the reaction mixture with IG2959 as a PI, which already means, that the reactivity of the mixture with Li-TPO is higher than the reactivity of the mixture with IG2959. Indeed, the data, presented in the Table 6 confirm this fact.

Table 6: Mixtures for determination of the best suited PI

Sample	Delay, s	Slope, $Pa*s^{-1}$	Time of 95%G'max, s	G'max, kPa
GelMOD5%_IG2959_2.23	108±1.8	5.4±0.3	630±8.8	1.6±0.1
GelMOD5%_LiTPO_2.23	24±1.5	17±1.7	590±3.5	2.3±0.2

First of all, delay of initiation is much more bigger in case of the mixture with IG2959. In case of reaction mixture with Li-TPO as a PI, cross-linking initiates already after 24 s after the shutter was opened, while mixture with IG2959 needs 108 s to start the reaction. The value of slope is bigger in case of Li-TPO also, which confirms, that the reactivity of this reaction mixture is higher. Time to reach 95% of the G'max is smaller in case of mixture with Li-TPO and the maximum value of storage modulus, G'max is higher, which means, that the formed hydrogel is stiffer.

It was important to see in this experiment how the properties of produced hydrogel layer will be changed in respect to the type of PI. Between two PIs studied in the present work, Li-TPO already showed the better results in terms of cytotoxicity and also spectra analysis, which were consider in details in Section 3. As long as it was already proved by UV-VIS spectra of IG2959

and Li-TPO, that efficiency of Li-TPO is higher, and from cytotoxicity tests it was demonstrated that concentration of Li-TPO 0.6 mM/L is comparable with cytotoxicity of IG2959 2.23 mM/L solution, the curves on the Figure 47 confirm our theory.

It was concluded, that Li-TPO is the better PI for our investigations and, therefore, will be used in all our further experiments.

4.4 Determination of an optimal PI concentration

Apart from the PI type, there are also two main factors, which can influence on the stiffness of a photo-crosslinkable material: concentration of PI and concentration of the polymer. For scientific and financial reasons, the optimal concentration of initial polymeric content of our reaction mixture, GelMOD, 5% have been chosen as a standard for all experiments, therefore, only variable concentration of PI Li-TPO was examined.

For determination of the optimal concentration of the PI in the reaction mixture, six mixtures with different concentrations of Li-TPO were prepared and the standard photorheometry measurements were performed. Table 7 shows the content of the analyzed mixtures for evaluation of the best PI concentration. The reaction mixtures were calculated to a polymer-content of GelMOD (DS: 70%) 5%, based on the whole formulation.

Table 7: Mixtures for evaluation of the best PI concentration

Sample	PI concentration [mM/L]
GelMOD5LiTPO-0.075	0.075
GelMOD5LiTPO-0.15	0.15
GelMOD5LiTPO-0.3	0.3
GelMOD5LiTPO-0.6	0.6
GelMOD5LiTPO-1.12	1.12
GelMOD5LiTPO-2.23	2.23

After the standard photorheometry measurements were performed, the curves, depicted on the Figure 48 below were obtained.

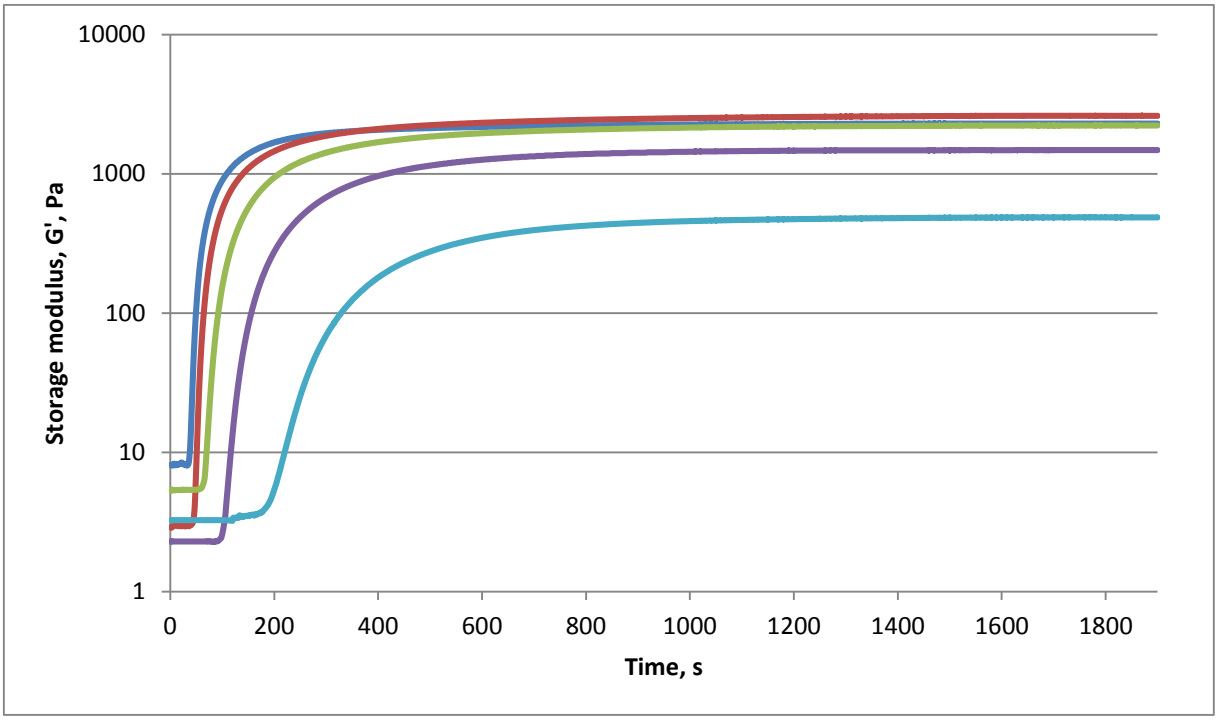

Fig.48: Image of photorheometry curves, obtained by measuring five reaction mixtures for evaluation of the best concentration of PI: GelMOD 5%, Li-TPO 2.23 mM/L (dark blue line), GelMOD 5%, Li-TPO 1.12 mM/L (red line), GelMOD 5%, Li-TPO 0.6 mM/L (green line), GelMOD 5%, Li-TPO 0.3 mM/L (violet line), GelMOD 5%, Li-TPO 0.15 mM/L (blue line).

The only curve, which is not depicted on the Figure 48 is a curve, corresponded to the reaction mixture with concentration of Li-TPO 0.075 mM/L. During the measurements it was shown, that this reaction mixture did not start within the time used for measuring the other samples (1900 s). This is because such a small PI content is, obviously, not enough to start the cross-linking reaction. Therefore, concentration of Li-TPO 0.075 mM/L was not analyzed anymore in this work. The concentration dependence can be clearly seen from the Figure 48, because one sees that the curves of reaction mixtures with less PI content are positioned lower than those with a higher PI content. In order to analyze the obtained photorheological curves, as usually, the standard calculations of the maximum value of storage modulus G'max, time after which 95% of G'max are reached, slope and delay of initiation were performed and compared. The results of these calculations are presented as the diagrams on Figures 49, 50, 51, 52 below.

It was important to see how the PI concentration can influence on the initiation of the photochemical reaction. Therefore, the delay of initiation in each reaction mixture was analyzed. The obtained time intervals are compared in Figure 49.

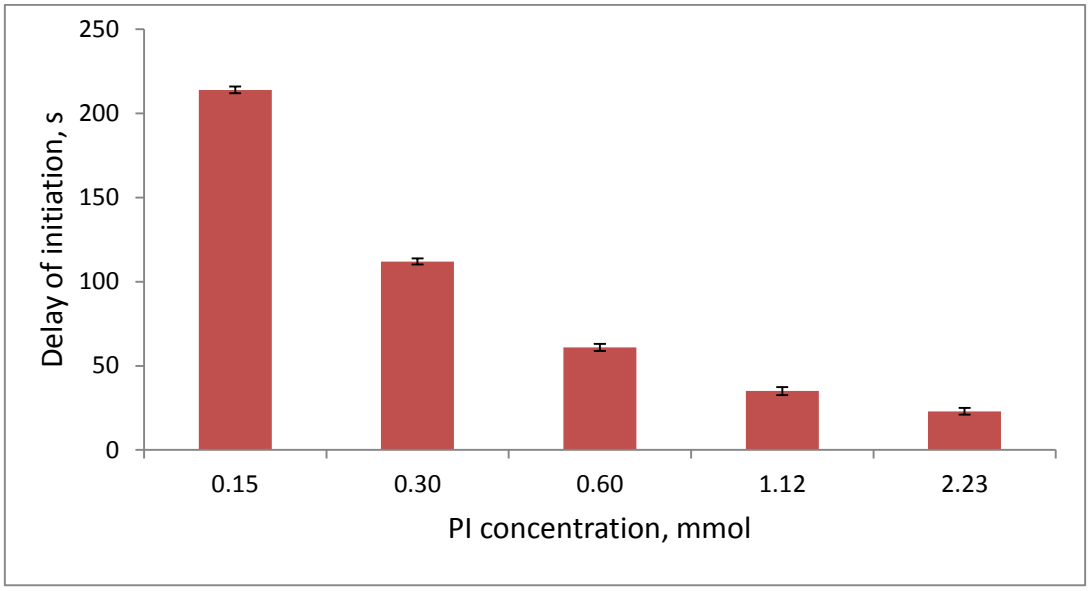

Fig. 49: Delay of initiation in mixtures of GelMOD5% with different concentrations of PI.

As it can be seen from the Figure 49, the delay of initiation strongly depends on the concentration of PI in the reaction mixture. The highest time of delay of initiation, almost 214 s, was observed in reaction mixture with the smallest PI concentration of 0.15 mM/L, while in reaction mixture with the highest PI content, 2.23 mM/L Li-TPO-L, the initiation starts already after 23 s. With an increasing amount of PI in the reaction mixture, a higher number of radicals can be generated in the beginning of light irradiation, and therefore, the probability for the radical to start a reaction increases. That is why the maximal PI concentration of 2.23 mM/L results in a smallest time of delay.

Slope, which indicates the reactivity of a system, was also analyzed and the calculated data are shown on the diagram below.

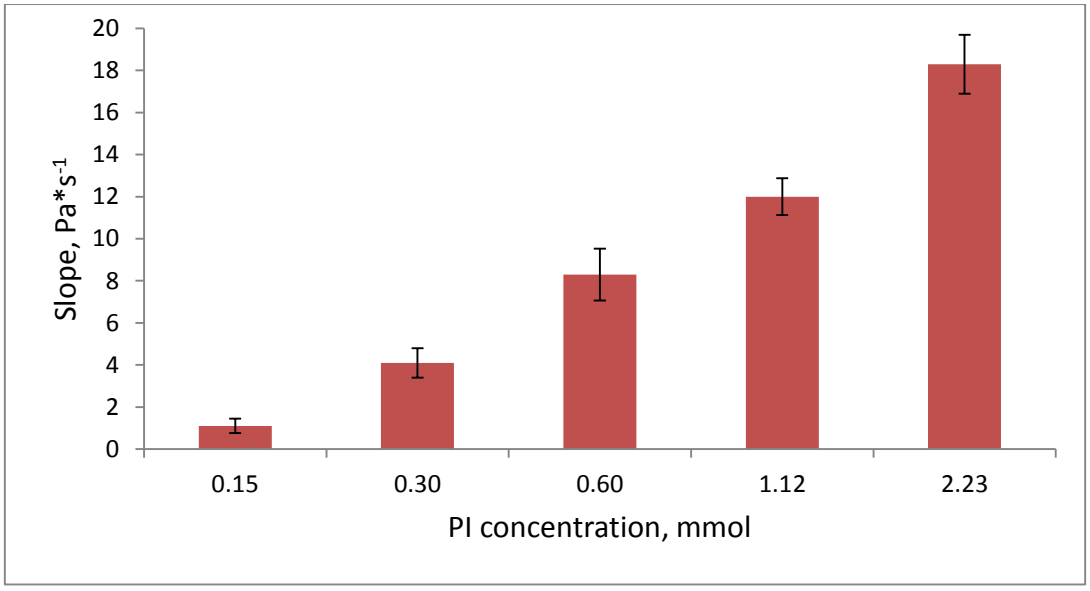

Fig.50: Slope of G' in the linear region in mixtures of GelMOD 5% with different concentrations of PI.

As it can be seen from the Figure 50, the smallest slope value has the mixture with the smallest PI concentration 0.15 mM/L and the highest slope value has the mixture with the highest PI concentration 2.23 mM/L. The slope values of other reaction mixtures are following the general tendency of elevation of the slope value with elevation of PI concentration. This increase of reactivity with elevation of PI content in the reaction mixture was expected for the same reason, as described for delay dependence from PI concentration: the higher amount of radicals is formed and react with more polymer molecules already in the beginning of irradiation.

For analyzing the values of maximal storage modulus, achieved for each reaction mixture, the dependence of G'max from concentration of PI is depicted as a diagram on the Figure 51 below. In order to see how fast 95% of G'max were reached in each case, the diagram on the Figure 52 was created.

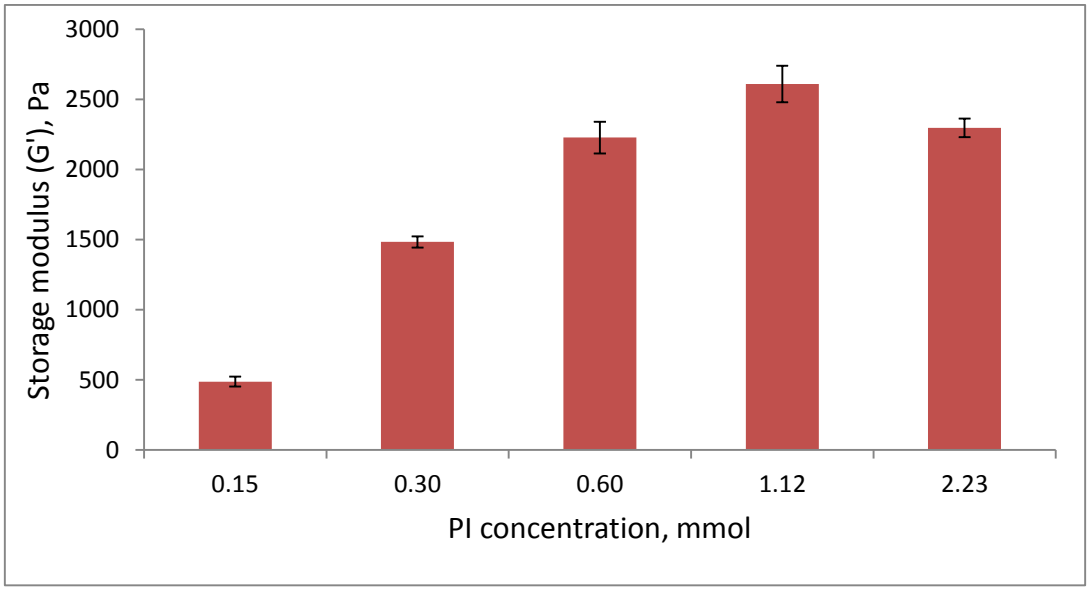

Fig.51: Maximum of storage modulus G' of reaction mixtures of GelMOD 5% with different concentrations of Li-TPO-L.

As it can be good seen from the Figures 51 and 52, the storage modulus, G', increases with an increasing concentration of Li-TPO. Again, this happens because the more PI content presents in the reaction mixture, the more free-radicals can be produced during the UV-light absorption, which leads to the most dense, cross-linked hydrogel formation. However, as one can see from the Figure 51, the maximal Li-TPO concentration of 2.23 mM/L does not fit to the general tendency of storage modulus elevation with elevation of PI concentration. This phenomenon can be easily explained: the highest PI concentration results in a too fast formation of many radicals, which undergo recombination process, probably also resulting in a short-chained polymers formation, which hinder the cross-linking of a hydrogel and makes reaction incomplete, which decreases the stiffness of the whole formed hydrogel.

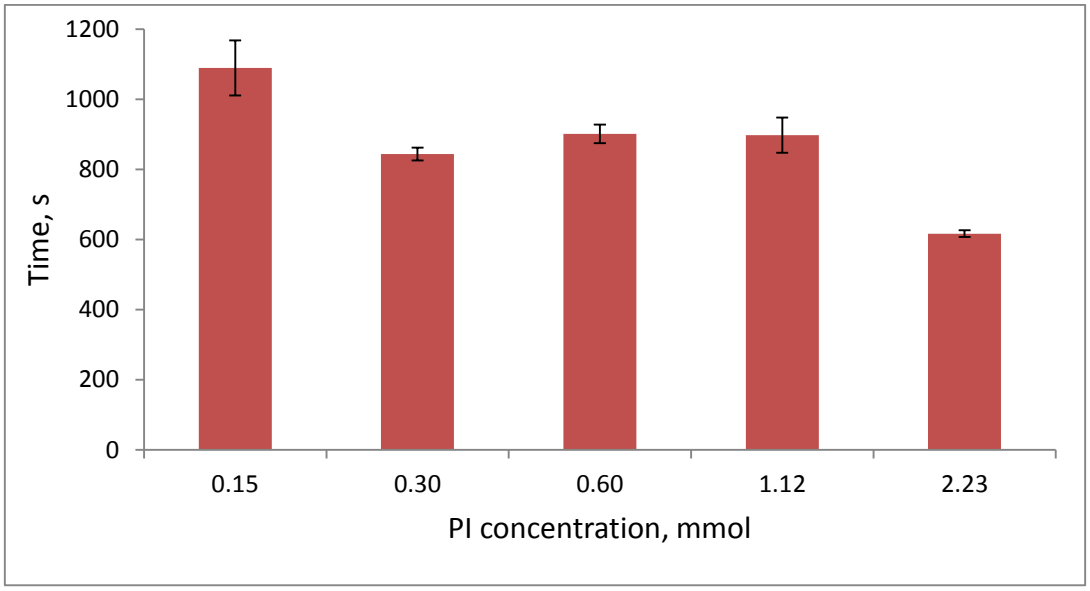

Fig.52: Time after which 95% of the maximum value of G' are reached in reaction mixtures of GelMOD 5% with different Li-TPO concentrations.

The fastest increase of a storage modulus and consequently the highest reactivity gives the reaction mixture with concentration of PI Li-TPO 2.23 mM/L, as it can be seen in Fig. 52.

Interestingly, the concentration of PI 0.3 mM/L does not fit to the general line, showing the smaller time of reaching 95% of G', as it can be good seen in the Figure 52. A possible explanation of this phenomena can be, that PI concentration of 0.3 mM/L is the edge concentration, where further evaluation of PI concentration leads to the possible formation of mono-reacted products, which leads to a little evaluation of the storage modulus, but also to decrease of mobility of the formed network, and therefore, an incompletely reached value of G'.

Another important observation is the gel-points shift phenomena in reaction mixtures with different concentrations of PI. It was interesting to find out, if in case of our reaction mixtures there is a certain dependence of the gel-points from concentration of PI and if it is so, then how this dependence looks like.

A point of gelation can be easily observed and calculated during the measurements: it is nothing else, but the point, where the value of storage modulus, G', becomes bigger, than a value of loss modulus, G". This intersection point represents a point of gelation of the sample.

Unfortunately, for reaction mixtures with 5% macromere concentration, it was impossible to determine the gel-points. The only exception were reaction mixtures with GelMOD (DS: 70%) 5% and Li-TPO 0.6 mM/L and 0.3 mM/L with gel-points at 47 s and 80 s respectively. Therefore, the concentration of macromere was elevated to 20%.

For this purpose 5 mixtures with different concentrations of Li-TPO were prepared and the increase of the storage, G', and loss, G", moduli were measured during irradiation with UV light. The reaction mixtures for this experiment were calculated with a constant content of GelMOD (DS: 70%) 20% and different concentrations of Li-TPO, listed in Table 8 below.

Table 8: PI concentration range in analyzed reaction mixtures

Sample name	PI concentration [mM/L]
GelMOD20%-LiTPO-0.075	0.075
GelMOD20%-LiTPO-0.15	0.15
GelMOD20%-LiTPO-0.3	0.3
GelMOD20%-LiTPO-0.6	0.6
GelMOD20%-LiTPO-2.23	2.23

Interestingly, the lowest PI concentration of 0.075 mM/L, which could not be analyzed with 5% of GelMOD (DS: 70%) content, could be analyzed by elevation of GelMOD (DS: 70%) content to 20%. Explanation of this phenomenon can be that in case of a very low concentrations of both PI and polymer in reaction mixtures are not enough to start the chain reaction, while evaluation of the macromere content in reaction mixture enables slow propagation of photochemical cross-linking reaction between the macromere chains and radicals, even if the radicals are very few.

In all previous sections the maximum value of the storage modulus, time to reach 95% of G'max, and the values of delay and slope had to be determined. Here, however, only that part of a photorheological curve, where the intersection point of G' and G" can be seen, is in the focus of our interest. Therefore, the gel-points of each reaction mixture were measured and depicted on a diagram, see Figure 53.

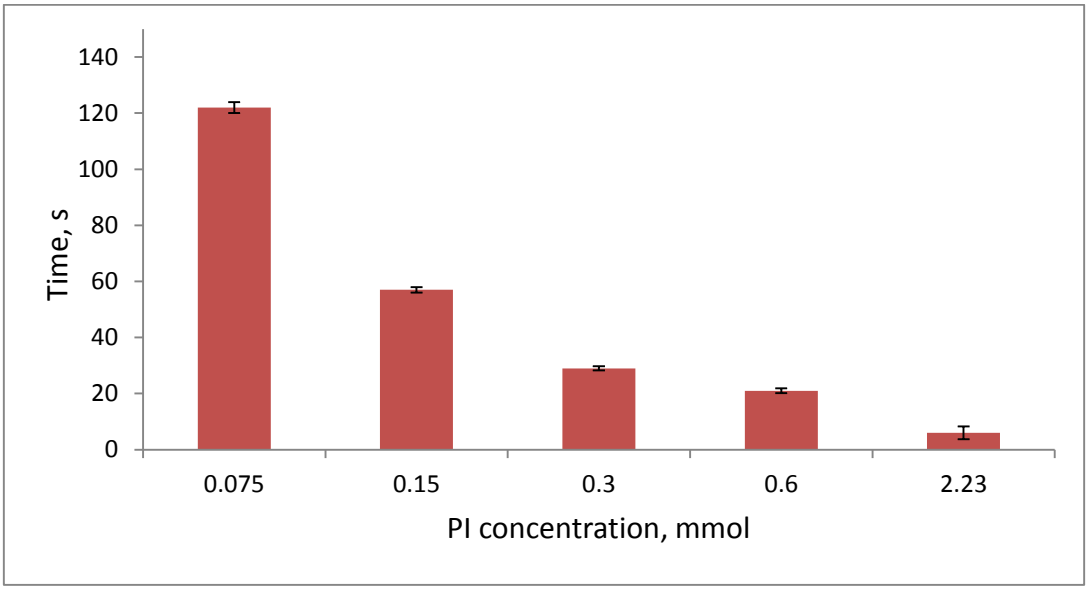

Fig.53: Gel-points shift diagram.

From the Figure 53 one sees, that the reaction mixture with a highest concentration of Li-TPO of 2.23 mM/L results in a fastest gelation of a reaction mixture, while the lowest concentration of Li-TPO-L of 0.075 mM/L leads to the slowest gelation process: in the first case gelation begins already at 6 s after the light irradiation begun, in the last case the gelation starts only after 122 s.

Therefore, from the conducted experiment, it can be concluded, that the higher concentration of PI in the reaction mixture is, the quicker gelation process is then induced.

4.5 Influence of macromere concentration

In order to distinguish the influence of macromere concentration on the properties of produced hydrogels, results obtained in the previous section (see Section 4.4) from reaction mixtures with 5% and 20% of macromere content were compared. As before, the maximum value of storage modulus G'max, time after which 95% of the maximum value of G'max are reached, slope, delay of initiation and the points of gelation were compared for each reaction mixture. The experimental data are depicted in the Table 9 below.

Table 9: Results, obtained from mixtures for establishing the influence of macromere concentration

Sample	Delay, s	Slope, $Pa*s^{-1}$	Time of 95%G'max, s	G'max, kPa	Gel-point, s
GelMOD5LiTPO-0.15	214	1	1070	0.5	-
GelMOD5LiTPO-0.3	112	4	824	1.5	80
GelMOD5LiTPO-0.6	61	8	882	2.2	47
GelMOD5LiTPO-2.23	23	18	597	2.3	-
GelMOD20LiTPO-0.15	200	32	930	20	57
GelMOD20LiTPO-0.3	110	130	670	33	29
GelMOD20LiTPO-0.6	54	285	720	72	21
GelMOD20LiTPO-2.23	17	680	315	78	6

As it can be good seen from the Table 9, some of the characteristics of reaction mixtures are influenced a lot by macromere concentration. Delay of initiation of reaction mixtures with 5% macromere content is not much higher than the delay of initiation of reaction mixtures with 20% macromere content, moreover, the tendency of decrease of delay with decreasing PI concentration is preserved in both cases. Slope values are strongly effected: for reaction mixtures with 20% macromere content, slope is incomparably greater. The slope for reaction mixture with 5% macromere content and minimal PI concentration (0.15 mM/L) is 1, whereas in case of 20% macromere content (PI also 0.15 mM/L), it is already 32. For the highest PI concentration (2.23 mM/L) for reaction mixture with 5% macromere slope value is 18 and for 20% already 680 $Pa*s^{-1}$. Time to reach 95% of G'max is also effected, but not as much as slope and it decreases with increasing PI concentration for both 5% and 20% reaction mixtures. G'max depends strongly on macromere concentration: reaction mixture with 5% macromere content and a maximal PI concentration (2.23 mM/L) gives 2.3 kPa, while reaction mixture with 20% macromere content and a maximal PI concentration (2.23 mM/L) gives 78 kPa, which is incomparable greater. Last but not least, gelation begins much more faster in case of reaction mixtures with 20% macromere content: gel-point in case of PI concentration 0.6 mM/L by 20%

macromere concentration comes at 21 s, by 5% macromere concentration only at 47 s, in case of PI concentration 0.3 mM/L by 20% macromere concentration at 29 s, by 5% macromere concentration only at 80 s. According to the obtained data, one can conclude, that the properties of the hydrogels strongly depend on the macromere concentration: the higher macromere concentration results in a faster gelation process and production of more dense cross-linked hydrogels.

4.6 Selection of the optimal formulation

The work, being undertaken in this section was aimed to distinguish the optimal experimental conditions and optimal formulation of reaction mixture for formation of hydrogel layers for our work.

Through conducted experiments it was discovered, that produced hydrogel layers undergo drying process and for prevention of it mineral oil is required. It was demonstrated, that the hydrogel layers do not possess a required mechanical stability, needed for the following experiments. A good solution of this problem was an enhancement of transportability and mechanical stability of the hydrogel layers with functionalized glass slides, which serve as a required support. It was shown, that GelMOD compound degrades with time, which can play a crucial role in our experiments. Finally, the best PI Li-TPO was selected due to its better characteristics compared to commercially used IG2959. Li-TPO possesses the better solubility in water, which is essential in our work, because the hydrogel layers were produced to be in contact with live cell culture, where water is the main solvent. Li-TPO showed the higher efficiency than IG2959, which was demonstrated on the UV-VIS absorption spectra, where both PIs were compared. At last, due to the higher efficiency, the required concentration of Li-TPO is 0.6 mM/L instead of 2.23 mM/L in case of IG2959. The cytotoxicity tests demonstrated that this concentration of Li-TPO is not dangerous for the cell culture. Therefore, the final formulation of our reaction mixture for production of the hydrogel layers is 5% of GelMOD (DS: 70%) as a polymeric content and 0.6 mM/L solution of Li-TPO as a PI content.

4.7 Double-bonds conversion

During UV exposure the chemical cross-linking of polymer chains of GelMOD proceeds via reaction of double bonds (DBs) in methacrylamide side groups. FTIR (Fourier transform infrared) Spectroscopy is a technique, which allows one to measure the amount of DBs in reaction mixture before exposure to UV-light and the amount of DBs remained after the photochemical cross-linking completed. Having these data, one can estimate the extent of photochemical cross-linking reaction. Photorheology, combined with FTIR Spectroscopy, enables ‘in real-time’ monitoring of UV-curing by measurement of double-bonds conversion (DBC) during the whole cross-linking process, and at the same time, measurement of the standard parameters, like maximum value of storage modulus G’, time to reach 95% of maximum value of G’, slope of the storage modulus in the linear region and delay of initiation.

Experiments for estimation of DBC were performed for reaction mixtures, calculated to 5% of GelMOD (DS: 70%) as a polymeric content and 0.6 mM/L solution of Li-TPO as a PI content. The measurements were performed as usual photorheological measurements, conducted in previous experiments, only this time the FTIR Spectrometer operated with experimental set-up.

The signals (or peaks) determining DBs on the IR spectrum can be seen in the regions: 6170, 3100, 1640, 1450 and 810 cm^{-1}. As long as water, which was used as a solvent in all previous experiments, has a very strong absorption in all these regions, first of all, it was necessary to choose a proper solvent for reaction mixtures. Heavy water (D_2O) was examined as a second possible solvent. Therefore, two spectra of pure H_2O and D_2O were measured at first and the result is depicted on the Figure 54 below.

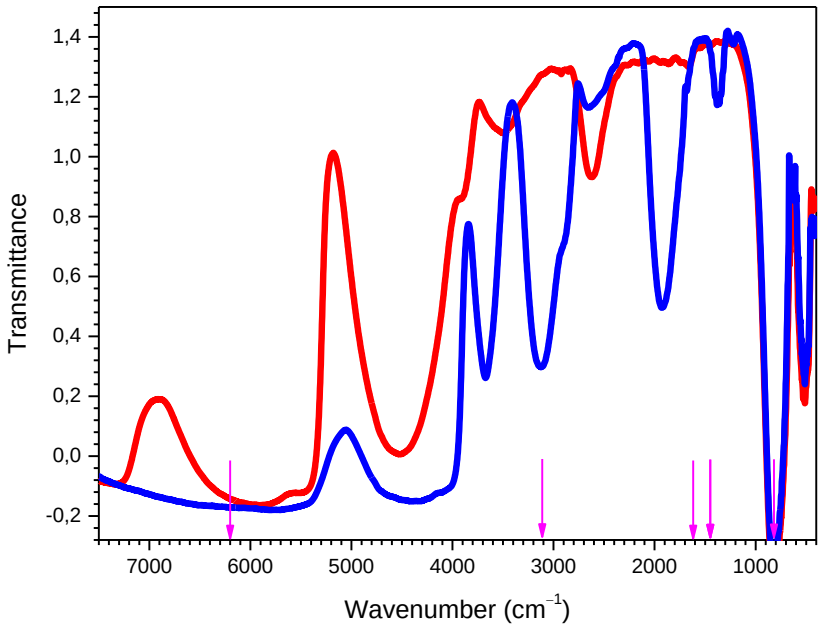

Fig. 54: IR-spectra of water (red) and D_2O (blue). With pink arrows are the areas marked, where one can see the peaks of double-bonds in hydrogels.

It can be clearly seen from the Figure 54, that in both cases (H_2O and D_2O) the absorption in all regions is too high to see any of the DBs signals, except for 6170 cm^{-1} wavelength. D_2O possesses, however, a lower absorption than H_2O at 6170 cm^{-1}, therefore reaction mixture with D_2O was prepared. Measurements were carried out as usually and the results are given below.

From the obtained spectra no DBs signal at 6170 cm^{-1} could be seen, as it is shown on the Figure 55.

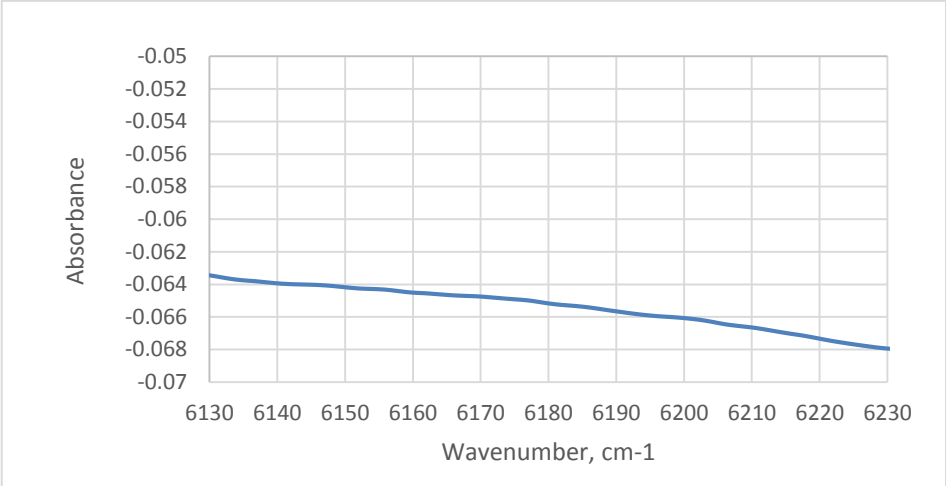

Fig.55: FTIR spectrum obtained from reaction mixture GelMOD (DS: 70%) 5%, Li-TPO-L 0.6 mM/L in D_2O.

It was decided, that the absence of peak in the expected area is due to the low concentration of polymeric component in the reaction mixture, because the amount of DBs depends on the amount of polymeric content. Therefore, concentration of GelMOD was increased from 5% to 20% for the next reaction mixture. Reaction mixture was calculated for 20% of GelMOD (DS: 70%) as a polymeric content and Li-TPO as a PI in concentration of 0.6 mM/L in heavy water (D_2O). However, even for this elevated concentration of GelMOD, the DBs peak could not be observed as well.

It was decided then to measure a reference reaction mixture with already well-studied PEGDA, which also contains DBs (see Figure 56), as a polymeric component.

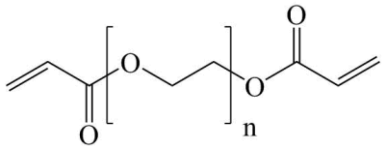

Fig.56: Chemical structure of PEGDA molecule.

Measurement of reaction mixture with polymeric content of 50% PEGDA (M=700 Da) and PI content of 0.2% IG2959 gave well-defined peak in the expected area of 6170 cm^{-1}, as it can be seen from the spectrum on the Figure 57 below.

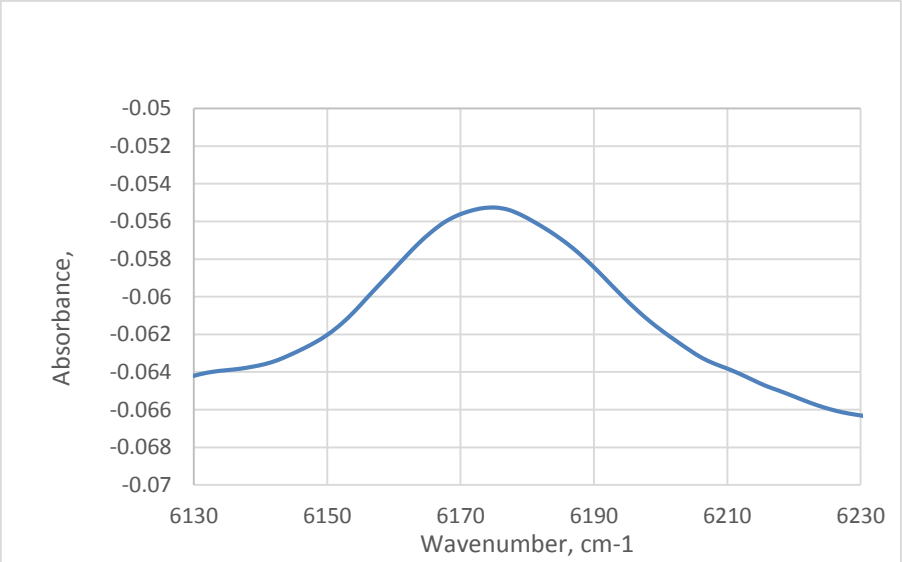

Fig.57: FTIR spectrum obtained from reaction mixture PEGDA (M=700 Da) 50%, IG2959 9 mM/L in D_2O.

Another reference sample was prepared with a lower concentration of PEGDA (M=700 Da) 20%, IG2959 9 mM/L in H_2O and measured. DBs signal at 6170 cm^{-1}could be observed in this case also. Spectra of both reference samples with PEGDA concentrations of 20% (in H_2O) and 50% (in D_2O) are depicted on the Figure 58 below.

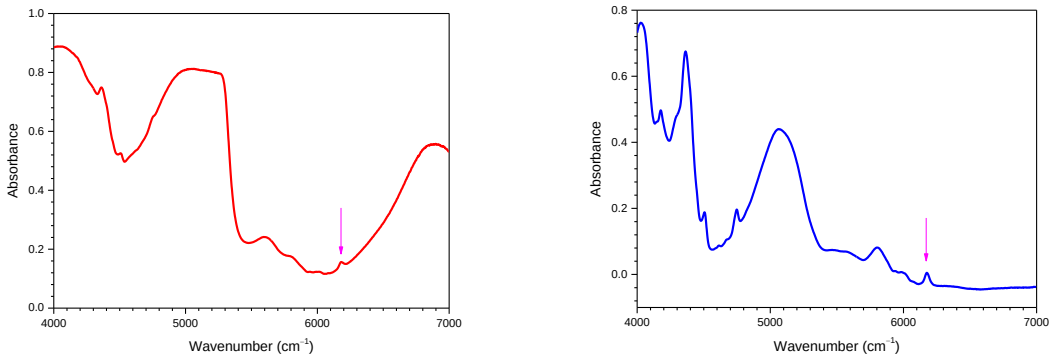

Fig.58: FTIR-spectra of 20% PEGDA (M=700 Da), IG2959 9mM/L in water (left) and 50% PEGDA (M=700 Da), IG2959 9 mM/L in D_2O (right).

One sees from the spectra on the Figure 58, that the peak at 6170 cm^{-1} can be better defined if the measurement is done in heavy water, then in water, because of a lower absorbance of heavy water in this region. Via interconnected photorheometer DB conversion, maximum value of storage modulus G', time to reach 95% of the maximum value of G', slope of the storage modulus in the linear region and the delay of initiation were measured for PEGDA sample. The resulting curves are depicted on the Figure 59 and the values in the Table 1.

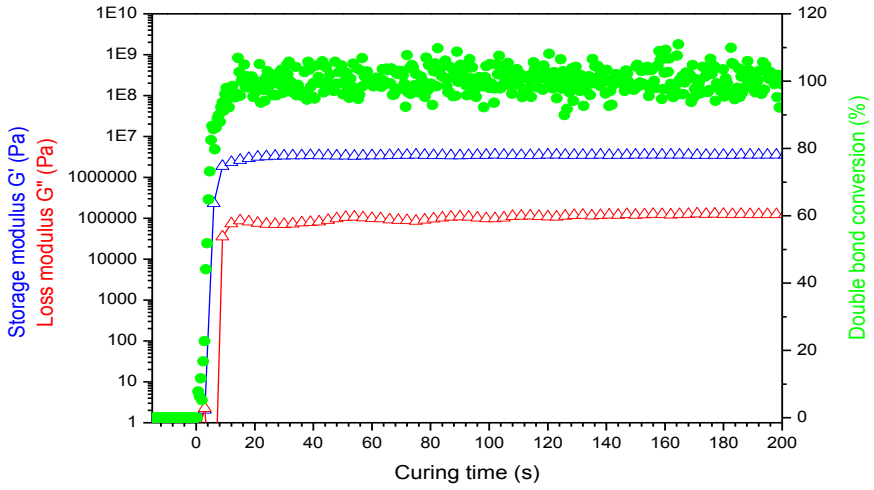

Fig.59: Curves, obtained by combined FTIR-Photorheometry: storage (blue) and loss (red) moduli, and DBC curve (green).

One can see from the Figure 59, that the DBC reached 100%, which indicates a full conversion of DBs in the PEGDA reaction mixture by the end of the cross-linking reaction.

As long as in the NIR region no DBs could be seen by observing the reaction mixture with GelMOD (DS: 70) 20%, our area of interest shifted to the MID-IR region (1640 cm^{-1}), where another signal from DBs can be observed. As long as both H_2O and D_2O have a very strong absorption, overlapping all other signals in this region, a new more proper solvent was required. The IR spectra of DMF, DMSO and DMSO-d6 were measured at first and are depicted below on the Figure 60.

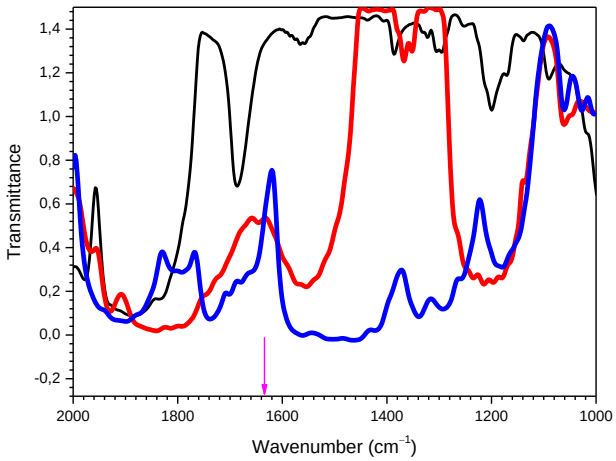

Fig.60: IR-Spektra of DMF (black), DMSO (red) and DMSO-d6 (blue). Rose arrow is for the region where we expect to see the DB signal.

As one can see from the Figure 60 above, DMF cannot be used, because the absorption in MID-IR region is too high. The less absorbance in desired region was detected by DMSO-d6, therefore it was chosen as a next solvent for further experiments.

'In real-time' DBC measurements were performed for two reaction mixtures: GelMOD (DS: 70%) 20%, Li-TPO 0.6 mM/L and PEGDA (700 Da) 10%, 9 mM/L IG2959. For both reaction mixtures DMSO-d6 was used as a solvent. Again, no DB peak could be observed for GelMOD sample, while DBC for PEGDA was successfully measured and the resulting spectra are shown on the Figure 61 below.

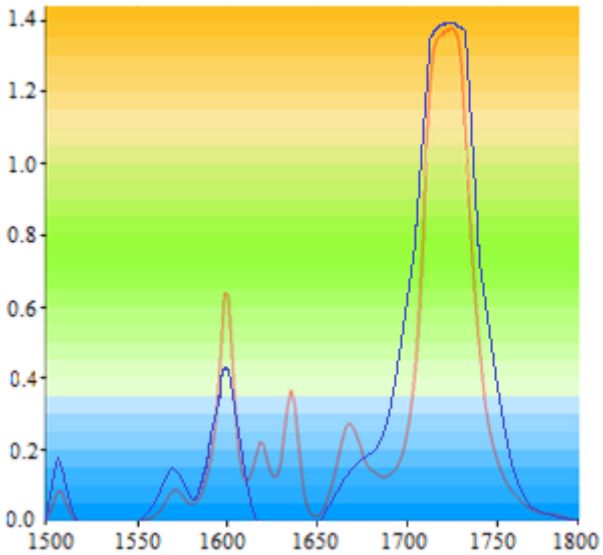

Fig.61: Monitoring of UV-curing by real-time FTIR-photorheology, PEGDA 10% with IG2959 9 mM/L in DMSO-d6.

Figure 61 demonstrates two time-points of the same cross-linking reaction for PEGDA sample: the beginning (red line) and the end (blue line) of reaction. On the red spectrum from Figure 61 the double-peak at 1630-1640 cm^{-1} can be observed, which disappears on the blue spectrum, indicating that the DBs were consumed during hydrogel formation. Again, maximum value of storage modulus G', time to reach 95% of the maximum value of G', slope of the storage modulus in the linear region and the delay of initiation were calculated for PEGDA sample. The curves, indicating DBC, storage and loss moduli are depicted below on the Figure 62.

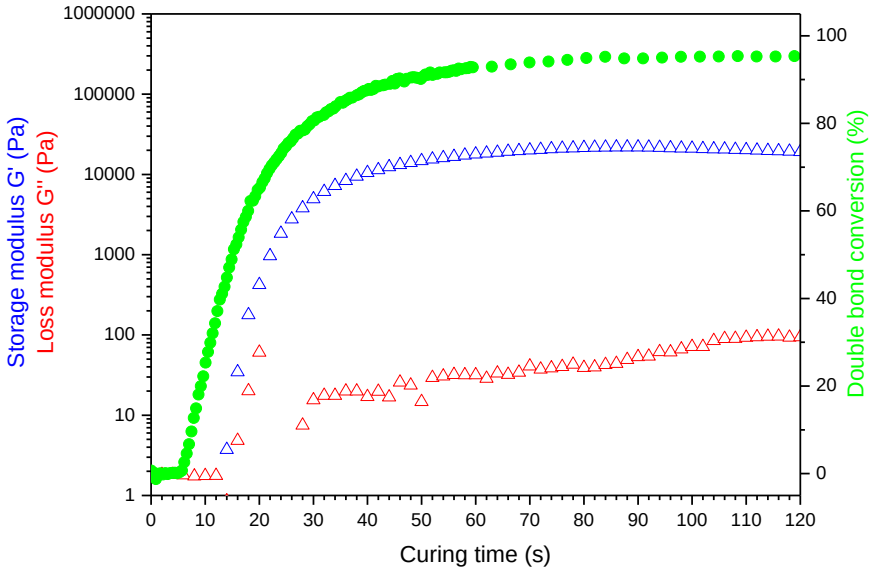

Fig.62: Curves, obtained by combined FTIR-Photorheometry: storage (blue) and loss (red) moduli, and DBC curve (green) for PEGDA 10% with 9 mM/L IG2959 in DMSO-d6.

As one can see from the Figure 62, DBC reached 97%, which indicates, that the cross-linking process was completed. All data, regarded to mechanical properties and reactivity of GelMOD and PEGDA reaction mixtures are given in the Table 10.

In order to find out why no DBs could be seen in any of examined GelMOD reaction mixtures, the calculations of DBs concentration in the mixtures: GelMOD (DS: 70%) 20% with Li-TPO 0.6 mM/L and PEGDA 20% and 50% with IG2959 9 mM/L were made. The results shown, that concentration of DBs in reaction mixture with 20% of GelMOD is 0.048 mol/L, while in reaction mixture with 20% of PEGDA it is 0.57 mol/L, which is almost 12 time greater. Concentration of DBs in reaction mixture with 50% of PEGDA is 1.43 mol/L, which is 30 times greater, than in reaction mixture with 20% GelMOD. Therefore, it can be concluded, that the absence of DB signals in reaction mixtures with GelMOD was due to the small concentration of DBs in those mixtures. However, it should be possible to measure DBC via combined FTIR-photorheology method, but only if the concentration of polymeric content (GelMOD concentration) will be elevated to the relevant values. Unfortunately, due to the time-frames established for this work, it was not possible to achieve here.

Table 10: Data, obtained by photorheometry measurements of GelMOD and PEGDA mixtures

Sample	Delay, s	Slope, $Pa*s^{-1}$	Time of 95%G'max, s	G'max, kPa
GelMOD5%_LiTPO_0.6	62	8	890	2.2
GelMOD20%_LiTPO_0.6	54	285	720	72
PEGDA10%_IG2959_9	12	2.3	79	23
PEGDA20%_IG2959_9	7	178	55	1820
PEGDA50%_IG2959_9	3	327	47	3700

From conducted experiments, one can conclude, that concentration of polymeric content, just as concentration of PI, also plays a crucial role: by increasing the GelMOD concentration from 5 to 20%, reaction starts earlier: delay of initiation decreases from 62 to 54 s. The same can be said about the second mixture: rising concentration of PEGDA (10, 20 and 50%) has a very strong influence on initiation of cross-linking – in the mixture with the highest (50%) PEGDA concentration it starts already within 3 seconds, whereas by 20% and 10% of PEGDA in 7 and 12 seconds, respectively. Reactivity of the systems is also polymer concentration-depndent: slope of the curves rises with rising concentration of polymeric content in both mixtures. For GelMOD by elevation of its concentration in reaction mixture from 5% to 20%, slope rises from 8 to 285 $Pa*s^{-1}$ and in case of PEGDA from 2.3 to 178 and 327 $Pa*s^{-1}$ by elevation of PEGDA content from 10% to 20% and 50% respectively. It must be admitted, that it takes longer time to reach 95% of G'max by GelMOD reaction mixture, then by PEGDA: already by 10%-concentrated solution of PEGDA, 95% of G'max is reached in 79 s and this value decreases to 47 s by its highest concentration of 50%. In case of GelMOD, 5%-concentrated solution reaches 95% of G'max only in 890 s and by 20% concentration of GelMOD in reaction mixture by 720 s, which indicates, that UV-curing process of reaction mixtures with GelMOD takes much longer, than in case of PEGDA. This phenomena can be simply explained: PEGDA possess a much higher cross-linking density, then GelMOD. The maximum value of G'max again, rises with rising concentration of polymer in reaction mixture: for GelMOD it evaluates from 2.2 kPa in 5%-concentrated solution to 72 kPa in 20%-concentrated solution and for PEGDA from 23 to 1820 and to 3700 kPa respectively in 10, 20 and 50%-concentrated solutions. Such difference in G'max values between GelMOD and PEGDA is, again, due to a greater cross-linking density of PEGDA hydrogel. The whole tendency is predictable, and can be explained in the similar way as in the previous chapter, where the same parameters of reaction mixtures were changed in the same way, but with increase of PI content: the higher amount of polymeric content in the reaction mixture results in the higher amount of DBs, which, first of all, faster undergo photo-induced radical polymerization, and secondly, results in formation of much more stiffer hydrogel. From obtained data, it can be established, that:

- mechanical properties and reactivity of GelMOD reaction mixtures are strongly dependent on polymer concentration and rise with its evaluation;
- mechanical properties and reactivity of PEGDA reaction mixtures are strongly dependent on polymer concentration and also rise with its evaluation;

- in general, hydrogels, produced from PEGDA exceed those, made of GelMOD in terms of initiation of cross-linking, reaction speed and hardness of final hydrogel material: the maximum value of G' for reaction mixture with 20% of GelMOD is 72 kPa, while for PEGDA of the same concentration it is already 1820 kPa and for PEGDA 50% 3700 kPa, which is incomparably higher. This fact again, supports our speculation about the higher concentration of DBs in PEGDA, than in GelMOD, because only with higher amount of DBs it is possible to produce more dense network from cross-linked polymeric chains and a harder hydrogel, respectively.

However, relying on conducted experiments, one can estimate for sure that from both reaction mixtures the higher reactivity has PEGDA reaction mixture: 95% of G'max is reached faster than in case of reaction mixture with GelMOD. For comparison, the value of 95% of G'max for GelMOD20% with LiTPO 0.6 mM/L is 720 s, while for PEGDA20% with IG2959 9 mM/L it is only 55 s. However, the concentration of IG2959 was much more greater (9 mM/L), than concentration of Li-TPO (0.6 mM/L), therefore, in order to compare GelMOD and PEGDA, one has to conduct experiments, using the same PI in the same concentrations for both reaction mixtures, which was not the direct aim of the present work, since our first interest was focused on measurement of DBs conversion during the cross-linking process of GelMOD.

4.8 Swellability

One of the important properties of hydrogel materials is swellability. Upon entering of a solvent into a polymer network of a hydrogel, the polymer chains have to stretch, which results in an opposite process: relaxation of the polymer chains to their initial state. Therefore, it will be an equilibrium reached between two confronting processes of swelling and relaxation. The swollen hydrogel can uptake only a certain amount of water, regarding to the equilibrium, and mechanical properties of the swollen hydrogel will be no more the same as those of non-swollen hydrogel.

Since produced hydrogel samples will be later treated in water-based environment, which is life-necessary for living cells, it was important to discover the swelling behaviour of hydrogel samples.

Reaction mixtures for determination of the swellability of hydrogels, produced from GelMOD were calculated to the established formulation of 5% of GelMOD (DS: 70%) as a polymeric content and 0.6 mM/L solution of Li-TPO as a PI content. At first, the measurements were performed as usual photorheological measurements, conducted in previous chapters. After, the produced hydrogelic samples were transferred into petri dishes and soaked in 2 mL of phosphate-buffered saline (PBS) and kept in the fridge for 24 h, afterwards measured on the photorheometer again with the same measuring parameters and instrument settings (see the corresponding experimental section). The experiment was made with 7 repetitions. As usually, standard parameters were measured: the values of delay, slope, time to reach 95% of G'max and G'max and are shown in the Table11 below.

Table11: Data, obtained by photorheological measurements of GelMOD (DS: 70%) 5%, Li-TPO 0.6 mM/L mixtures for investigation of the swellability of produced hydrogels.

Sample	G'max, kPa
GelMOD5%_LiTPO_0.6_nsw	2.2
GelMOD5%_LiTPO_0.6_sw	0.26

According to obtained data, the resulting value of G'max of the swollen sample is 0.26 kPa, which is 8.5 times less than G'max of the non-swollen sample, which is 2.2 kPa. Such drop in the stiffness of the hydrogel layer is due to swelling of PBS solution, which makes the material much softer, than a new-made non-swollen. The conducted experiment aims to predict the real stiffness of a hydrogel, when it will be immersed in a water-based cell media for further cell experiments. This is very important, because the cells are extremely sensitive to the stiffness of material, and will behave in accordance to it. Therefore, for reliability of obtained data, it is necessary to know exactly the value of stiffness of the hydrogel.

5 Multiphoton grafting

The structures for tissue engineering and, in particularly, for tissue regeneration, are aimed to mimic and replace (constantly or temporary) the natural cell matrix – extracellular matrix (ECM). As long as ECM possesses a very complex geometrical structure, it is important to find a technique, which could produce artificial structures of comparable architecture. Not only structural complexity of ECM, but also its biochemical environment plays a crucial role: ECM is not only a supportive carcase for cells, but also a mean of transport system, which is responsible for delivery of biochemical signals, nutrients and waste products. Being in a constant 'dialogue' with the cells, ECM regulates tissue function by regulating cells differentiation, proliferation and death, whereas the cells are able to rebuild ECM on demand. This is exactly the factor, which determines an inability of the most ECM-modelling techniques to mimic the natural ECM structure. Moreover, in order to perform systematic studies on cell culture, scaffolds have to be created in a reproducible manner, which is also difficult to achieve, using standard methods, such as phase separation, particulate leaching, gas foaming and numerous soft-chemistry approaches.

The aim of this work was not creation of scaffolds for tissue engineering. We wanted to enable observation of hydrogel matrix deformations induced by the cells. For this purpose it was decided to create a fluorescent grid on the hydrogel layer, which could be seen under laser scanning microscopy (LSM) due to its fluorescence. When cells, seeded on the top of such hydrogel will start to deform it, the grid will also be deformed. Observing the deformations of a fluorescent grid, it is possible to estimate the deformations of a hydrogel itself. However, to achieve it, a special technique, which will allow to create a stable fluorescent grid pattern on a hydrogel layer in a precise manner, with good spatial resolution and with high reproducibility was required.

Multiphoton grafting (MPG), which rises from a group of technologies, based on one working principle and named multiphoton processing (MPP) is exactly the technological platform, which fulfills all above mentioned criteria. In a work of A. Ovsianikov *et al.* it was demonstrated that MPG is capable to functionalize the matrices with high spatial resolution in 3D. As it was shown in recent studies, MPG is able to immobilize a single molecule into the matrix material.

MPG utilizes a laser irradiation to induce the multiphoton absorption of photoactive compound, or a grafting agent (GA). The selection criteria for GAs are planar π-conjugated systems, which contain a strong donor and/or acceptor groups. Commonly used compounds are aromatic azides, which are, however, potentially toxic to the living cells. When a GA absorbs a laser irradiation, its N-N bond dissociates and nitrogen and highly reactive electron-deficient nitrene species are formed. The formed nitrene intermediate inserts into the C-H bond of the matrix compound. The latest fact speaks about a potential of MPG to be applied for a very wide variety of matrices, containing C-H bonds. The main benefit of MPG is that this reaction takes place only in the focal spot of a laser beam. By moving the laser beam one can record a desired pattern.

5.1 Selection of a water-soluble grafting agent

As long as our samples are later to be applied for the living cells, where water is a natural medium, water-soluble GAs for creation of 2D fluorescent grids on hydrogel layers, are preferential. However, the first GA used in our work was an insoluble in water, reactive aromatic azide, 2,6-bis(4-diazidobenzylidene)-4-methylcyclohexanone (BAC-M), see Fig. 63.

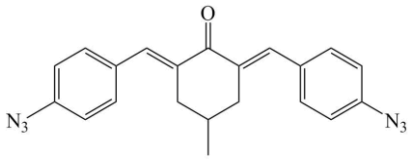

Fig. 63: Chemical structures of BAC-M molecule.

BAC-M was an only one available GA for multiphoton grafting experiment, which was already successfully applied in a work of A. Ovsianikov for selective functionalization of 3D PEG-based matrices.

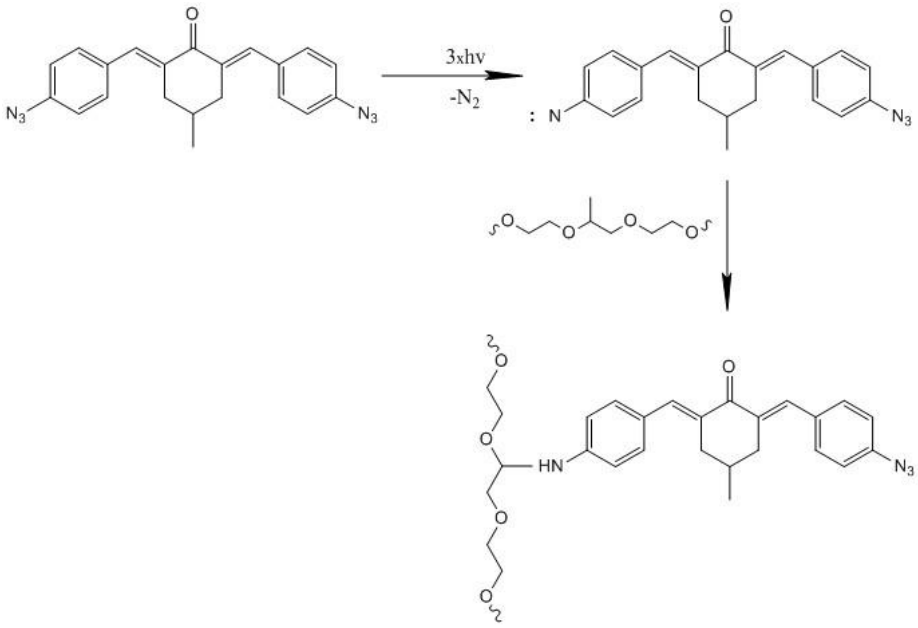

Fig.64: Photolysis reaction of BAC-M, followed by insertion reactions within the PEG sample.

On the Figure 64 the photolysis reaction of BAC-M, used for its immobilization into the matrix compound is depicted. As it was demonstrated in the work of A. Ovsianikov *et al.*, after grafting, either one or both azide groups of BAC-M were covalently linked to the matrix. In both cases the grafting products contain the ketocyanine chromophore, which exhibits strong fluorescence, which allowed to observe the grafted patterns via laser-scanning microscopy (LSM).

As long as in this work we pursued the same aim of being able to observe the grafted patterns under LSM, and also because BAC-M demonstrated good results in the work of Ovsianikov *et al.*, our first attempts were made with BAC-M. The problem of insolubility of BAC-M caused

an additional step to be performed in the whole procedure, namely a solvents exchange: firstly, before being grafted hydrogel layers were soaked in DMF with BAC-M, dissolved in it. After the grafting procedure being performed, the solvent was replaced with PBS for further experiments in cell-culture lab. The problem, automatically related to this procedure was how good the sample has been washed from the solvent. DMF is very toxic to the cells and even the minimal quantity of it can be deadly for the cells, placed on the hydrogel sample. That is why a solvent exchange procedure was very precise and time-consuming.

This problem, however, vanished after switching to another GA, which can be easily dissolved in water, 4, 4'-diazo-2, 2'-stilbenedisulfonic acid disodium salt tetrahydrate, see Figure 65. With this water-soluble salt a solvent-exchange step can be excluded and the whole procedure is significantly simplified.

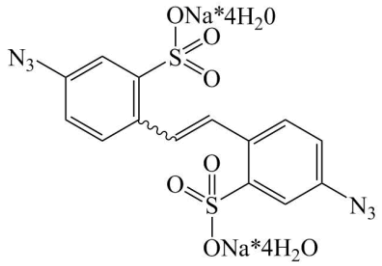

Fig.65: Chemical structure of 4, 4'-diazo-2, 2'-stilbenedisulfonic acid disodium salt tetrahydrate.

The photolysis reaction of the new GA follows the classical principle of photolysis of an aromatic azide and is depicted on the Figure 66 below.

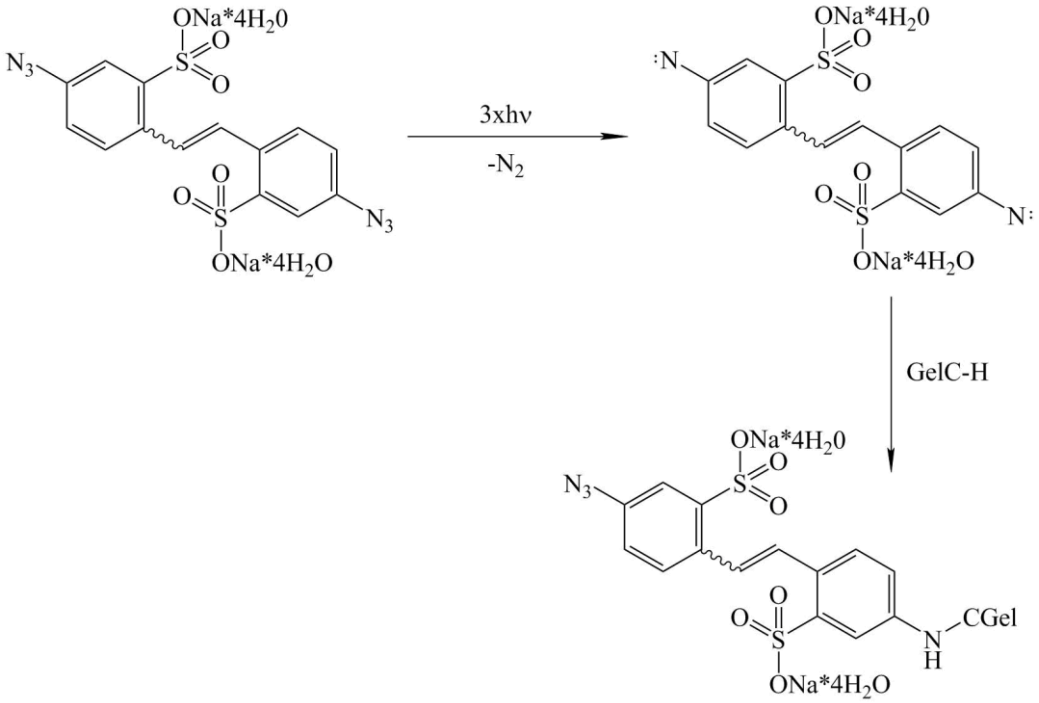

Fig.66: Photolysis reaction of BAC-M, followed by insertion reaction into the GelMOD structure.

Like in the case of BAC-M, the 4, 4'-diazo-2, 2'-stilbenedisulfonic acid disodium salt tetrahydrate can also react with azide groups from both sides, giving a strong fluorescence when observed via LSM, as it will be shown in the following experiments.

5.2 Evaluation of cytotoxicity of GA

As it was already discussed in a previous chapter, all aromatic azides are potentially toxic to the cell culture. Therefore, it was necessary to evaluate the cytotoxicity of 4, 4'-diazo-2, 2'-stilbenedisulfonic acid disodium salt tetrahydrate, which was used as a GA for MPG procedure, and also to estimate the optimal concentration, which will not be dangerous for the cells. All cytotoxicity tests, performed in this chapter were carried out by M. Markovic from the cell biology department.

The toxicity of 4, 4'-diazo-2, 2'-stilbenedisulfonic acid disodium salt tetrahydrate was tested with the L929 and MC3T3 cell lines according to the Presto Blue cell viability reagent protocol. For this purpose different concentrations of 4, 4'-diazo-2, 2'-stilbenedisulfonic acid disodium salt tetrahydrate were dissolved in Alpha Minimum Essential Medium (α-MEM, Thermo Fisher Scientific) with serum proteins.

A detailed explanation of the assay is described in Experimental Section. The sample solutions were put on the cells and left for 24h. Then the medium was exchanged and the fluorescence dye Presto Blue (PB) reagent was added and left for 1h. After 1 hour of incubation the fluorescence was measured in order to count the living cells. All substances were analyzed with 8 repetitions.

The cell counting is based on the metabolic reduction of the Presto Blue dye by living cells. When cells are viable, they maintain a reducing environment within their cytosol. The reduced dye exhibits fluorescence, which is measured by a plate reader and gives quantitative information proportional to the number of living cells.

Upon entering a living cell, Presto Blue reagent is reduced from resazurin, a blue compound with no intrinsic fluorescent value, to resorufin which is red in colour and highly fluorescent. This conversion is proportional to the number of metabolically active cells and therefore can be measured quantitatively.

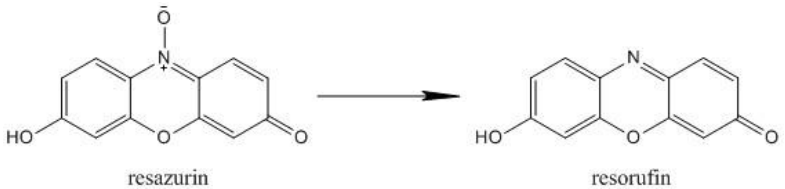

Fig. 67: Reduction of the dye in the Presto Blue assay by the reducing environment of the viable cell.

Figure 67 demonstrates the reaction of resazurin (the dye in the Presto Blue assay) to the fluorescence dye resorufin. Resazurin is a blue dye with no intrinsic fluorescence value, while

resorufin is red coloured and exhibits strong fluorescence at 586 nm, as it can be seen from the Figure 68.

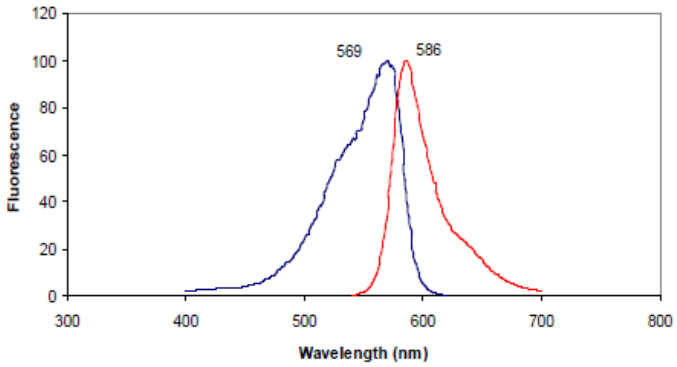

Fig.68: Reduction of Presto blue reagent: Excitation (blue) and emission (red) peaks for resorufin to measure fluorescence values.

The GA, 4, 4'-diazo-2, 2'-stilbenedisulfonic acid disodium salt tetrahydrate, as an aromatic azide, is toxic for the cells. However, one can minimize its toxic effect by choosing the right concentration. Via conducted cytotoxicity tests the optimal concentration can be found.

The effect of GA on cell metabolic activity was tested at the following dilutions of 20, 10, 5, 2.5, 1.25, 0.6, and 0.3 mM/L GA in medium. The experiment was performed in absolute darkness. Observed values were compared to the control samples, which were cells untreated with PI: a positive control (10% Presto Blue and 90% medium). As a negative control the highest possible concentration of GA of 20 mM/L was used. The results of the tests are depicted on Figure 69 below.

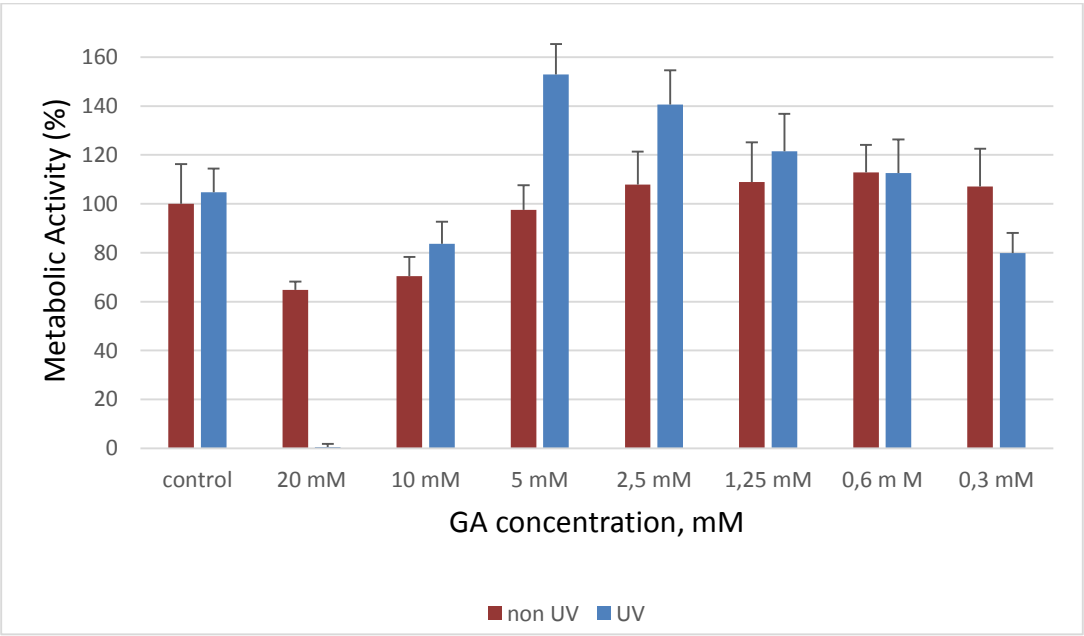

Fig. 69: Influence of different concentrations of GA on metabolic activity of L929 after 24 h and exposed/not exposed to UV light (PrestoBlue Cell Viability assay).

Figure 69 demonstrates the results of cytotoxicity test for the cell line L929 after 24h exposure to the GA. All values are presented as % of positive untreated with GA or UV light control sample, which was assumed to be 100%. As one can see from the Figure 69, the highest concentration of GA solution of 20 mM/L was deadly for the cells: there was no cell metabolic activity detected by this concentration after exposure to UV light. The lower concentration of 10 mM/L gives questionable results. Quite unusual observations were made with GA concentrations below 10 mM/L. As one can see from the Figure 69, such GA concentrations were not only less toxic to the cells, but even induced the cell metabolic activity with and also without UV-light. The highest metabolic activity of the cells was observed in samples with 5 and 2.5 mM/L concentration of PI. By lowest concentration of 0.3 mM/L, however, metabolic activity was again decreased after exposure to UV-light.

As it was previously mentioned, the toxicity tests were also performed for another cell line, MC3T3. Concentrations of GA solutions were the same. Positive control was performed as before. As long as the cytotoxicity tests were already performed for a PI IG2959, mentioned in a previous section, and it is already well-known how the cells will react to IG2959 at 2.23 mM/L concentration, for control of a process a reference sample, IG2959 2.23 mM/L was taken. The results of the test are shown below.

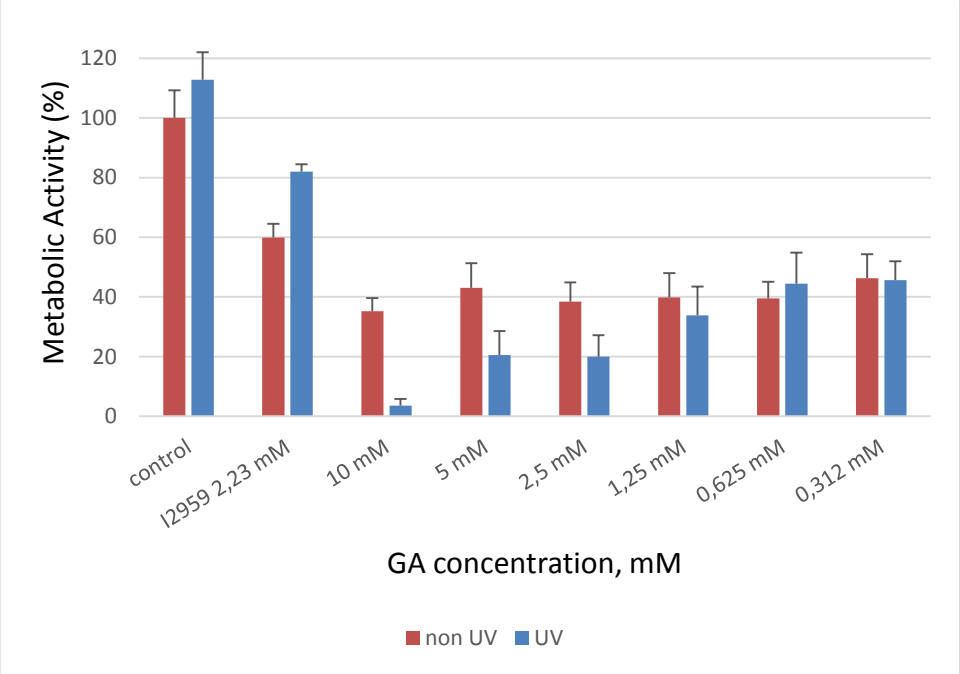

Fig.70: Influence of different concentrations of GA on metabolic activity of MC3T3-E1cell line after 24 h and exposed/not exposed to UV light (Presto Blue Cell Viability assay).

From the Figure 70 one can see, that reaction of MC3T3 cell line on the same GA was totally different. Almost no cell metabolic activity was observed by GA concentration of 10 mM/L, after irradiation with UV light, which was not critical for L929 cell line in the previous test. High toxicity without UV light was observed in all other samples with lower GA concentrations. With UV light 5 and 2.5 mM/L concentrations were toxic for cells. Lower concentrations of 1.25, 0.6 and 0.3 mM/L gave stable results with UV light.

From conducted experiment, we estimated the optimal concentration 2 mM/L of 4, 4'-diazo-2, 2'-stilbenedisulfonic acid disodium salt tetrahydrate, which is not dangerous for the cell cultureand will be used in all following experiments. Moreover, it was discovered, on the example of L929 and MC3T3-E1 cell lines, that different cell lines react differently on the same GA.

5.3 Determination of processing window

By using a MPG procedure, one has a very wide range of parameters, which can be adjusted to once need: laser power, laser writing speed, architecture of the desirable structure itself, and many others. In MP processes and MPG in subcase, all these parameters can be varied over the broad range still resulting in well-shaped structures. This broad range is known as a processing window. The broader processing windows are, the wider is diapason of adjustable parameters.

It is well-known, that the size of a processing window strongly depends on reactivity of the reactants, effectivity and concentration of grafting agent (GA), macromere concentration and also by limitations of the experimental set-up itself. However, in our work, the optimal concentrations of both components are determined rather by the needs of living cells. Therefore, concentration of GA, for example, cannot go beyond the toxicity limit, because otherwise it would be dangerous for the cells. For that reason, in our work only parameters of the MPG apparatus will be changed in order to determine the best processing window for our experiments. As it was demonstrated in a work of Zhiquan *et al.* [101], the fluorescence intensity of produced MPG patterns, which indicates the level of immobilization, is correlated with both laser power and scanning speed. Higher laser power combined with lower scanning speed provides more energy in the excited focal volume to produce 'brighter' patterns, where immobilization density is higher. Therefore, the immobilization density can be controlled via changing the laser intensity or exposure time, i.e. writing speed.

For determination of processing windows 11 samples were prepared. Hydrogel layers, produced on the photorheometer had the following constitution: 5% of GelMOD (DS: 70%) as a polymeric component, 0.6 mM/L Li-TPO as a PI. As it was previously described, reaction mixture was cross-linked via UV-light from the light source of the photorheometer directly on the functionalized glass slides. The glass slides were functionalized before being used in cross-linking procedure, as it was already discussed in a previous section. Functionalization of the glass slides was necessary because otherwise too weak adhesion of a hydrogel layer results in its slipping from the surface of a glass slide.

Prepared samples were put in the apparatus for MPG and the grids were printed on the top of the hydrogel layer with a laser power of 40 mW and the maximal writing speed of 555mm*s^{-1}. The grids had a square shape with a side of 200 µm and a hatch distance in 2 µm.

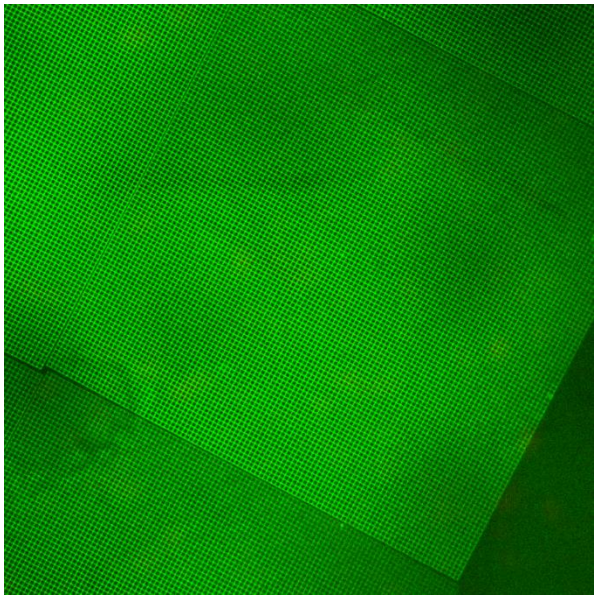

Fig. 71: LSM image of produced fluorescent grid.

Figure 71 demonstrates the LSM image of the fluorescent squared grids, produced via MPG process. This example shows that the structures produced via MPG possess a good shape and very precise microtopography.

First of all, it was necessary to distinguish the optimal laser power. For this reason an array of several grids was made, where the laser power varied from the maximum possible value to the minimum possible value, the writing speed was maximal in all cases. The maximum power of the laser set-up used in our experiments is 100 mW, which appeared to be too high for hydrogel samples, because the laser beam burned the holes inside of them. The first value, by which the laser beam did not damage the samples, was 40 mW, therefore all values, which exceeded this threshold were excluded. After being grafted the samples were washed several times in PBS before being analyzed under a LSM. Washing procedure is necessary because the residuals of GA must be removed before the analysis, otherwise the fluorescence of the remaining GA would overlap the fluorescence from the grids. Because of the fluorescence overlapping taking pictures with the LSM will be difficult.

For analyzing the samples under the LSM it was necessary to remove them from the petri-dishes and put them into a special samples holder, see Figure 72, because the plastic bottom of the petri-dish disturbs the observation. As it can be seen, the sample holder does not have any bottom and the grafted hydrogel layer can be observed directly through the glass slide, on which it is adhered.

Fig. 72: Image of the sample holder: left – in the assembled condition, right – in the disassembled condition.

Figure 72 demonstrates the sample holder made from stainless steel. After analysis with the LSM, one could observe an array of the well-shaped grids. All of them had the same structure, differing only in brightness and sharpness of the pattern, see Figure73.

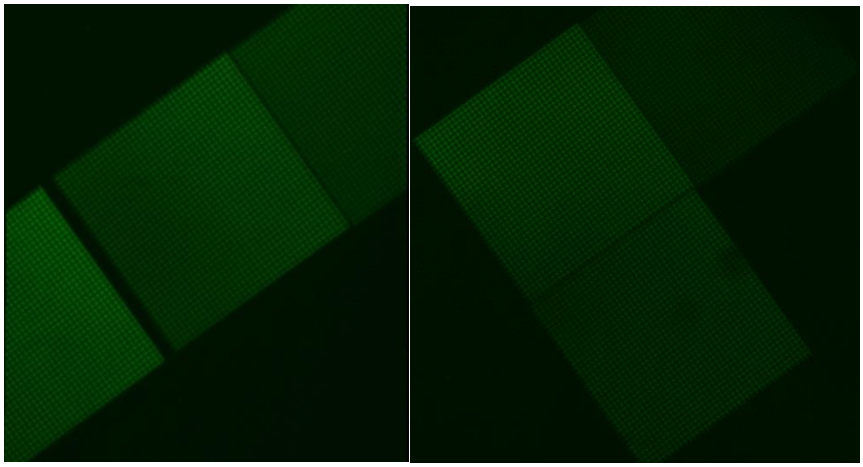

Fig.73: Images of fluorescent grids, produced with different laser-power. Left: first grid (from the left) by 40mW, second by 30mW, third 15mW; right: first (from the bottom) by 20mW, second (in the middle) by 30mW and third (up) 10mW.

Figure 73 demonstrates how the brightness of the grids changes with varying the laser power from 40 mW to 10 mW. The most bright and sharp grids were made with the higher laser power, the most indistinct images were taken from the grids created with a lower laser power. Obviously, the more power has a laser beam, the more fluorescent molecules it can bind to the hydrogel compound.

For analysis and selection of a suitable laser power parameter, the fluorescence intensities of produced grids were measured via another LSM option, see Fig.74, and compared.

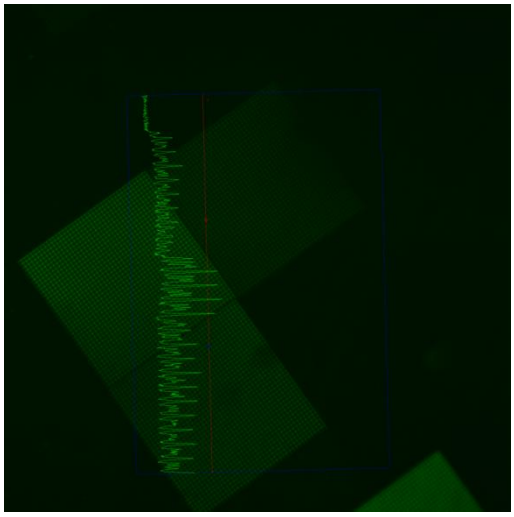

Fig.74: LSM image, showing the comparative fluorescence intensity of three grids, produced with different laser powers: first (from the bottom) by 20mW, second (in the middle) by 30mW and third (up) 10mW.

The dependence of the fluorescence intensity from the laser power is depicted as a diagram on the Fig.75 below. The vertical axis is made in logarithmic scale.

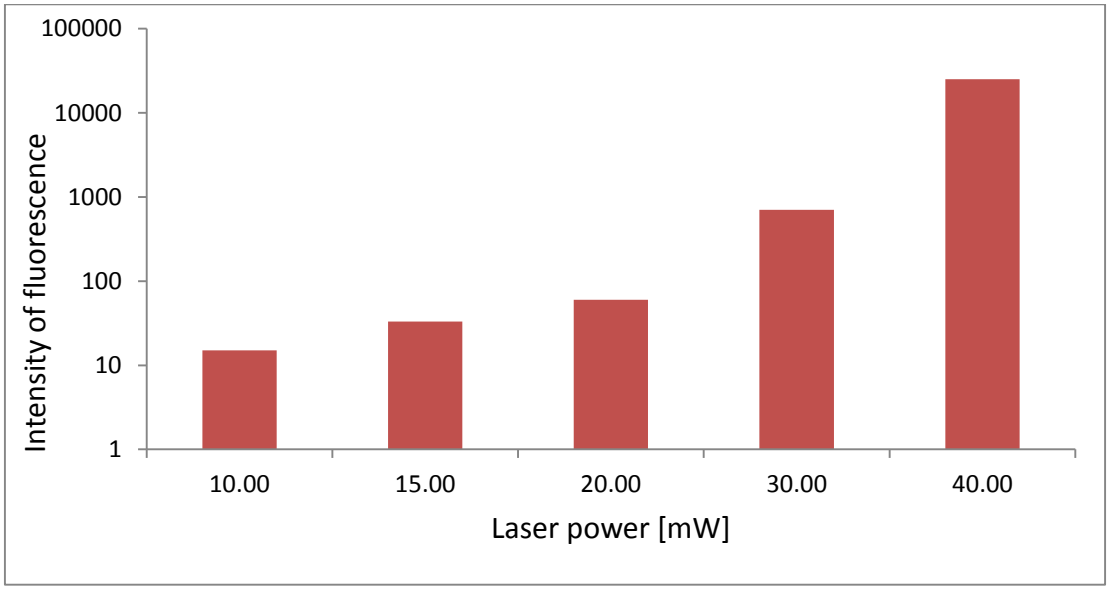

Fig.75: Diagram, showing dependence of an intensity of fluorescence from laser power.

In spite of the fact, that all observed laser powers (not exceeding 40 mW) resulted in well-shaped grids, which could be all good seen under LSM, based on the obtained results, the laser power in 20 mW was chosen as the optimal one. This laser power was enough for imagining the fluorescent structures with LSM obtaining good images of grids and at the same time there was no threat of destroying the hydrogel by this value of laser beam power.

5.4 Changing the hatch distance in a fluorescent grid

For the following biological experiments it was also interesting to find out if the hatch distance of the fluorescent grid has any influence on the visualization of the deformation of the hydrogel layer. For that reason 2 samples were prepared with the following formulation: GelMOD (DS: 70%) 5% as a polymeric content and Li-TPO 0.6 mM/L as a PI content. The hydrogels were attached to the functionalized glass slides as it was discussed in a previous section. The hydrogels were grafted with laser power of 20 mW and maximal writing speed. Grids with different hatch distances were created: 2 and 5 µm correspondingly. Produced grids are demonstrated on Figures 76 and 77.

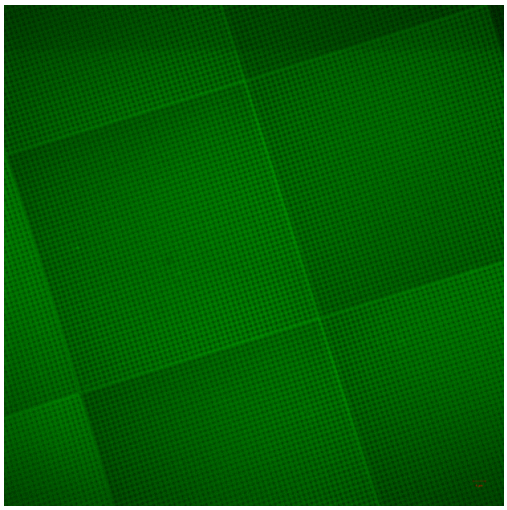

Fig.76: LSM images of the fluorescent grid with 2 µm hatch distance**.**

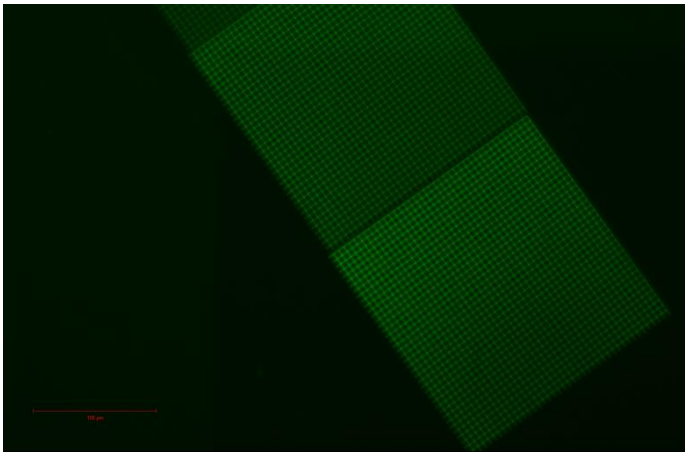

Fig.77: LSM images of the fluorescent grid with 5 µm hatch distance**.**

After the cells seeding procedure it must be clear which hatch distance is more appropriate for our investigations. When the cells will start to deform the fluorescent pattern of the grid, these deformations could be better seen on the grids with a broader hatch distance, rather than with the narrow hatch distance.

5.5 Changing the distance from the surface of hydrogel

It was interesting to find out how deep into the hydrogel material the cell can integrate. Theoretically, if the fluorescent grids will be created on the different heights, or in other words on the different distances from the surface of hydrogel material, the cell will start to deform those of grids, which are situated on the same distance from the surface as the cell itself. Using this rather rough analysis one can see how deep the cell has penetrated into the hydrogel material. This becomes possible by driving the focus of a laser beam deeper into the sample.

In order to check this speculation, five grids with the same parameters were created on the different distances from the surface of the hydrogel layer: one on the surface, and others 3, 5, 7 and 10 µm deep in the hydrogel material. All hydrogel layers had, as usually, the following formulation: GelMOD (DS: 70%) with 5% polymeric content and 0.6 mM/L PI Li-TPO. As usually the hydrogels were attached to the surface of functionalized glass slides and grafted according to the previously described procedure. Figure 78 demonstrates the LSM images of produced grids.

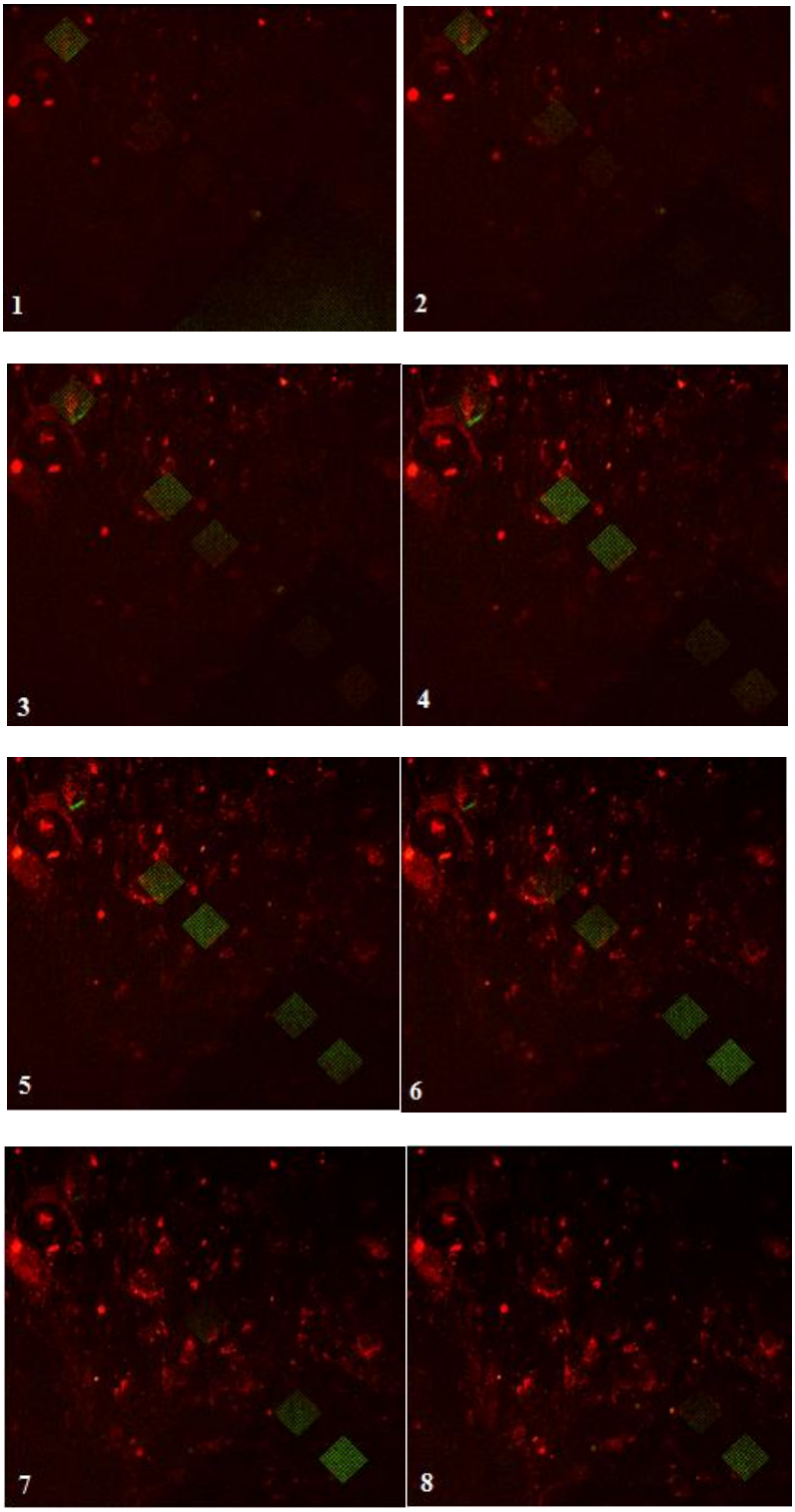

Fig.78: LSM images of five grids, grafted on different depths in the hydrogel layer: 1) - 2) grid on the top of the hydrogel layer; 3) - 4) second grid in the raw from top 3 µm deep; 5) third grid in the raw from top 5µm deep; 6) - 7) fourth grid in the raw from the top 7 µm deep; 8) the last visible grid in the raw 10 µm deep.

On the Figure 78 one can see the arrangement of the fluorescent grids: each following grid goes deeper into the hydrogel material than the previous one and the images of those grids, which are situated closely to the surface disappears as long as one observes the deeper layers

of material. Theoretically, if the cells will go deeper into the hydrogel material, they will deform only those grids, which are situated on the same depth as a cell. Knowing which grid is deformed and knowing its depth, we can say where exactly the cell is and how deep in the hydrogel it is.

6 Cell seeding

The final stage of our investigations was seeding of the grafted samples with living cells. For this purpose, there is a cells seeding procedure. The seeding procedure, like the cytotoxicity tests, discussed in the previous section, were provided by M. Markovic from the cell biology department.

6.1 Cell seeding procedure

The cells seeding procedure was carried out in a cell culture laboratory under the sterile flow hood, in order to prevent any contamination of the samples. Five previously grafted samples were washed with sterile PBS several times, then placed in sterile petri dishes and seeded with MC3T3-E1 subclone 4 preosteoblast type cells. The MC3T3-E1 subclone 4 line was grown in alpha-Minimum Essential Media – α-MEM (Thermo Fisher Scientific). Seeded hydrogel samples were left in the incubator by 37°C for three days.

If not otherwise mentioned, all manipulations with the samples with living cells were done under the sterile flow hood and the basic medium was α-MEM.

In our work we used MC3T3-E1 Subclone 4preosteoblast cells, because they are a good model for studying in vitro osteoblast differentiation, particularly extracellular matrix (ECM) signaling. They are also able to form ECM.

When observing some of samples with a light microscope, a yeast contamination was distinguished. The presence of such contaminations can be dangerous for the cell culture. In order to prevent yeast or bacterial contamination, all surfaces and tools with which the samples are in contact during the whole production procedure were periodically sprayed with isopropanol: also during photorheometry and multiphoton grafting (MPG) stages of the samples creation.

6.2. Life-dead staining procedure

After three days of incubating the five samples, prepared in Section 6.1 must be observed under LSM in order to check cell viability. For making the cells visible for laser scanning microscopy (LSM), one uses life-dead staining procedure. For this purpose, the live/dead viability assay was performed. Staining solution consists of Calcein AM (live stain) and propidium iodide (dead stain), which exhibit fluorescence, making cells visible under LSM, see Figures 79, 80.

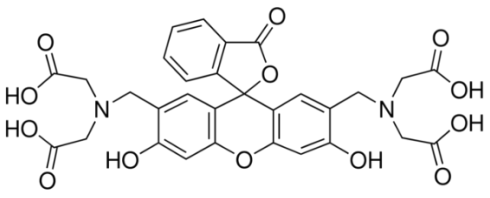

Fig.79: Chemical formula of calcein, used for life-dead staining.

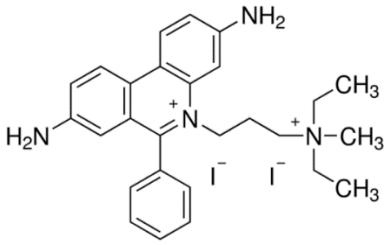

Fig.80: Chemical structure of propidiumiodide, used for life-dead staining.

After being stained, the samples were transferred into the sample holders and imaged using LSM. The cells, which are live have green fluorescence and the cells, which are dead have red fluorescence if observed under the LSM, as it can be seen on Figure 81 below.

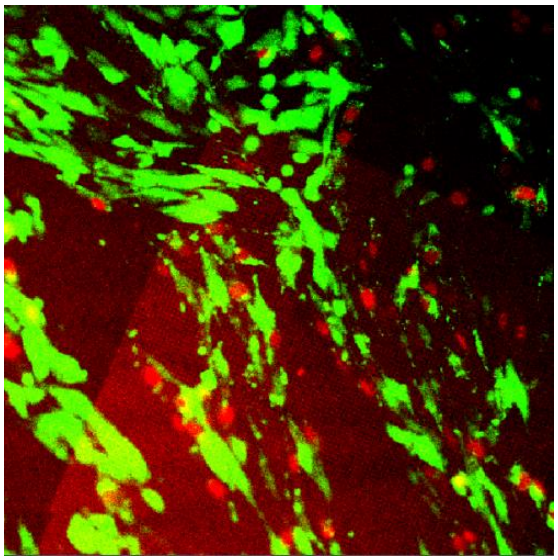

Fig.81: LSM image of the live (green) and dead (red) cells on the red fluorescent grids.

Figure 81 shows the LSM image of the cells on the top of the gel layer with a grid, which is stained red, on it. Living cells are stained green and dead cells red.

After LSM observation, the samples were again transferred into the sterile petri-dishes, PBS was exchanged with α-MEM and then the samples were put back to the cell culture incubator for further observations.

6.3 Integration of cells into the hydrogel layer

In order to see any deformations of the fluorescent grid, five samples, described in Section 6.2 were observed via LSM for the second time. The preparation procedure of the samples for LSM observations was carried out as usually. Obtained LSM image is demonstrated on the Figure 82, where the live cells stained green can be seen sitting on the grid, which is stained red.

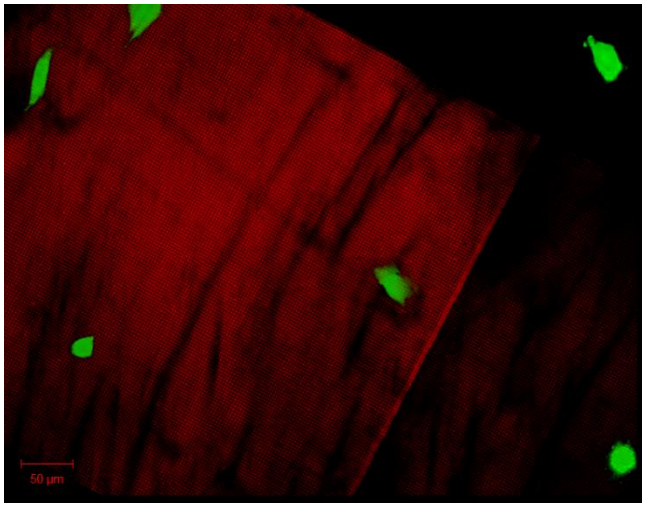

Fig.82: LSM image of live cells on the top of the hydrogel matrix with fluorescent grid on the second day.

With a higher magnification one can see that some of the cells integrated into the hydrogel, because one can see the cell from both sides of the fluorescent grid (also behind it), like it is demonstrated on Figure 83, 84.

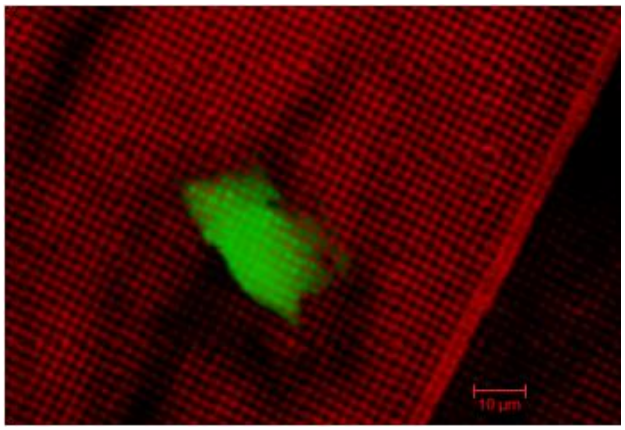

Fig. 83: LSM image of a single cell, integrated through the fluorescent grid with a hatch distance of 2 µm, observed with higher magnification.

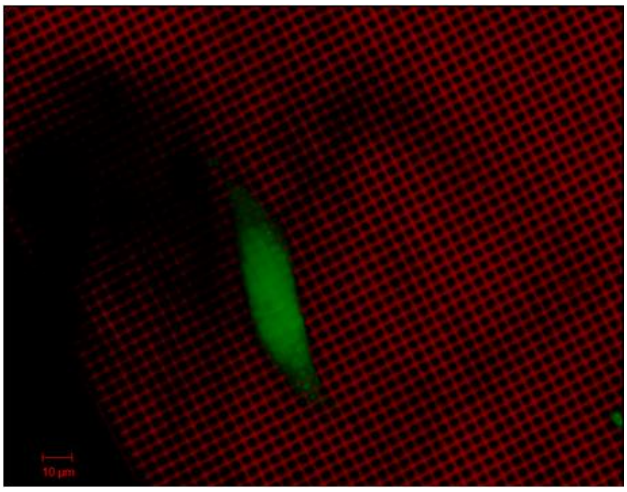

Fig.84: LSM image of a single cell on a fluorescent grid with a hatch distance of 5 µm, integrated into the hydrogel layer, observed with a higher magnification.

From the images above one can make a conclusion, that not only sit on the top of the fluorescent grid, but already on a second day the cells start to integrate into the hydrogel layer, which demonstrates that not only the samples are cell-friendly, but also that they have a potential for enabling constant high-quality observations of the cells life and fate.

Another option, which gives the LSM set-up is a creation of a 3D-images of a sample, a so-called z-stack. A z-stack image, where two single cells, sitting on the fluorescent grid, can be very good seen, see Fig. 85.

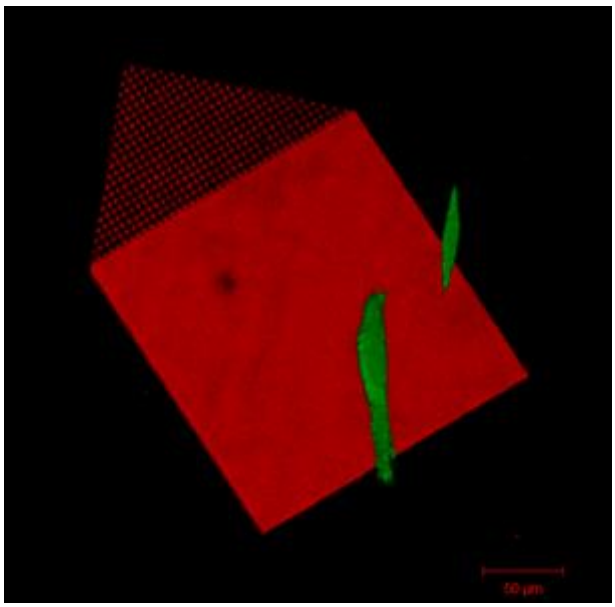

Fig.85: LSM z-stack image of two single cells, sitting on the fluorescent gridon the hydrogel layer.

6.4 Stability of the samples

Unfortunately, it was impossible to observe the samples, described in Section 6.3 once more under the LSM, because the hydrogel layer was slipping from the glass slide. The experiments were made with many repetitions, but not a single sample was stable already after the second day of observations.

As it was already established in this work, the hydrogel layers have a relatively strong adhesion to the functionalized glass slides and even locating in petri-dishes with PBS in a fridge for long periods, e.g. four till five weeks, could not lead to destruction of the samples. As long, as on this stage of the samples production they remained stable, it must be something in the following procedure, which causes destruction of the samples. The first possible cause is α-MEM cell-culture media, as long as it can be aggressive environment for the hydrogel material. Second one is an elevated temperature: all samples with cell cultures are placed in the incubator, where the temperature of 37°C is held all the time. The last possible reason for samples destruction is the cell culture: as long as cells live and proliferate, their metabolic activity could create the aggressive environment, or the cells could partially degrade the hydrogel material.

In order to find it out, there were 9 samples made. All of them were identical and produced via previously discussed procedure. 3 samples were put in sterile petri-dishes with only α-MEM alone and left in the fridge, 3 samples were put in sterile petri-dishes withα-MEM and transferred into the incubator, and 3 samples were put in sterile petri-dishes withα-MEM, seeded with cells and transferred into the incubator. After six days 9 samples were examined and the hydrodel layers on all of them were still firmly fixed to the glass slides. Subsequently, it must have been another reason why the samples were destroyed after being measured under the LSM.

Obviously, a lot of manipulations with the samples such as: daily exchanging of the cell media, washing the cells after each LSM observation, transferring them into the sample holders for LSM and after back into sterile petri dishes became the reason of detachment of the hydrogel layer from the surface of the functionalized glass slide. Therefore, because of mechanical instability of the samples by transportation, washing, changing media and other ordinary manipulations, it was impossible to observe the samples longer than two days. Such a short time of observations was definitely not enough for detecting any deformation of the fluorescent grid.

Experimental

2 Evaluation of monomer formulation

2.1 Hydrogel matrix

2.2 Support for hydrogel

Before starting the activation procedure, glass slides were at first cleaned in a Plasma-Cleaner, PDC-002 (230 V), Harrick Plasma. For this, 30 mm in diameter and 1.5 microns thick glass slides were put into a slide holder, see Figure 86, and then installed into the plasma-cleaner. After ignition of a plasma discharge, the slide holder with glass slides was held in the plasma-cleaner for 15 min.

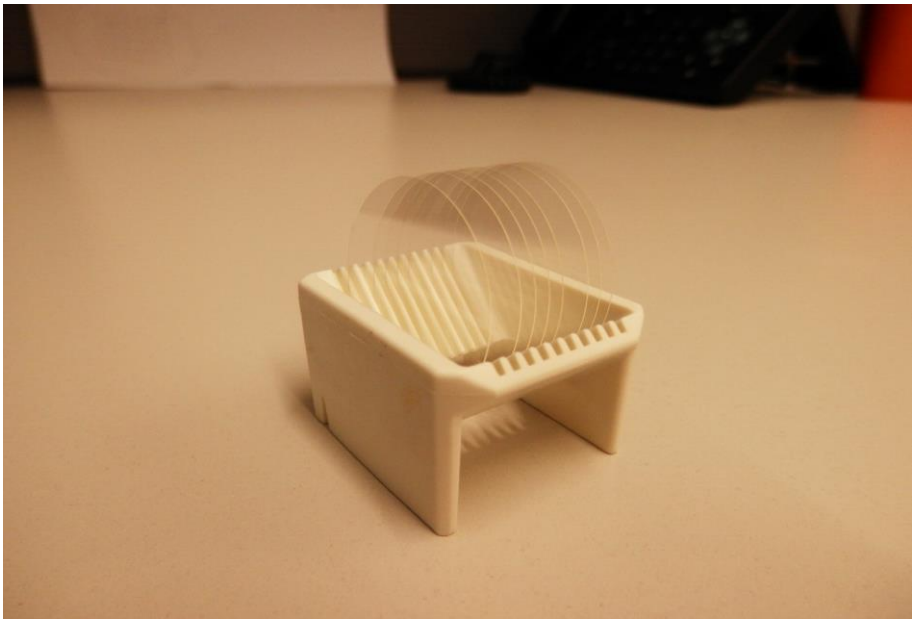

Fig.86: Image of a glass-holder with glass slides.

After the plasma-cleaning procedure, the glass slides were exposed to the activation procedure.

Chemical	M [g/mol]	V [ml]	n [mmol]	m [mg]
Trimethoxysilyl propyl methacrylate	248.35	2	8.42	2090
Ethanol	46	48	823	37858
Acetic acid	600	5.25	315	189000
Water	18	50	2778	50000

The silanization solution was prepared as following: in a 100 mL beaker with magnetic stirrer, 50 mL of deionized water was mixed with 48 ml of ethanol (Aldrich, CAS: 64-17-5, 98%, absolute) and 0.3 mL of acetic acid (Aldrich, CAS: 64-19-7, 99.7%). After that 2 ml of trimethoxysilyl propyl methacrylate (Aldrich, CAS: 2530-85-0, 98%), were slowly added dropwise to the solution and the reaction mixture then was stirred in a beaker for half an hour by room temperature. After being cleaned in a Plasma-Cleaner, glass slides with the glass-holder were put into the 100 mL beaker with silanization solution and magnetic stirrer and stirred for 15 minutes at room temperature. After that the glass holder with glass slides was taken from the beaker with the forceps and washed several times with deionized water. After that the glass slides in a holder were post-baked in a pre-heated convection oven by 110°C during half an hour.

3 Photoinitiator for Hydrogel

3.1 Selection of photoinitiator

3.2 Cytotoxicity of photoinitiator

MC3T3-E1 subclone 4 preosteoblast type cells were cultivated in alpha-Minimum Essential Media (α-MEM), Thermo Fisher Scientific, supplemented with 10% fetal bovine serum (FBS) and penicillin/streptomycin (100 IE/mL penicillin and 100 µg/mL streptomycin). The cells were provided from the Institute of Materials Science and Technology of the Technical University of Vienna. The medium was refreshed every second day and the cells were splitted with trypsin and EDTA once a week. The cell passage was 6 to 10.

For separation of cells and trypsin the cells were centrifuged and suspended in fresh medium. The cells were counted in a Neubauer chamber and afterwards seeded to a 96 well plate having 10 000 cells in each well.

The cells were left over night to attach to the wells and afterwards the medium was removed. The cells were stimulated with the prepared test-solutions in 8 repetitions. After exactly 24 hours the medium including the samples to be tested was removed and Presto Blue in fresh medium (ratio 1:10) was added. After 1 hour fluorescence was measured on BioTek Multiplate reader from Synergy.

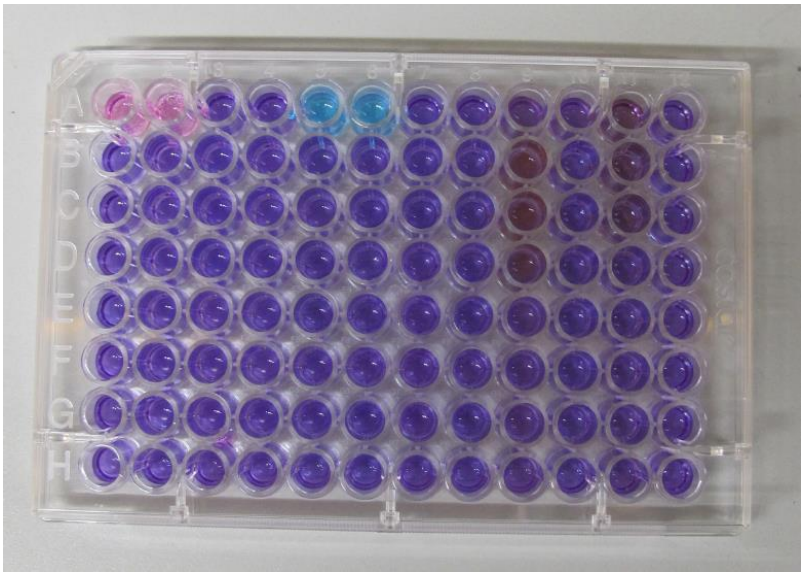

Fig.87: Photo of a well plate with Presto Blue dye in it.

Figure 87 shows an example of such a well plate filled with PB after measuring the fluorescence.

Photoinitiator (PI) Li-TPO-L was dissolved in α-MEM in order to reach the solutions of the following concentrations: 2.23, 1.12, 0.6, 0.3, 0.15 and 0.075 mM/L. As a comparison sample, also IG2959 was dissolved in medium to reach 2.23 mM/L concentrated solution.

Additional to the tested PIs some cavities were filled only with medium, cells and Presto Blue for positive control.

4 Rheology

4.1 Optimum setup

As it was already mentioned before, all rheology measurements involving irradiation of the sample were carried out on Anton-Paar Modular compact Rheometer MCR 302 WESP. A plate-to-plate measuring system with 25 mm diameter was used for all analysis with a gap size of 50 µm. The measurements were done in oscillation mode with a shear rate of 10 Hz and a strain of 10% at a constant temperature of 37°C. Light source was Omnicure Lamp, settled to λ=365 nm. The light output intensity was set to 1.45 W/cm^2 on the Omnicure system, which was calibrated with an Omnicure R2000 radiometer prior to usage.

Light intensity was measured directly on the top of the glass slide with a USB2000+ radiometer from Oceanoptics. The intensity was measured in the very centre and in distance of 0.6 cm and 1.25 cm from the centre, at 0°, 90°, 180° and 270°. The intensities are listed below in Table 12.

Table 12: Measured light intensity depending on position on the glass plate of the rheometer

Position	**Angle,** [°]	**Distance from centre, [cm]**	**Intensity,** [**mW*cm^{-2}**]
Centre	0	0	11
1	0	0.6	8
2	90	0.6	8
3	180	0.6	8
4	270	0.6	9
5	0	1.25	7
6	90	1.25	6
7	180	1.25	8
8	270	1.25	7

The measurements were done at 40 °C. The first 20 seconds of each measurement were done without UV irradiation and after this time span the UV light was turned on automatically via triggering of the rheometer. Data points were collected each second.

4.1.1 Protection of hydrogel from drying

For determination of drying process of the hydrogel, mixtures of methacryl modified gelatin (GelMOD) with degree of substitution (DS) 70% and a PI IG2959 were prepared with macromere content 20%, based on the whole formulation and PI content 2.23 mM/L. Stock solutions of PI were made at first and then mixed together with the macromere solutions. Table 13 shows the amounts of all constituents of reaction mixtures.

Table 13: Mixtures for determination of the drying process in the hydrogels

Sample	**m(mac), [mg]**	**c(PI_{final})[1], [mM/L]**	**c(PI-sol_{higher})[2], [mM/L]**	**V(PI-sol_{higher})[3], [µL]**	**V(PBS), [µL]**
GelMOD20%-IG2959	109	2.23	22.3	54.5	381.5

[1] $c(PI_{final})$ is the final PI concentration in the ready-to-use sample for rheometer measurements

[2] $c(\text{PI-}sol_{higher})$ is the concentration of the preceding higher concentrated stock solution used for the preparation of this solution

[3] $V(\text{PI-}sol_{higher})$ is the volume of the preceding higher concentrated stock solution used for the preparation of this solution

GelMOD was dissolved in phosphate-buffered saline (PBS) in a test tube. The test tube was ultrasonicated by 40°C for 30 min. After the GelMOD was completely dissolved, the test tube with the mixture was wrapped in an aluminium foil, and after that the PI was added. The test tube with the reaction mixture was ultrasonicated again by 40°C for 30 minutes without an access of visible light.

The reaction mixture in test tube, covered with the aluminium foil, was pre-heated and stored during the whole measurement in a 100 ml beaker with water at 40 °C. For the measurement 60 µl of reaction mixture was put on the transparent window of rheometer and measured with the standard parameters, mentioned in Section 4.1. In case of measuring with oil, before the measurement started several drops of mineral oil were put on the out-coming edges of the samples. Each measurement (with and without oil) was conducted with 7 repetitions. Table 14 below demonstrates obtained data with calculations of an average value and standard deviation, and a good reproducibility of the results.

Table 14: Data, demonstrating the reproducibility of the results, obtained from photorheometry

Sample	Delay, s	Slope, $Pa*s^{-1}$	Time of 95%G'max, s	G' max, kPa
GelMOD20%_IG2959_2.23_oil_1	101	150	545	46
GelMOD20%_IG2959_2.23_oil_2	100	171	574	52
GelMOD20%_IG2959_2.23_oil_3	99	164	530	45
GelMOD20%_IG2959_2.23_oil_4	97	180	571	47
GelMOD20%_IG2959_2.23_oil_5	102	143	575	35
GelMOD20%_IG2959_2.23_oil_6	97	157	592	43
GelMOD20%_IG2959_2.23_oil_7	98	138	600	44
Average Value	**99**	**158**	**570**	**45**
Standard Deviation	**0.8**	**6.2**	**10.11**	**2.1**
GelMOD20%_IG2959_2.23_no_oil_1	111	138	1400	150
GelMOD20%_IG2959_2.23_no_oil_2	108	119	1362	148
GelMOD20%_IG2959_2.23_no_oil_3	110	112	1374	155
GelMOD20%_IG2959_2.23_no_oil_4	109	128	1330	163
GelMOD20%_IG2959_2.23_no_oil_5	109	135	1355	172
GelMOD20%_IG2959_2.23_no_oil_6	112	124	1390	148
GelMOD20%_IG2959_2.23_no_oil_7	111	98	1320	133
Average Value	**110**	**122**	**1362**	**153**
Standard Deviation	**0.58**	**5.67**	**12.07**	**5.08**

4.1.2 Influence of glass supporter

For analyzing the difference between the hydrogel samples, made directly on the transparent window of rheometer and the samples, made on the glass slides, reaction mixture was prepared from GelMOD (DS: 70%) and Li-TPO-L with 20% of macromere content and 2.23 mM/L of PI content. Table 15 shows the amounts of all constituents of reaction mixtures.

Table 15: Mixtures for determination of the influence on the hydrogel properties of the presence of the glass slides

Sample	**m(mac)[mg]**	**c(PI_{final}), [mM/L]**	**c(PI-sol_{higher}), [mM/L]**	**V(PI-sol_{higher}), [µL]**	**V(PBS), [µL]**
GelMOD20%-LiTPO-glass	153	2.23	22.3	76.5	535.5
GelMOD20%-LiTPO-no glass	170	2.23	22.3	85	595

GelMOD was dissolved in PBS in a test tube. The test tube was ultrasonicated by 40°C for 30 min. After the GelMOD was completely dissolved, the test tube with mixture was wrapped in

an aluminium foil, and after that the PI was added. The test tube with the reaction mixture was ultrasonicated again by 40°C for 30 minutes without an access of visible light.

The reaction mixture in test tube, covered with the aluminium foil, was pre-heated and stored during the whole measurement in a 100 ml beaker with water at 40 °C. The measurments without glass supporter were conducted as described previously. Measurements, where supportive glass was used were conducted in a following way: a drop of water was put on a pre-heated transparent window of rheometer and then covered with a functionalized glass slide in each measurement. For the measurement 60 µl of the reaction mixture was put on the functionalized glass slide and measured with the standard parameters mentioned in Section 4.1. Mineral oil was added to each sample before the measurement started. Each measurement was conducted with 7 repetitions. Table 16 below demonstrates obtained data with calculations of an average value and standard deviation, and a good reproducibility of the results.

Table 16: Data, demonstrating the reproducibility of the results, obtained from the photorheometry experiment

Sample	Delay, s	Slope, $Pa*s^{-1}$	Time of 95%G'max, s	G'max, kPa
GelMOD20%_LiTPO2.23_glass_1	18	645	200	75
GelMOD20%_LiTPO2.23_glass_2	17	738	260	77
GelMOD20%_LiTPO2.23_glass_3	17	688	253	80
GelMOD20%_LiTPO2.23_glass_4	16	730	245	82
GelMOD20%_LiTPO2.23_glass_5	18	780	277	74
GelMOD20%_LiTPO2.23_glass_6	18	764	297	79
GelMOD20%_LiTPO2.23_glass_7	17	785	230	78
Average Value	**17**	**733**	**252**	**78**
Standard Deviation	**0.3**	**21**	**12.9**	**1.15**
GelMOD20%_LiTPO2.23_no_glass_1	19	643	300	68
GelMOD20%_LiTPO2.23_no_glass_2	20	600	283	70
GelMOD20%_LiTPO2.23_no_glass_3	18	590	207	69
GelMOD20%_LiTPO2.23_no_glass_4	18	643	273	77
GelMOD20%_LiTPO2.23_no_glass_5	17	670	295	75
GelMOD20%_LiTPO2.23_no_glass_6	17	697	243	73
GelMOD20%_LiTPO2.23_no_glass_7	19	568	267	71
Average Value	**18**	**630**	**267**	**72**
Standard Deviation	**0.46**	**19**	**13.32**	**1.35**

4.2 Storage stability of formulations

For observing the difference in photorheological properties of hydrogels, produced from the new-made and old reactions mixtures, there were 4 types of reaction mixtures prepared and tested. All reaction mixtures were containing GelMOD (DS: 70%) in concentration of 20%. For the first reaction mixture Li-TPO in concentration of 2.23 mM/L was used, and for the second mixture IG2959 in concentration of 2.23 mM/L was used. Two other mixtures were made one week before and had the same composition. Table 17 shows the amounts of all constituents of reaction mixtures.

Table 17: Mixtures for detecting the difference in properties of the hydrogels, produced from the new and old reaction mixtures.

Sample	**m(mac), [mg]**	**c(PI_{final}), [mM/L]**	**c(PI-sol_{higher}), [mM/L]**	**V(PI-sol_{higher}), [µL]**	**V(PBS), [µL]**
GelMOD20%-LiTPO-new	132.7	2.23	22.3	66.4	464.5
GelMOD20%-LiTPO-old	158	2.23	22.3	79	553
GelMOD20%-IG2959-new	147.5	2.23	22.3	73.8	516.3
GelMOD20%-IG2959-old	173	2.23	22.3	86.5	605.5

GelMOD was dissolved in PBS in a test tube. The test tube was ultrasonicated by 40°C for 30 min. After the GelMOD was completely dissolved, the test tube with reaction mixture was wrapped in an aluminium foil, and after that PI was added. The test tube with the reaction mixture was ultrasonicated again by 40°C for 30 minutes without an access of visible light.

The reaction mixture in test tube, covered with the aluminium foil was pre-heated and stored during the whole measurement in a 100 ml beaker with water at 40 °C. A drop of water was put on a pre-heated transparent window of rheometer and then covered with a functionalized glass slide in each measurement. For the measurement 60 µl of reaction mixture was put on the functionalized glass slide and measured with the standard parameters mentioned in Section 4.1. Mineral oil was added to each sample before the measurement started. Each measurement was conducted with 7 repetitions. Table 18 below demonstrates obtained data with calculations of an average value and standard deviation, and a good reproducibility of the results.

Table 18: Experimental results for mixtures for evaluation of degradability of formulation

Sample	Delay, s	Slope, $Pa*s^{-1}$	Time of 95%G'max, s	G' max, kPa
GelMOD20%_IG2959_2.23_new_1	99	267	500	71
GelMOD20%_IG2959_2.23_new_2	103	270	521	72
GelMOD20%_IG2959_2.23_new_3	100	290	527	70
GelMOD20%_IG2959_2.23_new_4	102	275	503	68
GelMOD20%_IG2959_2.23_new_5	100	285	510	70
GelMOD20%_IG2959_2.23_new_6	101	263	545	73
GelMOD20%_IG2959_2.23_new_7	102	295	519	69
Average Value	**101**	**278**	**517**	**70**
Standard Deviation	**0.58**	**5**	**6.4**	**0.7**
GelMOD20%_IG2959_2.23_old_1	114	107	521	33
GelMOD20%_IG2959_2.23_old_2	112	125	511	29
GelMOD20%_IG2959_2.23_old_3	109	132	548	34
GelMOD20%_IG2959_2.23_old_4	110	117	513	31
GelMOD20%_IG2959_2.23_old_5	111	122	519	33
GelMOD20%_IG2959_2.23_old_6	113	145	501	29
GelMOD20%_IG2959_2.23_old_7	108	110	528	32
Average Value	**111**	**123**	**520**	**32**
Standard Deviation	**0.9**	**5.4**	**6.13**	**0.8**
GelMOD20%_LiTPO_2.23_new_1	18	547	370	73
GelMOD20%_LiTPO_2.23_new_2	17	550	415	72
GelMOD20%_LiTPO_2.23_new_3	18	563	364	74
GelMOD20%_LiTPO_2.23_new_4	17	601	375	76
GelMOD20%_LiTPO_2.23_new_5	19	590	425	73
GelMOD20%_LiTPO_2.23_new_6	21	611	435	75
GelMOD20%_LiTPO_2.23_new_7	20	607	383	74
Average Value	**19**	**581**	**395**	**74**
Standard Deviation	**0.6**	**11.3**	**11.9**	**0.6**
GelMOD20%_LiTPO_2.23_old_1	25	211	435	37
GelMOD20%_LiTPO_2.23_old_2	23	226	427	38
GelMOD20%_LiTPO_2.23_old_3	24	230	410	41
GelMOD20%_LiTPO_2.23_old_4	22	218	414	42
GelMOD20%_LiTPO_2.23_old_5	27	253	412	40
GelMOD20%_LiTPO_2.23_old_6	25	238	400	38
GelMOD20%_LiTPO_2.23_old_7	27	247	405	39
Average Value	**25**	**232**	**415**	**39**
Standard Deviation	**0.77**	**6.2**	**5.03**	**0.74**

4.3 Evaluation of optimal photoinitiator

For determination of the best suited PI, reaction mixtures with GelMOD (DS: 70%) and IG2959 and Li-TPO respectively were prepared. Reaction mixtures were calculated to 5% of macromere content and 2.23 mM/L of each PI content. For this purpose stock solutions of both PIs were made at first and then mixed together with the macromere solutions. Table 19 shows the amounts of all constituents of reaction mixtures.

Table 19: Mixtures for determination of the most suitable PI

Sample	**m(mac), [mg]**	**c(PI_{final}), [mM/L]**	**c(PI-sol_{higher}), [mM/L]**	**V(PI-sol_{higher}), [µL]**	**V(PBS), [µL]**
GelMOD5%-IG2959	50	2.23	22.3	100	850
GelMOD5%-LiTPO	52	2.23	22.3	104	884

GelMOD was dissolved in PBS in two test tubes. The test tubes were ultrasonicated by 40°C for 30 min. After the GelMOD was completely dissolved, the test tubes with the mixtures were wrapped in an aluminium foil, and after that the corresponding PI was added to each tube. The test tubes with the reaction mixture were ultrasonicated again by 40°C for 30 minutes without an access of visible light.

The samples in test-tubes, covered with the aluminium foil were pre-heated and stored in a 100 ml beaker with water at 40 °C. At first a drop of water was put on the pre-heated transparent window of rheometer and covered with a functionalized glass slide. For the measurement 60 µl were put on the functionalized glass slide and measured with the standard parameters, mentioned in Section 4.1. Mineral oil was added to each sample before the measurement started. Each measurement was conducted with 7 repetitions. Table 20 below demonstrates obtained data with calculations of an average value and standard deviation, and a good reproducibility of the results.

Table 20: Results for reaction mixtures for evaluation of the best PI type

Sample	Delay, s	Slope, $Pa*s^{-1}$	Time of 95%G'max, s	G' max, kPa
GelMOD5%_IG2959_2.23_1	107	5.3	617	1.7
GelMOD5%_IG2959_2.23_2	109	5.5	620	1.5
GelMOD5%_IG2959_2.23_3	108	5.1	629	1.6
GelMOD5%_IG2959_2.23_4	105	5.8	635	1.8
GelMOD5%_IG2959_2.23_5	106	5.7	640	1.7
GelMOD5%_IG2959_2.23_6	110	4.9	638	1.6
GelMOD5%_IG2959_2.23_7	109	5.2	633	1.5
Average Value	**108**	**5.4**	**630**	**1.6**
Standard Deviation	**0.74**	**0.13**	**3.6**	**0.05**
GelMOD5%_LiTPO_2.23_1	23	18	588	2.2
GelMOD5%_LiTPO_2.23_2	22	17	591	2.0
GelMOD5%_LiTPO_2.23_3	24	15	595	2.3
GelMOD5%_LiTPO_2.23_4	25	20	590	2.3
GelMOD5%_LiTPO_2.23_5	22	18	585	2.4
GelMOD5%_LiTPO_2.23_6	26	19	592	2.5
GelMOD5%_LiTPO_2.23_7	24	16	594	2.2
Average Value	**24**	**17**	**590**	**2.3**
Standard Deviation	**0.6**	**0.7**	**1.4**	**0.07**

4.4 Determination of an optimal photoinitiator concentration

To analyze the influence of the PI concentration on the photorheological properties and to choose an optimal one, reaction mixtures of GelMOD (DS: 70%) 5% concentrated with Li-TPO in the following concentrations: 2.23, 1.12, 0.6, 0.3, 0.15 and 0.075 mM/L were prepared. Table 21 shows the amounts of all constituents of reaction mixtures.

Table 21: Mixtures for analysis of the hydrogels behavior dependent from concentration of PI

Sample	**m(mac), [mg]**	**c(PI_{final}), [mM/L]**	**c(PI-sol_{higher}), [mM/L]**	**V(PI-sol_{higher}), [µL]**	**V(PBS), [µL]**
GelMOD5%-LiTPO2.23	49	2.23	22.3	98	833
GelMOD5%-LiTPO1.12	53	1.12	22.3	53	954
GelMOD5%-LiTPO0.6	47	0.6	22.3	23.5	869.5
GelMOD5%-LiTPO0.3	49.6	0.3	22.3	12.4	930
GelMOD5%-LiTPO0.15	48.7	0.15	22.3	6	919
GelMOD5%-LiTPO0.075	47.9	0.075	22.3	3	907

GelMOD was dissolved in PBS in 6 test tubes. The test tubes were ultrasonicated by 40°C for 30 min. After the GelMOD was completely dissolved, the test tubes with mixtures were wrapped in an aluminium foil, and after that the corresponding concentrations of PI were added to each tube. The test tubes with the reaction mixtures were ultrasonicated again by 40°C for 30 minutes without an access of visible light.

The reaction mixtures in test-tubes, covered with the aluminium foil were pre-heated and stored during the whole measurement in a 100 mL beaker with water at 40 °C. At first a drop of water was put on the pre-heated transparent window of rheometer and covered with a functionalized glass slide. For the measurement 60 µl of each reaction mixture were put on the functionalized glass slide and measured with the standard parameters mentioned in Section 4.1. Mineral oil was added to each sample before the measurement started. Each measurement was conducted with 7 repetitions. Table 22 below demonstrates obtained data with calculations of an average value and standard deviation, and a good reproducibility of the results.

Table 22: Results for reaction mixtures for evaluation of an optimal PI concentration

Sample	Delay, s	Slope, $Pa*s^{-1}$	Time of 95%G'max, s	G' max, kPa
GelMOD5%_LiTPO_2.23_1	23	19	610	2.2
GelMOD5%_LiTPO_2.23_2	21	17	598	2.1
GelMOD5%_LiTPO_2.23_3	25	17	595	2.3
GelMOD5%_LiTPO_2.23_4	25	19	591	2.3
GelMOD5%_LiTPO_2.23_5	22	18	585	2.4
GelMOD5%_LiTPO_2.23_6	25	16	593	2.3
GelMOD5%_LiTPO_2.23_7	22	18	595	2.3
Average Value	**23**	**18**	**597**	**2.3**
Standard Deviation	**0.7**	**0.46**	**3.15**	**0.04**
GelMOD5%_LiTPO_1.12_1	33	14	889	2.6
GelMOD5%_LiTPO_1.12_2	35	13	876	2.7
GelMOD5%_LiTPO_1.12_3	36	10	865	2.7
GelMOD5%_LiTPO_1.12_4	35	12	890	2.5
GelMOD5%_LiTPO_1.12_5	37	14	882	2.3
GelMOD5%_LiTPO_1.12_6	35	13	867	2.5
GelMOD5%_LiTPO_1.12_7	34	11	878	2.6
Average Value	**35**	**12**	**878**	**2.6**
Standard Deviation	**0.53**	**0.62**	**4.01**	**0.06**
GelMOD5%_LiTPO_0.6_1	62	8	879	2.2
GelMOD5%_LiTPO_0.6_2	60	7	890	2.0
GelMOD5%_LiTPO_0.6_3	62	6	878	2.1
GelMOD5%_LiTPO_0.6_4	61	10	892	2.3
GelMOD5%_LiTPO_0.6_5	59	8	885	2.4
GelMOD5%_LiTPO_0.6_6	58	9	873	2.1
GelMOD5%_LiTPO_0.6_7	60	8	880	2.2
Average Value	**61**	**8**	**882**	**2.2**
Standard Deviation	**0.6**	**0.53**	**2.8**	**0.06**
GelMOD5%_LiTPO_0.3_1	114	3	818	1.5
GelMOD5%_LiTPO_0.3_2	112	4	822	1.2
GelMOD5%_LiTPO_0.3_3	109	5	817	1.4
GelMOD5%_LiTPO_0.3_4	111	4	830	1.3
GelMOD5%_LiTPO_0.3_5	112	4	820	1.4
GelMOD5%_LiTPO_0.3_6	113	3	835	1.6
GelMOD5%_LiTPO_0.3_7	110	5	830	1.7
Average Value	**112**	**4**	**824**	**1.5**
Standard Deviation	**0.7**	**0.33**	**2.9**	**0.1**
GelMOD5%_LiTPO_0.15_1	213	0.8	1080	0.5
GelMOD5%_LiTPO_0.15_2	212	1	1082	0.6

GelMOD5%_LiTPO_0.15_3	214	1.5	1090	0.3
GelMOD5%_LiTPO_0.15_4	215	2	1075	0.4
GelMOD5%_LiTPO_0.15_5	213	1	1070	0.3
GelMOD5%_LiTPO_0.15_6	211	0.9	1063	0.7
GelMOD5%_LiTPO_0.15_7	217	1	1054	0.5
Average Value	**214**	**1**	**1070**	**0.5**
Standard Deviation	**0.81**	**0.2**	**5**	**0.1**

To analyze the influence of the PI concentration on the gel-point shift, 5 mixtures of GelMOD (DS: 70%) in concentration of 20% with Li-TPO in concentrations of: 2.23, 0.6, 0.3, 0.15 and 0.075 mM/L were prepared. Table 23 shows contents of all used formulations.

Table 23: Mixtures for evaluation of the influence of PI concentration

Sample	**m(mac), [mg]**	**c(PI_{final}), [mM/L]**	**c(PI-sol_{higher}), [mM/L]**	**V(PI-sol_{higher}), [µL]**	**V(PBS), [µL]**
GelMOD20%-LiTPO2.23	110	2.23	22.3	55.2	386
GelMOD20%-LiTPO0.6	113	0.6	22.3	14	438
GelMOD20%-LiTPO0.3	132	0.3	22.3	8.3	519.8
GelMOD20%-LiTPO0.15	168	0.15	22.3	5.3	667
GelMOD20%-LiTPO0.075	148	0.075	22.3	2.30	589.7

GelMOD was dissolved in PBS in 5 test tubes. The test tubes were ultrasonicated by 40°C for 30 min. After the GelMOD was completely dissolved, the test tubes with the mixtures were wrapped in an aluminium foil, and after that the corresponding concentration of PI was added to each tube. The test tubes with the reaction mixtures were ultrasonicated again by 40°C for 30 minutes without an access of visible light.

The reaction mixtures in test-tubes, covered with the aluminium foil were pre-heated and stored during the whole measurement in a 100 ml beaker with water at 40 °C. At first a drop of water was put on the pre-heated transparent window of rheometer and covered with a functionalized glass slide. For the measurement 60 µl were put on the functionalized glass slide and measured with the standard parameters, mentioned in Section 4.1. Mineral oil was added to each sample before the measurement started. Each measurement was conducted with 7 repetitions. Table 24 below demonstrates obtained data with calculations of an average value and standard deviation, and a good reproducibility of the results.

Table 24: Results for reaction mixtures for evaluation of the best PI type

Sample	Gel-point time, s
GelMOD20%_LiTPO_2.23	6
GelMOD20%_LiTPO_2.23	5
GelMOD20%_LiTPO_2.23	6
GelMOD20%_LiTPO_2.23	7
GelMOD20%_LiTPO_2.23	5
GelMOD20%_LiTPO_2.23	6
GelMOD20%_LiTPO_2.23	5
Average Value	**6**
Standard Deviation	**0.31**
GelMOD20%_LiTPO_0.6	22
GelMOD20%_LiTPO_0.6	21
GelMOD20%_LiTPO_0.6	20
GelMOD20%_LiTPO_0.6	21
GelMOD20%_LiTPO_0.6	22
GelMOD20%_LiTPO_0.6	22
GelMOD20%_LiTPO_0.6	23
Average Value	**21**
Standard Deviation	**0.4**
GelMOD20%_LiTPO_0.3	30
GelMOD20%_LiTPO_0.3	29
GelMOD20%_LiTPO_0.3	31
GelMOD20%_LiTPO_0.3	28
GelMOD20%_LiTPO_0.3	27
GelMOD20%_LiTPO_0.3	30
GelMOD20%_LiTPO_0.3	31
Average Value	**29**
Standard Deviation	**0.62**
GelMOD20%_LiTPO_0.15	55
GelMOD20%_LiTPO_0.15	56
GelMOD20%_LiTPO_0.15	55
GelMOD20%_LiTPO_0.15	57
GelMOD20%_LiTPO_0.15	57
GelMOD20%_LiTPO_0.15	58
GelMOD20%_LiTPO_0.15	58
Average Value	**57**
Standard Deviation	**0.52**
GelMOD20%_LiTPO_0.075	123
GelMOD20%_LiTPO_0.075	122
GelMOD20%_LiTPO_0.075	121

GelMOD20%_LiTPO_0.075	122
GelMOD20%_LiTPO_0.075	123
GelMOD20%_LiTPO_0.075	119
GelMOD20%_LiTPO_0.075	120
Average Value	**122**
Standard Deviation	**0.62**

4.5 Influence of macromere concentration

4.6 Selection of the optimal formulation

During the above described experiments the optimal formulation of a reaction mixture was selected: GelMOD in concentration of 5% as a polymer component and Li-TPO in concentration of 0.6 mM/L as a PI component.

4.7 Double-bonds conversion

For determination of double-bonds conversion (DBC) during the UV-curing of the hydrogel, the IR-spectrometer Bruker Vertex 80 was connected to rheometer setup. Two mixtures of GelMOD (DS: 70%) and Li-TPO was prepared with macromere content 5% and 20% and PI content 0.6 mM/L. As reference samples three reaction mixtures of PEGDA (700 Da) and IG2959 were prepared with macromere content 10, 20 and 50% and PI content 0.2%. Table 25 shows the amounts of all constituents of reaction mixtures.

Table 25: Mixtures for determination of the DBC in the hydrogels

Sample	**m(mac), [mg]**	**c(PI_{final}), [mM/L]**	**c(PI-sol_{higher}), [mM/L]**	**V(PI-sol_{higher}), [µL]**	**V(PBS), [µL]**
GelMOD5%-LiTPO_0.6	109	0.6	22.3	54.5	381.5
GelMOD20%-LiTPO_0.6	110	0.6	22.3	55	386
PEGDA10%-IG2959_9	114	9	22.3	103	923
PEGDA20%-IG2959_9	107	9	22.3	43	385
PEGDA50%-IG2959_9	115	9	22.3	12	103

GelMOD was dissolved in PBS in 2 test tubes to obtain 5 and 20% concentrated solutions. PEGDA was dissolved in PBS in 3 test tubes to obtain 10, 20 and 50% concentrated solutions. The test tubes were ultrasonicated by 40°C for 30 min. After the GelMOD and PEGDA were completely dissolved, the test tubes with the mixtures were wrapped in an aluminium foil, and after that the PIs in corresponding concentrations were added to each tube. The test tubes with the reaction mixtures were ultrasonicated again by 40°C for 30 minutes without an access of visible light.

The samples in test-tubes, covered with the aluminium foil were pre-heated and stored during the whole measurement in a 100 ml beaker with water at 40 °C. At first a drop of water was put on the pre-heated transparent window of rheometer and covered with a functionalized glass slide. For the measurement 60 µl were put on the functionalized glass slide and measured with the standard parameters, mentioned in Section 4.1. Mineral oil was added to each sample before the measurement started. Each measurement was conducted with five repetitions. Table 26 below demonstrates obtained data with calculations of an average value and standard deviation, and a good reproducibility of the results.

Table 26: Data, demonstrating the reproducibility of the results, obtained from photorheometry

Sample	Delay, s	Slope, $Pa*s^{-1}$	Time of 95%G'max, s	G' max, kPa	DBC,%
GelMOD5%_LiTPO_0.6_1	59	8	900	2.2	
GelMOD5%_ LiTPO_0.6_2	60	9	885	2.3	
GelMOD5%_ LiTPO_0.6_3	65	8	907	2.0	
GelMOD5%_ LiTPO_0.6_4	61	7	905	2.1	
GelMOD5%_ LiTPO_0.6_5	63	7	880	2.5	
Average Value	**62**	**8**	**890**	**2.2**	
Standard Deviation	**1.2**	**0.42**	**6.09**	**0.1**	
GelMOD20%_LiTPO_0.6_1	53	285	723	73	
GelMOD20%_ LiTPO_0.6_2	52	286	718	68	
GelMOD20%_ LiTPO_0.6_3	55	286	721	78	
GelMOD20%_ LiTPO_0.6_4	53	284	724	67	
GelMOD20%_ LiTPO_0.6_5	54	287	720	72	
Average Value	**54**	**285**	**720**	**72**	
Standard Deviation	**0.57**	**0.57**	**1.19**	**2.2**	
PEGDA10%_IG2959_9_1	13	2.2	77	26	100
PEGDA10%_IG2959_9_2	12	2.4	84	25	94
PEGDA10%_IG2959_9_3	12	2.4	80	24	95
PEGDA10%_IG2959_9_4	10	2.2	76	20	98
PEGDA10%_IG2959_9_5	11	2.3	81	21	97
Average Value	**12**	**2.3**	**79**	**23**	**97**
Standard Deviation	**0.57**	**0.05**	**1.6**	**1.29**	**1.19**
PEGDA20%_IG2959_9_1	8	180	54	1822	
PEGDA20%_IG2959_9_2	6	179	55	1819	
PEGDA20%_IG2959_9_3	7	178	57	1818	
PEGDA20%_IG2959_9_4	7	173	56	1821	
PEGDA20%_IG2959_9_5	5	177	53	1823	
Average Value	**7**	**178**	**55**	**1820**	
Standard Deviation	**0.57**	**1.35**	**0.79**	**1.04**	
PEGDA50%_IG2959_9_1	3	324	44	3720	100
PEGDA50%_IG2959_9_2	4	326	46	3750	98
PEGDA50%_IG2959_9_3	3	330	47	3685	97
PEGDA50%_IG2959_9_4	2	326	48	3700	99
PEGDA50%_IG2959_9_5	2	328	47	3690	95
Average Value	**3**	**327**	**47**	**3700**	**98**
Standard Deviation	**0.42**	**1.14**	**0.76**	**13.28**	**0.96**

4.8 Swellability

For studying the swelling process of the hydrogel, mixture of GelMOD (DS: 70%) and Li-TPO was prepared with macromere content 5% and PI content 0.6 mM/L. Stock solutions of PI were made at first and then mixed together with the macromere solutions. Table 27 shows the amounts of all constituents of reaction mixtures.

Table 27: Mixture for determination of the drying process in the hydrogels

Sample	**m(mac), [mg]**	**c(PI_{final}), [mM/L]**	**c(PI-sol_{higher}), [mM/L]**	**V(PI-sol_{higher}), [µL]**	**V(PBS), [µL]**
GelMOD5%-LiTPO_0.6	115	0.6	22.3	73.5	546.5

GelMOD was dissolved in PBS in a test tube. The test tube was ultrasonicated by 40°C for 30 min. After the GelMOD was completely dissolved, the test tube with the mixture was wrapped in an aluminium foil, and after that the PI was added. The test tube with the reaction mixture was ultrasonicated again by 40°C for 30 minutes without an access of visible light.

The reaction mixture in test tube, covered with the aluminium foil was pre-heated and stored during the whole measurement in a 100 ml beaker with water at 40 °C. At first a drop of water was put on the pre-heated transparent window of rheometer and covered with a functionalized glass slide. For the measurement 60 µl of reaction mixture were put on the functionalized glass slide and measured with the standard parameters, mentioned in Section 4.1. Mineral oil was added to each sample before the measurement started. Each measurement was conducted with five repetitions. After the measurement was accomplished, the samples were put into the fridge for 24 h and after that measured again also with 5 repetitions. Table 28 below demonstrates obtained data with calculations of an average value and standard deviation, and a good reproducibility of the results.

Table 28: Data, demonstrating the reproducibility of the results, obtained from photorheometry

Sample	Delay, s	Slope, $Pa*s^{-1}$	Time of 95%G'max, s	G' max, kPa
GelMOD5%-LiTPO_0.6_sw_1	63	8	894	2.5
GelMOD5%-LiTPO_0.6_sw_2	64	9	885	2
GelMOD5%-LiTPO_0.6_sw_3	62	11	895	1.9
GelMOD5%-LiTPO_0.6_sw_4	60	7	878	2.3
GelMOD5%-LiTPO_0.6_sw_5	61	7	900	2.2
Average Value	**62**	**8**	**890**	**2.2**
Standard Deviation	**0.79**	**0.84**	**4.4**	**0.12**
GelMOD5%-LiTPO_0.6_nsw_1				0.21
GelMOD5%-LiTPO_0.6_nsw_2				0.23
GelMOD5%-LiTPO_0.6_nsw_3				0.25
GelMOD5%-LiTPO_0.6_nsw_4				0.27
GelMOD5%-LiTPO_0.6_nsw_5				0.28
Average Value				**0.26**
Standard Deviation				**0.01**

5 Multiphoton grafting

5.1 Selection of a water-soluble grafting agent

5.2 Evaluation of cytotoxicity of grafting agent

Experiment was conducted with two different cell cultures: L929 and MC3T3-E1 Subclone 4 preosteoblast type cells. Both cell cultures were cultivated separately in alpha-Minimum Essential Media (α-MEM) (Thermo Fisher Scientific) supplemented with 10% fetal bovine serum (FBS) and penicillin/streptomycin (100 IE/ml penicillin and 100 µg/mL streptomycin). The cells were provided from the Institute of Materials Science and Technology of the Technical University of Vienna. The medium was refreshed every second day and the cells were splitted with trypsin and EDTA once a week. The cell passage was 6 to 10.

For separation of cells and trypsin the cells were centrifuged and suspended in fresh medium. The cells were counted in a Neubauer chamber and afterwards seeded to a 96 well plate having 10 000 cells in each well.

The cells were left over night to attach to the wells and afterwards the medium was removed. The cells were stimulated with the prepared test-solutions in 8 repetitions. After exactly 24 hours the medium including the samples to be tested was removed and Presto Blue in fresh medium (ratio 1:10) was added. After 1 hour fluorescence was measured on BioTek Multiplate reader from Synergy.

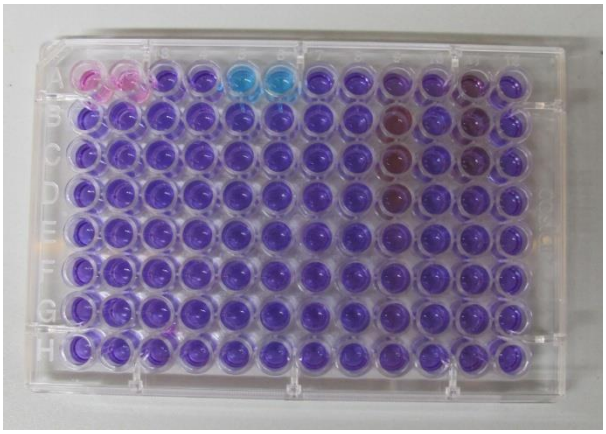

Fig.88: Photo of a well plate with Presto Blue dye in it.

Figure 88 shows an example of such a well plate filled with PB after measuring the fluorescence.

4, 4’-diazo-2, 2’-stilbenedisulfonic acid disodium salt tetrahydrate was dissolved in α-MEM in order to reach the solutions of the following concentrations: 20, 10, 5, 2.5, 1.25, 0.6, and 0.3 mM/L. As a comparison sample, also IG2959 was dissolved in medium to reach 2.23 mM/L concentrated solution. The experiment was performed in absolute darkness. Observed values were compared to the control samples, which were cells untreated with PI: a positive control (10% Presto Blue and 90% medium). As a negative control the highest possible concentration of GA of 20 mM/L was used.

5.3 Determination of processing window

For determination of processing window, mixture of GelMOD (DS: 70%) and Li-TPO was prepared with macromere content 5% and PI content 0.6 mM/L. Stock solutions of PI were made at first and then mixed together with the macromere solutions. Table 29 shows the amounts of all constituents of reaction mixtures.

Table 29: Mixture for determination of the drying process in the hydrogels

Sample	**m(mac), [mg]**	**c(PI_{final}), [mM/L]**	**c(PI-sol_{higher}), [mM/L]**	**V(PI-sol_{higher}), [µL]**	**V(PBS), [µL]**
GelMOD5%-LiTPO_0.6	117	0.6	22.3	89.7	690

GelMOD was dissolved in PBS in a test tube. The test tube was ultrasonicated by 40°C for 30 min. After the GelMOD was completely dissolved, the test tube with the mixture was wrapped in an aluminium foil, and after that the PI was added. The test tube with the reaction mixture was ultrasonicated again by 40°C for 30 minutes without an access of visible light.

The reaction mixture in test tube, covered with the aluminium foil was pre-heated and stored during the whole measurement in a 100 ml beaker with water at 40 °C. At first a drop of water was put on the pre-heated transparent window of rheometer and covered with a functionalized glass slide. For the measurement 60 µl of reaction mixture were put on the functionalized glass slide and measured with the standard parameters, mentioned in Section 4.1. Mineral oil was added to each sample before the measurement started. There were 11 samples made.

After being prepared, the samples were transferred into the petri-dishes with solutions of 2 mM/L concentrated grafting agent (GA) 4, 4'-Diazido-2, 2'-stilbenedisulfonic acid disodium salt in PBS and left overnight without an access of light by room temperature.

On the next day the GA solutions were aspirated from the petri-dishes with samples and the samples were ready for grafting. For the structuring procedure, each sample was put in the specimen holder and moved until the focal point of the objective was in formulation. All parameters for the structuring: laser power, writing speed, structure that should be grafted, grid size, hatch distances, depth of writing were configured with the software. Studied laser power values were: 100, 90, 80, 70, 60, 50, 40, 30, 20, 15, and 10 mW. Writing speed was in all cases maximal 555 $mm*s^{-1}$. The structures were square grids with a side 200 mµ and a hatch distance 2 mµ. After the set up was done the grafting was carried out and could be also monitored with use of a charge coupled device (CCD) camera. The samples were grafted on the surface of the hydrogel layers with a Mai Tai DeepSee ultrafast laser, which utilizes over 2.4 W of average power and 350 nm (690-1040 nm) in useable tuning range.

After grafting procedure was accomplished, the samples were prepared for observations under laser scanning microscopy (LSM), LSM 700, Zeiss. For this purpose, the rest of unreacted GA was aspirated the samples were washed several times with PBS and put in the new sterile

Petri-dishes. After the samples were transferred into the stainless steel sample holders and analyzed with LSM.

5.4 Changing the hatch distance in a fluorescent grid

Two hydrogel layers on the functionalized glass slides, were prepared according to the procedure, described in Section 5.3. After being prepared, the samples were transferred into the petri-dishes with solutions of 2 mM/L concentrated GA 4, 4'-Diazido-2, 2'-stilbenedisulfonic acid disodium salt in PBS and left overnight without an access of light by room temperature.

On the next day the solutions were aspirated from the petri-dishes with samples and the samples were ready for grafting. For the structuring procedure, each sample was put in the specimen holder and moved until the focal point of the objective was in formulation. Laser power was set to 20 mW, writing speed to 555 mm*s^{-1}, square grids with site 200 mμ and hatch distances 2 and 5 mμ, were grafted on the surface of the hydrogel layer.

After the grafting procedure was accomplished, the samples were prepared for observations under LSM: the rest of unreacted GA was removed by putting the samples in the new sterile Petri-dishes and washing them several times with PBS. After that samples were transferred into the stainless steel sample holders and analyzed with LSM.

5.5 Changing the distance from the surface of hydrogel

Five hydrogel layers on the functionalized glass slides, were prepared according to the procedure, described in Section 5.3. After being prepared, the samples were transferred into the petri-dishes with solutions of 2 mM/L concentrated GA 4, 4'-Diazido-2, 2'-stilbenedisulfonic acid disodium salt in PBS and left overnight without an access of light by room temperature.

On the next day the solutions were aspirated from the petri-dishes with samples and the samples were ready for grafting. For the structuring procedure, each sample was put in the specimen holder and moved until the focal point of the objective was in formulation. Laser power was set to 20 mW, writing speed to 555 mm*s^{-1}, square grids with site 40 mμ and hatch distance 2 mμ, were grafted on the surface of the hydrogel layer, 3, 5, 7 and 10 mμ deep into the hydrogel layer.

After grafting procedure was accomplished, the samples were prepared for observations under LSM: the rest of unreacted GA was removed by putting the samples in the new sterile Petri-dishes and washing them several times with PBS. After that samples were transferred into the stainless steel sample holders and analyzed with LSM.

6 Cell seeding

6.1 Cell seeding procedure

The cells seeding procedure was carried out in a cell culture laboratory under the sterile flow hood, in order to prevent any contamination of the samples. Five samples were produced in accordance to the procedure, described in Section 5.3. After the produced hydrogel layers were grafted with a standard maximal speed of 555 $mm*s^{-1}$ and laser power of 20 mW on the surface and 3, 5, 7, 10 µm deep. Three grafted grids had the hatch distances of 2 µm and two grids had 5 µm. Samples were washed with sterile PBS several times, then placed in sterile petri dishes and seeded with MC3T3-E1 Subclone 4 preosteoblast type cells. The MC3T3-E1 Subclone 4 line was grown in α-MEM (Thermo Fisher Scientific). Seeded hydrogel samples were left in the incubator by 37°C for three days.

6.2 Life-dead staining procedure

After three days in incubator, five samples described in Section 6.1 were prepared for observing on LSM in order to check cell viability. For this purpose the LIVE/DEAD viability assay (Thermo Fisher Scientific) was used to assess cell viability according to manufacturer's instructions. α-MEM was aspirated, the samples were washed with sterile PBS several times and the staining solution with 0.2 M Calcein AM (live stain) and 0.6 M propidium iodide (dead stain) was added for 20 min at 37 °C.

After that the staining solution was removed, the samples were washed with sterile PBS several times and 2 ml of sterile PBS was added to each sample. After that samples were transferred into the stainless steel sample holders and analyzed with LSM.

LSM with excitation/emission filter set at 488/530 nm to observe living cells (green) and 530/580 nm to detect dead (red) cells was used. In order to prevent the contamination of the samples, the sample holder and some parts of the LSM microscope were periodically sprayed with isopropanol.

After LSM observation, the samples were again transferred in sterile petri-dishes, and α-MEM was added. Then the samples were put back to the cell culture incubator for further observations.

6.3 Integration of cells into the hydrogel layer

The samples, described in Section 6.2 were prepared for LSM observations once more in order to see the possible deformations of the fluorescent grid.

α-MEM was aspirated, the samples were washed with sterile PBS several times and the staining solution with 0.2 M Calcein AM (live stain) and 0.6 M propidium iodide (dead stain) was added for 20 min at 37 °C.

After that the staining solution was removed, the samples were washed with sterile PBS several times and 2 ml of sterile PBS was added to each sample. After that samples were transferred into the stainless steel sample holders and analyzed with LSM.

LSM with excitation/emission filter set at 488/530 nm to observe living cells (green) and 530/580 nm to detect dead (red) cells was used. In order to prevent the contamination of the samples, the sample holder and some parts of the LSM microscope were periodically sprayed with isopropanol. For a better observation of integration process several images with higher magnification were made.

After LSM observations, the samples were again transferred in sterile petri-dishes, and α-MEM was added. Then the samples were put back to the cell culture incubator for further observations.

6.4 Stability of the samples

The samples, observed in Section 6.3 were prepared for LSM observations again. Unfortunately, it was discovered that the hydrogel layers were slipped from the glass slides. All five samples were inappropriate for observations.

9 hydrogel samples were made, according to the procedure, described in Section 5.3. After being prepared, the samples were transferred into the petri-dishes with solutions of 2 mM/L concentrated grafting agent (GA) 4, 4'-Diazido-2, 2'-stilbenedisulfonic acid disodium salt in PBS and left overnight without an access of light by room temperature.

On the next day the GA solutions were aspirated from the petri-dishes with samples and the samples were ready for grafting. Grafting parameters were 20 mW laser power, 555 $mm*s^{-1}$ writing speed, hatch distance 2 µm, grid site 200 µm. All structures were grafted on the surface of the hydrogel layers. 3 samples were put in sterile petri-dishes with only α-MEM alone and left in the fridge, 3 samples were put in sterile petri-dishes with α-MEM and transferred into the incubator, and 3 samples were put in sterile petri-dishes with α-MEM, seeded with cells and transferred into the incubator. After six days 9 samples were examined.

Summary

The aim of this work was the creation of novel system, allowing a comprehensive monitoring and also quantitative and qualitative characterization of live cells-induced deformations in a hydrogelic matrix material. Hydrogel layers, made from photoactive mixtures of biocompatible and enzymatically degradable GelMOD with a new PI Li-TPO-L, were cross-linked utilizing photorheometry technique on the surface of modified glass slides. Toxicity studies with MC3T3 preosteoblast cells were performed in order to estimate the optimal type and concentration of PI for production of hydrogel. For this, cytotoxicity tests were performed where cytotoxicity of a new PI Li-TPO-L and commonly used IG2959 were compared.It was demonstrated, that Li-TPO-L used in concentration of 2.23 mM/L was similar to the DMSO control, where metabolic activity of cells dropped to only 17%, however lower concentrations of Li-TPO-L showed comparatively same cell toxicity as a commonly used PI IG2959 in its optimal concentration of 2.23 mM/L.

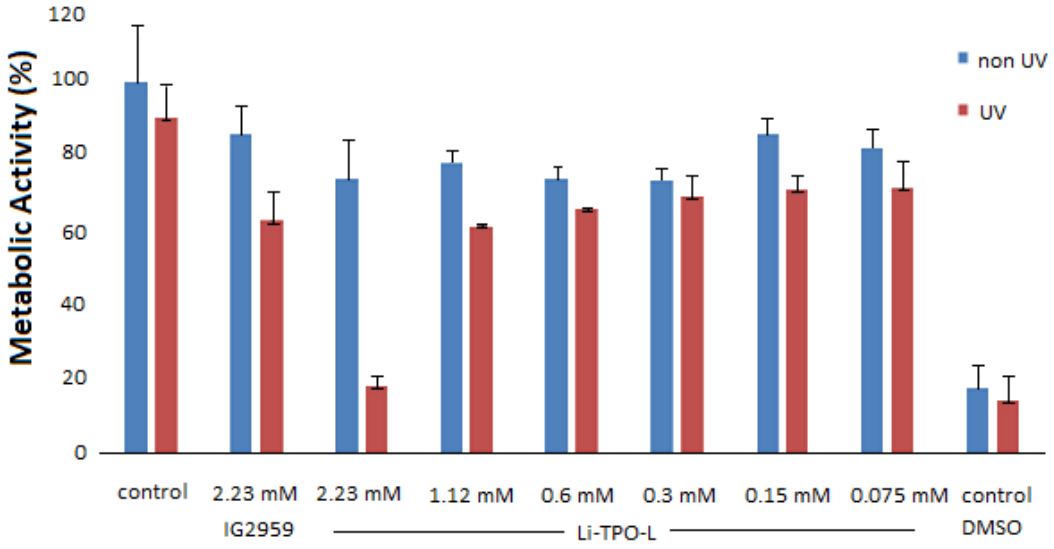

S.1.1: Results from the cell-toxicity analysis of Li-TPO-L in different concentrations, compared with IG2959 in its optimal concentration of 2.23 mM/L, negative control performed with DMSO and positive untreated control.

Photorheological studies were performed for characterization of mechanical properties of cross-linked hydrogels, concerning composition of initial reaction mixtures: concentrations of polymer and type and concentrations of PI. For analysis of the reaction mixtures, maximum storage modulus G'max, slope in the linear region of the increase of G', the time until 95% of G'max value is reached and finally the delay of initiation were determined. It was demonstrated that Li-TPO in comparison to IG2959 results in better mechanical properties of produced cross-linked hydrogels by lower concentrations. Therefore, the optimal formulation with polymeric content of GelMOD 5% and concentration of PI Li-TPO of 0.6 mM/L was selected and used in all further experiments.

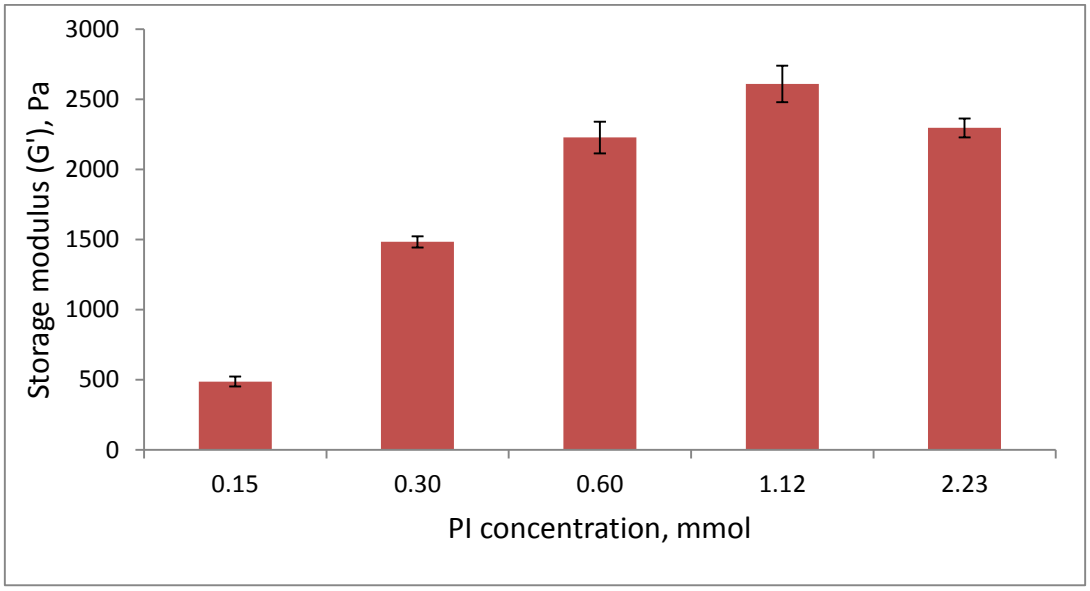

Figure S.1.2: Maximum storage modulus G' of analyzed reaction mixtures with different concentrations of Li-TPO.

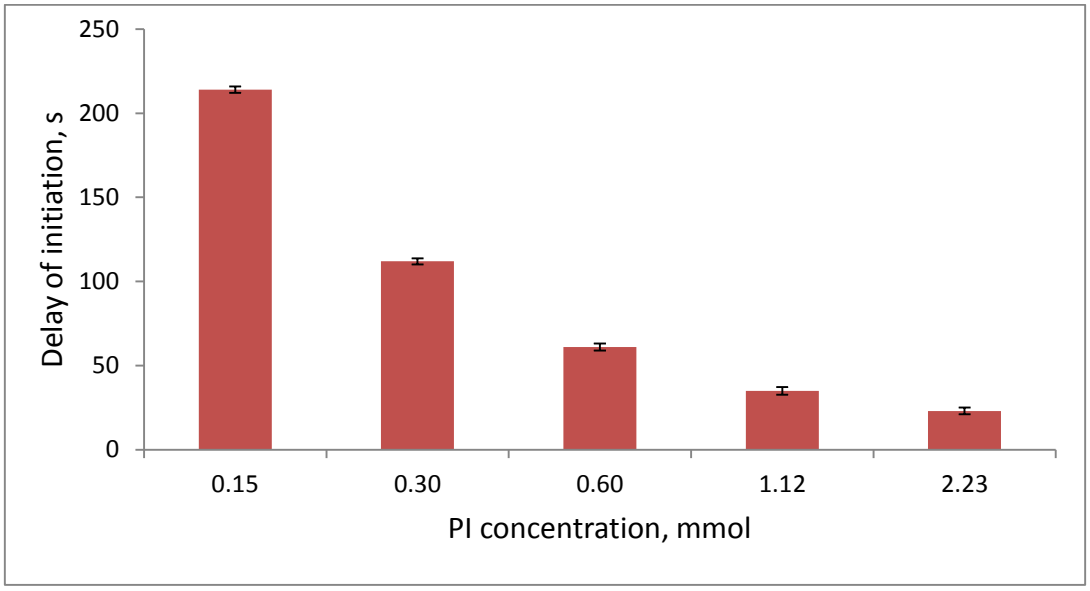

Figure S.1.3: Delay of initiation in analyzed reaction mixtures with different concentrations of Li-TPO.

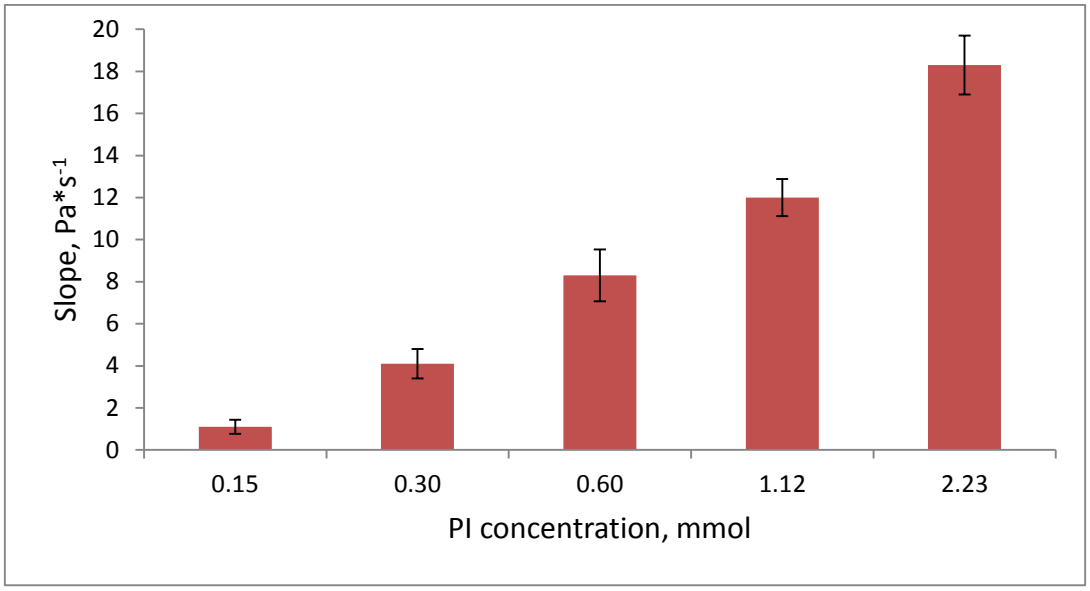

Figure S.1.4: Slope of G' in the linear region in reaction mixtures with different concentrations of Li-TPO.

The higher reactivity was observed, as it was expected, in reaction mixtures with higher PI content. The gradual stiffness increase was observed in reaction mixtures with gradual evaluation of PI concentration. However, maximum stiffness (maximal G' value) was obtained in mixture with concentration of PI 1.12 mM/L, further evaluation of PI concentration gave reverse results: G'max of produced hydrogel dropped by concentration of PI 2.23 mM/L. This could happen because of decreased mobility of high-molecular weight macromers, preventing the full conversion of cross-linking reaction.

Via combined FTIR-Spectroscopy and Photorheometry, double-bonds conversion (DBC) experiments were conducted. After comparison of GelMOD with a reference sample: PEGDA, it was established, that the amount of double bonds (DBs) in reaction mixtures with 20% concentrated GelMOD is much lower, than in reaction mixtures with 20% concentrated PEGDA. Mechanical properties of resulting hydrogels: from GelMOD and PEGDA were also compared. Mechanical properties of hydrogels made of GelMOD in dependence from its concentration in reaction mixture were also studied.

Produced samples were then prepared for multiphoton grafting (MPG) procedure. For this purpose, a suitable grafting agent (GA) was firstly selected. An insoluble in water 2,6-bis(4-diazidobenzylidene)-4-methylcyclohexanone (BAC-M), previously used in works of Ovsianikov et al. was compared with a new GA 4, 4'-diazo-2, 2'-stilbenedisulfonic acid disodium salt tetrahydrate, which is more preferable, due to its watersolubility. Aromatic azides are known to be toxic for the cells, however the right concentration can help to minimize toxicity. Therefore, cytotoxicity tests for 4, 4'-diazo-2, 2'-stilbenedisulfonic acid disodium salt tetrahydratewere performed with two different cell lines: MC3T3 preosteoblast cells and L929 cells.

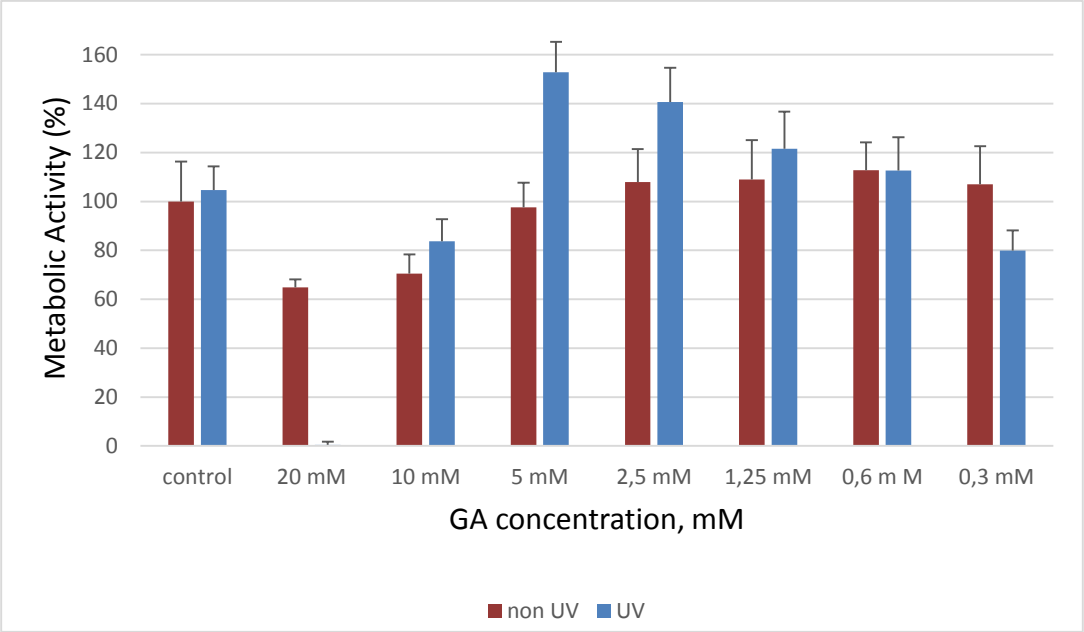

Figure S.1.5: Influence of different concentrations of GA on metabolic activity of L929 after 24 h and exposed/not exposed to UV light (PrestoBlue Cell Viability assay).

Results demonstrated, that the highest concentration of GA solution of 20 mM/L was deadly for the cells: there was no cell metabolic activity detected by this concentration after exposure to UV light. Unusual results were obtained with GA concentrations below 10 mM/L: the induced cell metabolic activity was observed.

The toxicity tests, performed for another cell line, MC3T3 with same concentrations of GA demonstrated that no cell metabolic activity was observed by GA concentration of 10 mM/L, after irradiation with UV light, which was not critical for L929 cell line in the previous test. High toxicity without UV light was observed in all other samples with lower GA concentrations. With UV light only lower concentrations of 1.25, 0.6 and 0.3 mM/L gave good results. Therefore, an optimal concentration 2 mM/L of 4, 4'-diazo-2, 2'-stilbenedisulfonic acid disodium salt tetrahydrate was estimated for further MPG process, which will also be used in all further experiments.

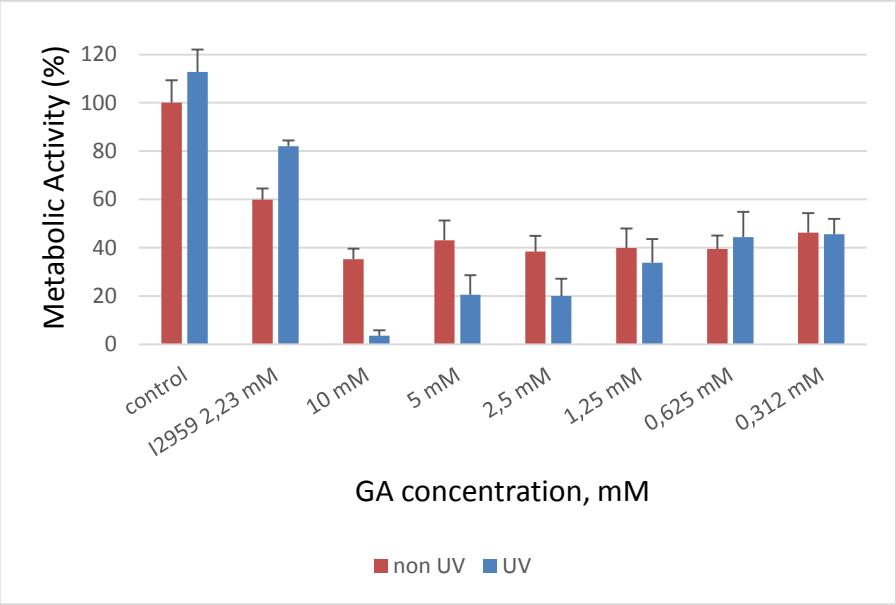

Figure S.1.6: Influence of different concentrations of GA on metabolic activity of MC3T3-E1cell line after 24 h and exposed/not exposed to UV light (PrestoBlue Cell Viability assay).

A processing window was then determinated for chosen formulation. An optimal laser power of 20 mW was chosen with maximal writing speed of 555 mm*s^{-1}. Well-shaped grid patterns, which could be good seen via laser scanning microscopy (LSM) were demonstrated after performing MPG procedure.

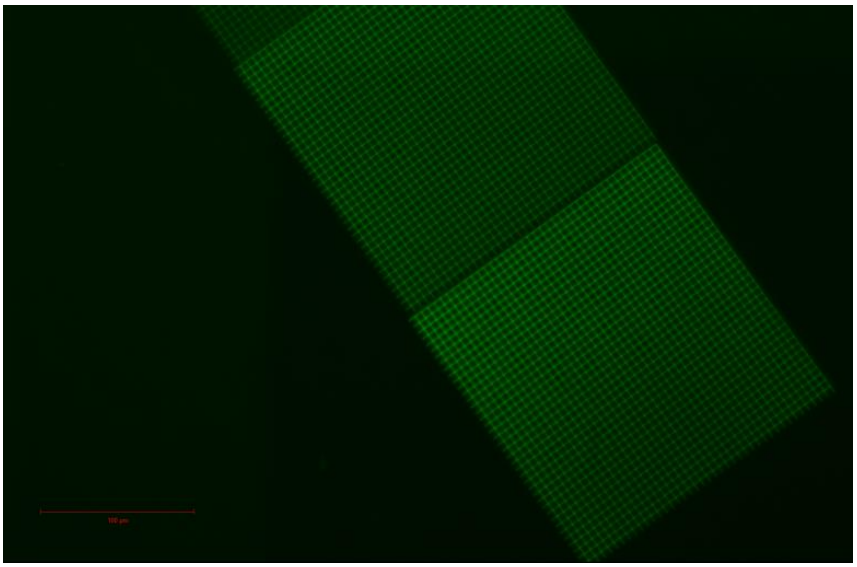

Figure S.1.7: An LSM image of a fluorescent grid grafted on the surface of hydrogel layer.

After the grids were grafted, the samples were seeded with cells and after a certain incubating time were observed via LSM. It was demonstrated that the cells behaved well on the first day of observations and on a second day some cells were even seen to be integrated in the hydrogel layer, which could be monitored via fluorescent grid, which speaks for a good cytocompatibility of created system.

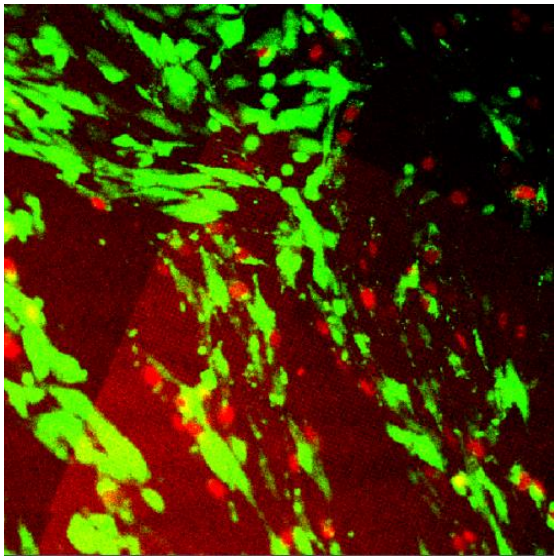

Figure S.1.8: LSM image of the live (green) and dead (red) cells on the red fluorescent grids.

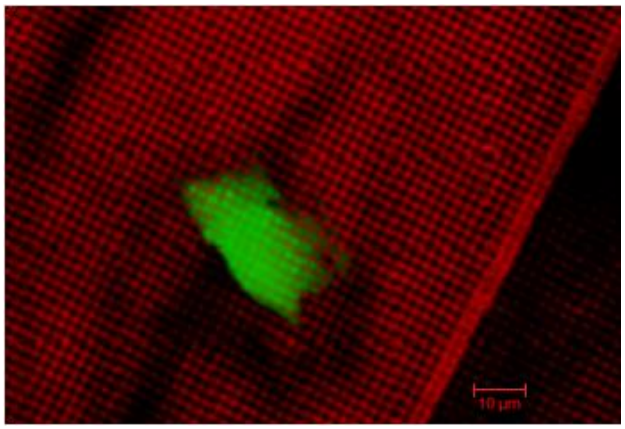

Figure S.1.9: LSM image of a single cell, integrated through the fluorescent grid with a hatch distance of 2 µm, observed with higher magnification.

However it was impossible to image the samples more than two days, because of their poor sustainability to periodical manipulations, like cell-medium change, transportations and others.

As long as via fluorescent grid it was possible to detect integration of cells into a hydrogel layer, it can be concluded that if the problem of storage stability of the whole system will be improved, it can still bring success in studying of cell-induced deformations of the biocompatible matrices. On the example of this work, further improvements of created system can be made in the future:

- to achieve better adhesion of a hydrogel layer to the glass surface it is necessary to try some other methods for modification of glass slides surfaces;
- a new system should be invented for non-invasive transportation of grafted samples with cells, which should reduce the amount of required manipulations with samples;
- More broad parameter window should be tested with variations of such grid parameters like hatch distance, distance from the surface of a hydrogel, etc.

Materials and Methods

Rheology

Photorheology measurements were performed on an Anton-Paar Modular Compact Rheometer MCR 302 WESP. All measurements were done at a constant temperature of 37 °C. Light source was an OmniCure 2000 lamp from EXFO with high pressure mercury lamp, combined with a two-headed light guide. The lamp was triggered by rheometer. Omnicure 2000 light source was calibrated with an R2000 radiometer from EXFO.

The light intensity was measured directly on the glass plate with an Ocean Optics USB2000+ radiometer. All measurements were carried out at a constant temperature of 25 °C in plate-to-plate mode with a 25 mm in diameter steel plate measuring system (PP25). To assure reproducibility of the obtained results, the planarity of the glass plate was checked before each series of measurements.

Multiphoton Grafting

For the multiphoton grafting experiments a Mai Tai DeepSee ultrafast laser utilizing over 2.4 W of average power and 350 nm (690-1040 nm) was used. Obtained structures could be monitored with use of a CCD camera.

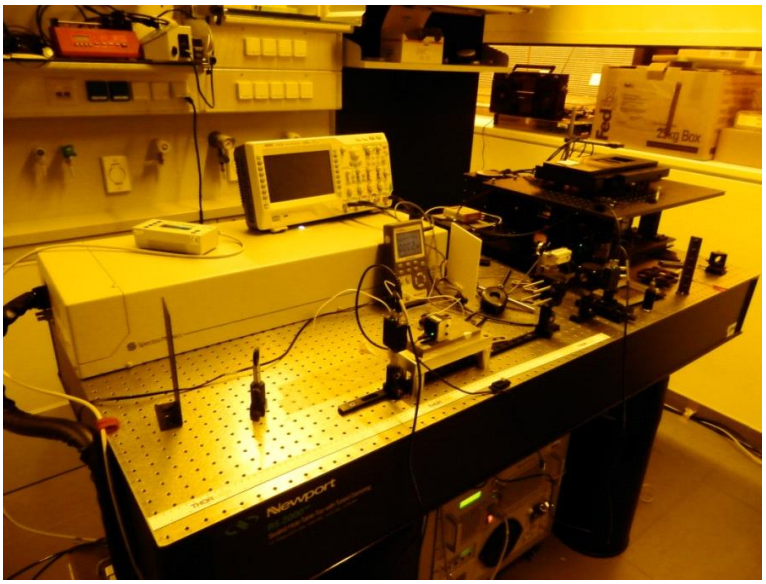

Figure M.1.1: Image of setup for MPG.

Microscope

An Axioskop microscope from Zeiss with an LD Achroplan (20x) objective was used for analyzing grafted samples before they were seeded with cells and after that.

For the laser scanning microscopy (LSM) of obtained patterns a Axio Observer Z1 from Zeiss was used in combination with an LSM 700 scanning head. The excitation wavelength was 490 nm and for data processing ZEN 2011 software from Zeiss was used. The following objectives were used in combination with the LSM: 10x EC Plan Neofluar 10x/03, 20x EC Plan Neofluar 20x/05 and 63x Plan Achromat 63x/1.40 with immersion oil.

Ultrasonic bath

For a better and faster dissolving of compounds, an ultrasonic bath Sonorex Digitec from Bandelin company was used.

Plasma Cleaner

A plasma cleaner from Harrick Plasma was used for purification of glass slides and also for their surface activation.

Abbreviations

TE	Tissue engineering
TES	Tissue engineering scaffold
ECM	extracellular matrix
GF	growth factor
PI	photoinitiator
GA	grafting agent
MPP	multiphoton processing
MPA	multiphoton absorption
TPA	two-photon absorption
2PP	two-photon polymerization
MPG	multiphoton grafting
2PP	two-photon polymerisation
DMSO	dimethylsulfoxide
DS	degree of substitution
IG2959	Irgacure 2959
GelMOD	chemically modified gelatin
NMR	nuclear magnetic resonance
PEG	poly(ethylene glycol)
PEGDA	poly(ethylene glycol) diacrylate
PVA	poly(vinylalcohol)
UV	ultra-violet
GF	growth factor
HA	hyaluronic acid
PGA	poly(glycolic acid)
PLA	poly(lactic acid)
PLGA	poly(lactic-co-glycolic acid)

PCL	poly-caprolactone
PGS	poly(glycerol sebacate)
PEGDMA	poly(ethylene glycol) dimethacrylate
MSCs	mesenchymal stem cells
hMSCs	human mesenchymal stem cells
AFM	atomic force microscopy
TFM	traction force microscopy
FRET	fluorescence resonance energy transfer
SAMs	self-assembled monolayers
LSM	laser scanning microscopy
EDX	Energy dispersive X-ray
Li-TPO	Lithium benzoyl phenylphosphonat
α-MEM	Alpha Minimum Essential Medium
PB	PrestoBlue
BAC-M	2,6-bis(4-diazidobenzylidene)-4-methylcyclohexanone
SAM	self-assembled monolayer
DB	double-bond
DBC	double-bond conversion
FTIR	Fourier transform infrared
IR	infrared
PBS	phosphate-buffered saline

Bibliography

[1] Tsang KY, Cheung MCH, Chan D, Cheah KSE. The developmental roles of the extracellular matrix: beyond structure to regulation. Cell Tissue Res. 339, 93–110 (2009).

[2] Langer R, Vacanti J. Tissue engineering. Science 260(5110), 920–926 (1993).

[3] Meng D, Erol M, Boccaccini AR. Processing technologies for 3D nanostructured tissue engineering scaffolds. Adv. Eng. Mater. 12(9), B467–B487 (2010).

[4] Hutmacher DW. Scaffold design and fabrication technologies for engineering tissues – state of the art and future perspectives. J. Biomater. Sci. Polym. Ed. 12(1), 107–124 (2001).

[5] Langer R, Vacanti J. Tissue engineering. Science 260(5110), 920–926 (1993).

[6] Guilak F, Cohen DM, Estes BT, Gimble JM, Liedtke W, Chen CS. Control of stem cell fate by physical interactions with the extracellular matrix. Cell Stem Cell 5(1), 17–26 (2009).

[7] Wheeldon I, Farhadi A, Bick AG, Jabbari E, Khademhosseini A. Nanoscale tissue engineering: spatial control over cell– materials interactions. Nanotechnology 22(21), 212001 (2011).

[8] Dvir T, Timko BP, Kohane DS, Langer R. Nanotechnological strategies for engineering complex tissues. Nat. Nanotechnol. 6(1), 13–22 (2010).

[9] Zohreh Izadifar, Xiongbiao Chen and William Kulyk. Strategic Design and Fabrication of Engineered Scaffolds for Articular Cartilage Repair. J. Funct. Biomater. 2012, 3, 799-838.

[10] Cukierman, E. and Bassi, D.E. (2010) Physico-mechanical aspects of extracellular matrix influences on tumorigenic behaviors. Semin. Cancer Biol. 20, 139–145.

[11] Tibbitt, M.W. and Anseth, K.S. (2009) Hydrogels as extracellular matrix mimics for 3D cell culture. Biotechnol. Bioeng. 103, 655–663

[12] Hutmacher, D.W. Scaffolds in tissue engineering bone and cartilage. Biomaterials 2000, 21, 2529–2543.

[13] Malda, J.; Woodfield, T.B.F.; van der Vloodta, F.; Wilsond, C.; Martensc, D.E.; Tramperc, J.; van Blitterswijk, C.A.; Rieslea, J. The effect of PEGT/PBT scaffold architecture on the composition of tissue engineered cartilage. Biomaterials 2005, 26, 63–72.

[14] Hwang, N.S.; Kim, M.S.; Sampattavanich, S.; Baek, J.H.; Zhang, Z.; Elisseeff, J. Effects of three-dimensional culture and growth factors on the chondrogenic differentiation of murine embryonic stem cells. Stem Cells 2006, 24, 284–291.

[15] Liu, H.; Lin, J.; Roy, K. Effect of 3D scaffold and dynamic culture condition on the global gene expression profile of mouse embryonic stem cells. Biomaterials 2006, 27, 5978–5989.

[16] Gelain, F. et al. (2007) Designer self-assembling peptide scaffolds for 3-d tissue cell cultures and regenerative medicine. Macromol. Biosci. 7, 544–551

[17] Ashe, H.L. and Briscoe, J. (2006). The interpretation of morphogen gradients. Development 133, 385–394

[18] Hutmacher, D.; Woodfield, T.; Dalton, P.D.; Lewis, J.A. Scaffold design and fabrication In Tissue Engineering; van Blitterswijk, C., Thomsen, P., Hubbell, J., Cancedda, R., de Bruijn, J., Lindahl, A., Sohier, J., Williams, D.F., Eds.; Elsevier Academic Press: London, UK, 2008; pp. 403–454.

[19] Billiet T, Vandenhaute M, Schelfhout J, Van Vlierberghe S, Dubruel P. A review of trends and limitations in hydrogel-rapid prototyping for tissue engineering. Biomaterials 2012;33:6020e41.

[20] Malda J, Woodfield TBF, van der Vloodt F, Kooy FK, Martens DE, Tramper J, et al. The effect of PEGT/PBT scaffold architecture on oxygen gradients in tissue engineered cartilaginous constructs. Biomaterials 2004;25:5773, 80.

[21] Eggli, P.S.; Hunziker, E.B.; Schenk, R.K. Quantitation of structural features characterizing weight- and less- weight-bearing regions in articular cartilage: A stereological analysis of medial femoral condyles in young adult rabbits. Anat. Rec. 1988, 222, 217–227.

[22] Nehrer, S.; Breinan, H.A.; Ramappa, A.; Young, G.; Shortkroff, S.; Louie, L.K.; Sledge, C.B.; Yannas, I.V.; Spector, M. Matrix collagen type and pore size influence behaviour of seeded canine chondrocytes. Biomaterials 1997, 18, 769–776.

[23] LiVecchi, A.B.; Tombes, R.M.; LaBerge, M. In vitro chondrocyte collagen deposition within porous HDPE: Substrate microstructure and wettability effects. J. Biomed. Mater. Res. 1994, 28, 839–850.

[24] Bhardwaj, T.; Pilliar, R.M.; Grynpas, M.D.; Kandel, R.A. Effect of material geometry on artilagenous tissue formation in vitro. J. Biomed. Mater. Res. 2001, 57, 190–199.

[25] Woodfield, T.B.F.; Bezemer, J.M.; Pieper, J.S.; van Blitterswijk, C.A.; Riesle, J. Scaffolds for tissue engineering of cartilage. Crit. Rev. Euk. Gene Exp. 2002, 12, 207–235.

[26] Zein, I.; Hutmacher, D.W.; Tan, K.C.; Teoh, S.H. Fused deposition modeling of novel scaffold architectures for tissue engineering applications. Biomaterials 2002, 23, 1169–1185.

[27] Murphy, W.L.; Dennis, R.G.; Kileny, J.L.; Mooney, D.J. Salt fusion: An approach to improve pore interconnectivity within tissue engineering scaffolds. Tissue Eng. 2002, 8, 43–52.

[28] Silva, M.M.; Cyster, L.A.; Barry, J.J.; Yang, X.B.; Oreffo, R.O.; Grant, D.M.; Scotchford, C.A.; Howdle, S.M.; Shakesheff, K.M.; Rose, F.R. The effect of anisotropic architecture on cell and tissue infiltration into tissue engineering scaffolds. Biomaterials 2006, 27, 5909–5917.

[29] Ayoubi, R.; Degrandpre, C.; Diraddo, R.; Yousef, A.M. design and dynamic culture of 3D-scaffolds for cartilage tissue engineering. J. Biomater. Appl. 2011, 25, 429–444.

[30] Lavik, E.; Langer, R. Tissue engineering: Current state and perspectives. Appl. Microbiol. Biotechnol. 2004, 65, 1–8.

[31] Mikos, A.G.; Herring, S.W.; Ochareon, P.; Elisseeff, J.; Lu, H.H.; Kandel, R.; Schoen, F.J.; Toner, M.; Mooney, D.; Atala, A.; Van Dyke, M.E.; Kaplan, D.; Vunjak-Novakovic, G. Engineering complex tissues. Tissue Eng. 2006, 12, 3307–3339.

[32] Athanasiou, K.A.; Niederauer, G.G.; Agrawal, C.M. Sterilization, toxicity, biocompatibility and clinical applications of polylactic Acid/Polyglycolic acid copolymers. Biomaterials 1996, 17, 93–102.

[33] Cima, L.G.; Vacanti, J.P.; Vacanti, C.; Ingber, D.; Mooney, D.; Langer, R. Tissue engineering by cell transplantation using degradable polymer substrates. J. Biomech. Eng. 1991, 113, 143–151.

[34] Freed, L.E.; Vunjak-Novakovic, G.; Biron, R.J.; Eagles, D.B.; Lesnoy, D.C.; Barlow, S.K.; Langer, R. Biodegradable polymer scaffolds for tissue engineering. Biotechnology 1994, 12, 689–693.

[35] Mikos, A.G.; Bao, Y.; Cima, L.G.; Ingber, D.E.; Vacanti, J.P.; Langer, R. Preparation of poly(glycolic acid) bonded fiber structures for cell attachment and transplantation. J Biomed. Mater. Res. 1993, 27, 183–189.

[36] Niklason, L.E.; Langer, R. Prospects for organ and tissue replacement. JAMA 2001, 285, 573–576.

[37] Goldberg, M.; Langer, R.; Jia, X. Nanostructured materials for applications in drug delivery and tissue engineering. J. Biomater. Sci. Polym. Ed. 2007, 18, 241–268.

[38] Athanasiou, K.A.; Darling, E.M.; Hu, J.C. Articular cartilage tissue engineering. In Synthesis Lectures on Tissue Engineering, 1st ed.; Athanasiou K.A., Leach J.K., Eds.; Morgan &Claypool: San Rafael, CA, USA, 2009; pp. 1–182.

[39] Stoop, R. Smart biomaterials for tissue engineering of cartilage injury. Int. J. Care Injured 2008, 39, 77–87.

[40] Moutos, F.T.; Guilak, F. Composite scaffolds for cartilage tissue engineering. J. Biorheol. 2008, 45, 501–512.

[41] Kemppainen, J.M.; Hollister, S.J. Tailoring the mechanical properties of 3D-designed poly(glycerol sebacate) scaffolds for cartilage applications. J. Biomed. Mater. Res. A 2010, 94, 9–18.

[42] Chang, C.H.; Lin, F.H; Kuo, T.F.; Liu, H.C. Cartilage tissue engineering. Biomed. Eng. Appl. Basis Comm. 2005, 17, 1–11.

[43] Reddy, N.; Yang, Y. Potential of plant proteins for medical applications. Trends Biotechnol. 2011, 29, 490–498.

[44] Thierry, D. (2012) In situ forming polysaccharide-based 3D-hydrogels for cell delivery in regenerative medicine. Carbohydr. Polym. 87, 1013–1019.

[45] Orive, G. et al. (2009) Bioactive cell-hydrogel microcapsules for cellbaseddrug delivery. J. Control. Release 135, 203–210.

[46] Li, W.J.; Laurencin, C.T.; Caterson, E.J.; Tuan, R.S.; Ko, F.K. Electrospun nanofibrous structure: a novel scaffold for tissue engineering. J. Biomed. Mater. Res. 2002, 60, 613–621.

[47] Sechriest, V.; Miao, Y.; Niyibizi, C.; Westerhausen-Larson, A.; Matthew, H.; Evans, C.H.; Fu, F.H.; Suh, J.K. GAG-augmented polysaccharide hydrogel: A novel biocompatible and biodegradable material to support chondrogenesis. J. Biomed. Mater. Res. 2000, 49, 534–541.

[48] Lin, Y.J.; Yen, C.N.; Hu, Y.C.; Wu, Y.C.; Liao, C.J.; Chu, I.M. Chondrocytes culture in three-dimensional porous alginate scaffolds enhanced cell proliferation, matrix synthesis and gene expression. J. Biomed. Mater. Res. Part A 2009, 88, 23–33.

[49] Perka, C.; Schultz, O.; Spitzer, R.; Lindenhayn, K. The influence of transforming growth factor beta1 on mesenchymal cell repair of full-thickness cartilage defects. J. Biomed. Mater. Res.2000, 52, 543–552.

[50] Mouw, J.K.; Case, N.D.; Guldberg, R.E.; Plaas, A.H.; Levenston, M.E. Variations in matrix composition and gag fine structure among scaffolds for cartilage tissue engineering. Osteoarth.Cart. 2005, 13, 828–836.

[51] Rahfoth, B.; Weisser, J.; Sternkopf, F.; Aigner, T.; von der Mark, K.; Brauer, R. Transplantation of allograft chondrocytes embedded in agarose gel into cartilage defects of rabbits. Osteoarth.Cart. 1996, 6, 50–65.

[52] Khalil S, Nam J, Sun W. Multi-nozzle deposition for construction of 3d

biopolymer tissue scaffolds. Rapid Prototyping J 2005, 11, 9-17.

[53] Wang XH, Yan YN, Pan YQ, Xiong Z, Liu HX, Cheng B, et al. Generation of three-dimensional hepatocyte/gelatin structures with rapid prototyping system. Tissue Eng 2006; 12, 83-90.

[54] Fedorovich NE, Dewijn JR, Verbout AJ, Alblas J, Dhert WJA. Three-dimensional fiber deposition of cell-laden, viable, patterned constructs for bone tissue printing. Tissue Eng Part A 2008;14:127e33.

[55] Kireev V.V., High-molecular compounds, Vysschaya Shkola, 1992.

[56] Fouassier, J. P. in Photoinitiation, Photopolymerization and Photocuring: Fundamentals and Applications; Hanser: Munich, Vienna, 1995, pp 1 – 7, p 174.

[57] Wei, H.; Lee, T. Y.; Miao, W.; Fortenberry, R.; Magers, D. H.; Hait S.; Guymon, A. C.; Jonsson, S. E.; Hoyle, C. E.; "Characterization and photopolymerization of divinyl fumarate"; Macromolecules; 2007; 40; 6172 – 6180.

[58] Kilambi, H.; Reddy, S. K.; Schneidewind, L.; Lee, T. Y.; Stansbury, J. W.; Bowman, C. N.; "Design, development, and evaluation of monovinyl acrylates characterized by secondary functionalities as reactive diluents to diacrylates."; Macromolecules; 2007; 40; 6112 – 6118.

[59] Gruber, H.F.; "Photoinitiators for free radical polymerization"; Progress in Polymer Science; 1992; 17; 953.

[60] Jonsson, E. S., Hoyle, C. E.; "Monomeric photoinitiators" in Photochemistry and UV-Curing: New trends, 2006, (Ed. J.P. Fouassier); Research Signpost: Trivandrum, India; 2006; 165-175.

[61] Crivello, J. V.; Dietliker, K.; "Photoinitiators for free radical cationic and anionic photopolymerization. Chemistry & Technology of UV & EB Formulations for coatings, inks & paints"; (Ed. G. Bradley); 2nd ed.; SITA Technology Ltd., 1991; Vol. III.; p 20-21.

[62] Source: http://web.uvic.ca/ail/techniques/Jablonski.jpg

[63] Knistle, J. F.; "Polymerization by UV radiation. II. Free radical homopolymerization in liquid systems"; Journal of Radiation Curing; 1974; 1; 2.

[64] Osborn C. L.; „Photoinition systems and their role in UV-curable coatings and inks";Journal of Radiation Curing; 1976; 3; 3.

[65] Davidson R. S.; Orton S. P.; "Photo-induced electron-transfer reactions. Fragmentation of 2-aminoethanols"; Journal of the Chemical Society Chemical Communications; 1974; 6; 209-210.

[66] Fouassier, J. P.; “Photochemistry and UV-curing: a brief survey of the latest trends.”; in Photochemistry and UV Curing: New Trends 2006; Research Signpost, Kerula, India; 2006; 1-8.

[67] Fouassier, J. P.; "Radiation curing in polymer science and technology"; in Elsevier Applied Science Vol.II: Photoinitiating Systems, 1993, 717.

[68] Chen, Y. C.; Ferracane, J. L.; Prahl, S. A.; “Quantum yield of conversion of the photoinitiator camphorquinone”; Dental Materials; 2007, 23; 655-664.

[69] Andrzejewska, E.; Zych-Tomkowiak, D.; Andrzejewski, M.; Hug, G. L.; Marciniak, B.; “Heteroaromatic thiols as co-initiators for Type II photoinitiating systems based on camphorquinone and isopropylthioxanthone.”; Macromolecules; 2006; 39(11); 3777-3785.

[70] Becker, H. G. O. in „Einführung in die Photochemie“; DVW, 1991, p 358.

[71] Cohen, S. G.; Parola, A.; Parsons Jr., G. H.; "Photoreduction by Amines"; Chemical Reviews; 1973; 73(2); 141-161.

[72] Paczkowski, J.; "Electron-transfer photoinitiators of free radical polymerization. The effect of co-initiator structure on photoinitiation ability"; in Photochemistry and UV Curing: New Trends 2006; (Ed. J.P. Fouassier); Research Signpost, Kerula, India; 2006; 101-115.

[73] Brimage, D. R. G.; Davidson, R. S.; "Photoreactions of polycyclic aromatic hydrocarbons with N-aryl-glycines"; Journal of the Chemical Society Perkin Transactions 1: Organic and Bio-Organic Chemistry; 1973; 5; 496-499.

[74] Crivello, J. V.; Dietliker, K.; "Photoinitiators for free radical cationic and anionic photopolymerization. Chemistry & Technology of UV & EB Formulations for coatings, inks & paints"; (Ed. G. Bradley); 2nd ed.; SITA Technology Ltd., 1991; Vol. III.; 71-82.

[75] Hageman, H. J.; "Photoinitiators and photoinitiation. Part 12. The aromatic ketone/tert-amine type-II photoinitiation system. Identification of the initiating species"; Macromolecular Rapid Communications; 1997; 18(5); 443 – 449.

[76] Clarke, S. R.; Shanks, R. A.; "Factors affecting the ultraviolet-initiated polymerization of vinyl monomers "; Journal of Macromolecular Science Part A; 1982; 17(1); 77 – 85.

[77] Nguyen, K. T.; West, J. L. Biomaterials 2002, 23, 4307-4314.

[78] Mooney DJ, Baldwin DF, Suh NP, Vacanti JP, Langer R. Novel approach to fabricate porous sponges of poly(d,l-lactic-co-glycolic acid) without the use of organic solvents. Biomaterials 17(14), 1417–1422 (1996).

[79] Mikos AG, Thorsen AJ, Czerwonka LA et al. Preparation and characterization of poly(l-lactic acid) foams. Polymer 35, 1068 (1994).

[80] Kumbar SG, James R, Nukavarapu SP, Laurencin CT. Electrospun nanofiber scaffolds: engineering soft tissues. Biomed. Mater. 3(3), 034002 (2008).

[81] Van Vlierberghe, S.; Cnudde, V.; Dubruel, P.; Masschaele, B.; Cosijns, A.; De Paepe, I.; Jacobs, P. J. S.; Van Hoorebeke, L.; Remon,J. P.; Schacht, E. Biomacromolecules 2007, 8, 331–337.

[82] Lee, J.; Cuddihy, M. J.; Kotov, N. A. Tissue Eng., Part B 2010, 14, 61–86.

[83] Hutmacher, D. W.; Sittinger, M.; Risbud, M. V. Trends Biotechnol. 2004, 22, 354–362.

[84] Yeong, W.; Chua, C.; Leong, K.; Chandrasekaran, M. Trends Biotechnol 2004, 22, 643–652.

[85] Arcaute, K.; Mann, B.; Wicker, R. Acta Biomater. 2010,6, 1047–1054.

[86] Choi, J.; Wicker, R.; Lee, S.; Choi, K.; Ha, C.; Chung, I. J. Mater. Process. Technol. 2009, 209, 5494–5503.

[87] Baudis, S.; Heller, C.; Liska, R.; Stampfl, J.; Bergmeister, H.; Weigel, G. J. Polym. Sci., Part A: Polym. Chem. 2009, 47, 2664–2676.

[88] Cheah, C.; Chua, C.; Leong, K.; Chua, S. Int. J. Adv. Manuf. Technol. 2003, 21, 291–301.

[89] Naing, M.; Chua, C.; Leong, K.; Wang, Y. Rapid Prototyping J. 2005, 11, 249–259.

[90] Ramanath, H.; Chua, C.; Leong, K.; Shah, K. J. Mater. Sci.: Mater. Med. 2008, 19, 2541–2550.

[91] Ramanath, H.; Chandrasekaran, M.; Chua, C.; Leong, K.; Shah, K. D. Key Eng. Mater. 2007, 334-335, 1241–1244.

[92] Too, M.; Leong, K.; Chua, C.; Du, Z.; Yang, S.; Cheah, C.; Ho, S. Int. J. Adv. Manuf. Technol. 2002, 19, 217–223.

[93] Yeong, W.; Chua, C.; Leong, K.; Chandrasekaran, M.; Lee, M. J. Biomed. Mater. Res. 2007, 82B, 260–266.

[94] Yeong, W.; Chua, C.; Leong, K.; Chandrasekaran, M.; Lee, M.Rapid Prototyping J. 2006, 12, 229–237.

[95] Tan, J. Y.; Chua, C. K.; Leong, K. F. Virtual Phys. Prototyping 2010, 5, 45–53.

[96] Liu X, Ma PX. Phase separation, pore structure, and properties of nanofibrous gelatin scaffolds. Biomaterials 30(25), 4094–4103 (2009).

[97] Moroni L, Schotel R, Hamann D, de Wijn JR, van Blitterswijk CA. 3D Fiber-deposited electrospun integrated scaffolds enhance cartilage tissue formation. Adv. Funct. Mater. 18(1), 53–60 (2008).

[98] Pitts JD, Campagnola PJ, Epling GA, Goodman SL. Submicron multiphoton free-form fabrication of proteins and polymers: studies of reaction efficiencies and applications in sustained release. Macromolecules 33(5), 1514–1523 (2000).

[99] Z. Li, et al., Opt. Mater., 2013, DOI: 10.1016/j.optmat.2013.04.007.

[100] M. Rumi , S. Barlow , J. Wang , J. W. Perry , S. R. Marder , in Photoresponsive Polymers (Eds: S.R. Marder , K.-S. Lee), Springer, Berlin, Heidelberg 2008, 1 – 95 .

[101] B. H. Cumpston, S. P. Ananthavel, S. Barlow, D. L. Dyer, J. E. Ehrlich, L. L. Erskine, A. A. Heikal, S. M. Kuebler , I.-Y. S. Lee, D. McCord-Maughon, J. Qin, H. Rockel, M. Rumi, X.-L. Wu, S. R. Marder, J. W. Perry, Nature 1999, 398 , 51 – 54 .

[102] N. Pucher , A. Rosspeintner , V. Satzinger , V. Schmidt , G. Gescheidt , J. Stampfl , R. Liska , Macromolecules 2009 , 42 , 6519 – 6528 .

[103] Aleksandr Ovsianikov, Andrea Deiwick, Sandra Van Vlierberghe, Peter Dubruel, Lena Möller, Gerald Dräger, and Boris Chichkov. Laser Fabrication of Three Dimensional CAD Scaffolds from Photosensitive Gelatin for Applications in Tissue Engineering. Biomacromolecules 2011, 12, 851–858

[104] Ovsianikov A, Schlie S, Ngezahayo A, Haverich A, Chichkov BN. Two-photon polymerization technique for microfabrication of CAD-designed 3D scaffolds from commercially available photosensitive materials. J. Tissue Eng. Regen. Med. 1(6), 443–449 (2007).

[105] Claeyssens F, Hasan EA, Gaidukeviciute A et al. Three-dimensional biodegradable structures fabricated by two-photon polymerization. Langmuir 25(5), 3219–3223 (2009).

[106] Mizutani M, Matsuda T. Photocurable liquid biodegradable copolymers: in vitro hydrolytic degradation behaviors of photocured films of coumarin-endcapped poly(e-caprolactone-co-trimethylene carbonate). Biomacromolecules 3(2), 249–255 (2002).

[107] Weiß T, Schade R, Laube T et al. Two-photon polymerization of biocompatible photopolymers for microstructured 3D biointerfaces. Adv. Eng. Mater. 13(9), B264–B273 (2011).

[108] Melissinaki V, Gill AA, Ortega I et al. Direct laser writing of 3D scaffolds for neural tissue engineering applications. Biofabrication 3(4), 045005 (2011).

[109] Kaehr B. Guiding neuronal development with in situ microfabrication. Proc. Natl Acad. Sci. USA 101(46), 16104–16108 (2004).

[110] Jeon H, Hidai H, Hwang DJ, Healy KE, Grigoropoulos CP. The effect of micronscale anisotropic cross patterns on fibroblast migration. Biomaterials 31(15), 4286–4295 (2010).

[111] Kiyan Y, Limbourg A, Kiyan R et al. Urokinase receptor associates with myocardin to control vascular smooth muscle cells phenotype in vascular disease. Arterioscler. Thromb. Vasc. Biol. 32(1), 110–122 (2011).

[112] Aleksandr Ovsianikov, Vladimir Mironov, Jürgen Stampfl1 and Robert Liska. Engineering 3D cell-culture matrices: multiphoton processing technologies for biological & tissue engineering applications.

[113] Adam J. Engler, Maureen A. Griffin, Shamik Sen, Carsten G. Bönnemann, H. Lee Sweeney, and Dennis E. Discher, Myotubes differentiate optimally on substrates with tissue-like stiffness pathological implications for soft or stiff microenvironments, J Cell Biol. 2004 Sep 13; 166(6): 877–887.

[114] Adam J. Engler, Shamik Sen, H. Lee Sweeney, Dennis E. Discher, Matrix Elasticity Directs Stem Cell Lineage Specification, Cell, Volume 126, Issue 4, p677–689, 25 August 2006

[115] Ingber DE, Tensegrity-based mechanosensing from macro to micro, Prog Biophys Mol Biol. 2008 Jun-Jul; 97(2-3):163-79.

[116] Matrix elasticity directs stem cell lineage specification.Engler AJ, Sen S, Sweeney HL, Discher DE Cell. 2006 Aug 25; 126(4):677-89.

[117] Engler AJ, Sweeney HL, Discher DE. Biophys. J.2005;88:500A–500A.

[118] Chen CS, Mrksich M, Huang S, Whitesides GM, Ingber DE. Science. 1997;276:1425–1428.

[119] Singhvi R, Kumar A, Lopez GP, Stephanopoulos GN, Wang DIC, Whitesides GM, Ingber DE. Science.1994;264:696–698.

[120] Mammoto A, Ingber DE. Curr. Opin. Cell Biol. 2009;21:864–870.

[121] Mammoto A, Huang S, Moore K, Oh P, Ingber DE. J. Biol. Chem. 2004;279:26323–26330.

[122] Bryant SJ, Anseth KS, Lee DA, Bader DL. J. Orthop. Res. 2004;22:1143–1149.

[123] Fairbanks BD, Schwartz MP, Halevi AE, Nuttelman CR, Bowman CN, Anseth KS. Adv. Mater. 2009 In press.

[124] Lutolf MP, Raeber GP, Zisch AH, Tirelli N, Hubbell JA. Adv. Mater. 2003;15:888.

[125] Dr. AM Kloxin,Dr. CJ Kloxin, CN Bowman, Prof., and KS Anseth, Prof. Mechanical properties of cellularly responsive hydrogels and their experimental determination, Adv Mater. 2010 Aug 17; 22(31): 3484–3494.

[126] Mechanisms of 3-D migration and matrix remodeling of fibroblasts within artificial ECMs.Raeber GP, Lutolf MP, Hubbell JA Acta Biomater. 2007 Sep; 3(5):615-29.

[127] A photo-modulatable material for probing cellular responses to substrate rigidity.Frey MT, Wang YL Soft Matter. 2009; 5():1918-1924.

[128] Giepmans BN, Adams SR, Ellisman MH, Tsien RY Science. 2006 Apr 14; 312(5771):217-24.

[129] Van Engelenburg SB, Palmer AE Curr Opin Chem Biol. 2008 Feb; 12(1):60-5.

[130] Destaing O, Saltel F, Jurdic P, Bard FA. Mol. Biol. Cell.2001;12:1621.

[131] Zhang J, Campbell RE, Ting AY, Tsien RY Nat Rev Mol Cell Biol. 2002 Dec; 3(12):906-18.

[132] Wolf K, Wu YI, Liu Y, Geiger J, Tam E, Overall C, Stack MS, Friedl P Nat Cell Biol. 2007 Aug; 9(8):893-904.

[133] Particle-tracking microrheology of living cells: principles and applications.Wirtz D Annu Rev Biophys. 2009; 38():301-26.

[134] Extracellular matrix stiffness and architecture govern intracellular rheology in cancer.Baker EL, Bonnecaze RT, Zaman MH Biophys J. 2009 Aug 19; 97(4):1013-21.

[135] Quantifying cellular traction forces in three dimensions.Maskarinec SA, Franck C, Tirrell DA, Ravichandran G Proc Natl Acad Sci U S A. 2009 Dec 29; 106(52):22108-13.

[136] Cell-cell mechanical communication through compliant substrates.Reinhart-King CA, Dembo M, Hammer DA Biophys J. 2008 Dec 15; 95(12):6044-51.

[137] Poly(ethylene glycol) hydrogels conjugated with a collagenase-sensitive fluorogenic substrate to visualize collagenase activity during three-dimensional cell migration.Lee SH, Moon JJ, Miller JS, West JL Biomaterials. 2007 Jul; 28(20):3163-70.

[138] Noninvasive probing of the spatial organization of polymer chains in hydrogels using fluorescence resonance energy transfer (FRET).Kong HJ, Kim CJ, Huebsch N, Weitz D, Mooney DJ J Am Chem Soc. 2007 Apr 18; 129(15):4518-9.

[139] S.K. Sia, G.M. Whitesides, Microfluidic devices fabricated in poly(dimethylsiloxane) for biological studies, Electrophoresis 24 (2003) 3563–3576.

[140] J. Moorthy, D.J. Beebe, Organic and biomimetic designs for microfluidic systems—new strategies offer a flexible approach to designing microscale devices, Anal. Chem. 75 (2003) 292A–301A.

[141] E. Delamarche, A. Bernard, H. Schmid, B. Michel, H. Biebuyck, Patterned delivery of immunoglobulins to surfaces using microfluidic networks, Langmuir 276 (1997) 779–781.

[142] J. Yakovleva, R. Davidsson, M. Bengtsson, T. Laurell, Microfluidic enzyme immunosensors with immobilised protein A and G using chemiluminescence detection emneus, J. Biosens. Bioelectron. 19 (2003) 21–34.

[143] E. Delamarche, A. Bernard, H. Schmid, B. Michel, H. Biebuyck, Patterned delivery of immunoglobulins to surfaces using microfluidic networks, Langmuir 276 (1997) 779–781.

[144] P. Mela, S. Onclin, M.H. Goedbloed, S. Levi, M.F. Garcia-Parajo, N.F. van Hulst, B.J. Ravoo, D.N. Reinhoudt, A. van den Berg, Monolayerfunctionalized microfluidics devices for optical sensing of acidity, Lab Chip 5 (2005) 163–170.

[145] E. Delamarche, G. Sundarababu, H. Biebuyck, B. Michel, C. Gerber, H. Sigrist, H. Wolf, H.J. Ringsdorf, N. Xanthopoulos, H. Mathieu, Immobilization of antibodies on a photoactive self-assembled monolayer on gold, Langmuir 12 (1996) 1997–2006.

[146] A. Schwarz, J.S. Rossier, E. Roulet, N. Mermod, M.A. Roberts, H.H. Girault, Micropatterning of biomolecules on polymer substrates, Biophys. Appl. Nanosci. 14 (1998) 5526–5531.

[147] J. Yakovleva, R. Davidsson, M. Bengtsson, T. Laurell, Microfluidic enzyme immunosensors with immobilised protein A and G using chemiluminescence detection emneus, J. Biosens. Bioelectron. 19 (2003) 21–34.

[148] H. Zhu, M. Snyder, Current opinion in chemical biology, Protein Chip Technol. 7 (2003) 55–63.

[149] Z.R. Lu, P. Kopeckova, Kopecek, Polymerizable Fab' antibody fragments for targeting of anticancer drugs, J. Nat. Biotechnol. 17 (1999) 1101– 1104.

[150] Robert P. Sebra, Andrea M. Kasko, Kristi S. Anseth, Christopher N. Bowman. Synthesis and photografting of highly pH-responsive polymer chains. Sensors and Actuators B 119 (2006) 127–134.

[151] C. B. Herbert , T. L. McLernon , C. L. Hypolite , D. N. Adams , L. Pikus , C.-C. Huang, G. B. Fields, P. C. Letourneau, M. D. Distefano, W.-S. Hu, Chem. Biol. 1997, 4, 731 – 737.

[152] Zhiquan Li, Evaldas Stankevicˇius, Aliasghar Ajami, Gediminas Racˇiukaitis, Wolfgang Husinsky, Aleksandr Ovsianikov, Jürgen Stampfl and Robert Liska*. 3D alkyne–azide cycloaddition: spatiotemporally controlled by combination of aryl azide photochemistry and two-photon grafting†. Chem. Commun.

[153] E. Alsberg , H. A. von Recum , M. J. Mahoney , Expert Opin. Biol. Ther. 2010 , 6, 847– 866.

[154] Aleksandr Ovsianikov, Zhiquan Li, Jan Torgersen, Jürgen Stampfl, Robert Liska. Selective Functionalization of 3D Matrices Via Multiphoton Grafting and Subsequent Click Chemistry. Adv. Funct. Mater. 2012.

[155] M. F. Budyka, M. M. Kantor and M. V. Alfimov, Russ. Chem. Rev., 1992, 61, 25.

[156] M. S. Hahn , J. S. Miller , J. L. West , Adv. Mater. 2006 , 18 , 2679 –2684.

[157] J. E. Leslie-Barbick , C. Shen , C. Chen , J. L. West , Tissue Eng. Part A 2010.

[158] Hahn MS, Miller JS, West JL. Three-dimensional biochemical and biomechanical patterning of hydrogels for guiding cell behavior. Adv. Mater. 18(20), 2679–2684 (2006).

[159] Lee S-H, Moon JJ, West JL. Three-dimensional micropatterning of bioactive hydrogels via two-photon laser scanning photolithography for guided 3D cell migration. Biomaterials 29(20), 2962–2968 (2008).

[160] Seidlits SK, Schmidt CE, Shear JB. High-resolution patterning of hydrogels in three dimensions using direct-write photofabrication for cell guidance. Adv. Funct. Mater. 19, 3543–3551 (2009).

[161] Wylie RG, Shoichet MS. Two-photon micropatterning of amines within an agarose hydrogel. J. Mat. Chem. 18(23), 2716–2721 (2008).

[162] Wosnick JH, Shoichet MS. Three-dimensional chemical patterning of transparent hydrogels. Chem. Mat. 20(1), 55–60 (2008).

[163] Wylie RG, Ahsan S, Aizawa Y, Maxwell KL, Morshead CM, Shoichet MS. Spatially controlled simultaneous patterning of multiple growth factors in three-dimensional hydrogels. Nat. Mat. 10(10), 799–806 (2011).

[164] M. Rumi , S. Barlow , J. Wang , J. W. Perry , S. R. Marder , in Photoresponsive Polymers (Eds: S.R. Marder , K.-S. Lee), Springer, Berlin, Heidelberg 2008 , 1 – 95.

[165] B. H. Cumpston , S. P. Ananthavel , S. Barlow , D. L. Dyer , J. E. Ehrlich , L. L. Erskine , A. A. Heikal , S. M. Kuebler , I.-Y. S. Lee , D. McCord-Maughon , J. Qin , H. Rockel , M. Rumi , X.-L. Wu , S. R. Marder , J. W. Perry , Nature 1999 , 398 , 51 – 54 .

[166] N. Pucher , A. Rosspeintner , V. Satzinger , V. Schmidt , G. Gescheidt , J. Stampfl, R. Liska , Macromolecules 2009 , 42 , 6519 – 6528 .

[167] R. Pinard , J. E. Heckman , J. M. Burke , J. Mol. Biol. 1999 , 287 , 239 – 251.

[168] Zhiquan Li, Evaldas Stankevicˇius, Aliasghar Ajami, Gediminas Racˇiukaitis, Wolfgang Husinsky, Aleksandr Ovsianikov, Jürgen Stampflc and Robert Liska. 3D alkyne–azide cycloaddition: spatiotemporally controlled by combination of aryl azide photochemistry and two-photon grafting, Chem. Commun.

[169] Charles J. Shields, Douglas R. Chrisope, Gary B. Schuster, Andrew J. Dixon, Martyn Poliakoff, and James J. Turner; Photochemistry of Aryl Azides: Detection and Characterization of a Dehydroazepine by Time-Resolved Infrared Spectroscopy and Flash Photolysis at Room Temperature; American Chemical society, J. Am. Chem. SOC. 1987, 109, 4723-4726.

[170] W.E. Doering, R.A. Odum, Tetrahedron, 1966, 22, 81 – 93.

[171] S.E. Carroll, B. Nay, E.F.V. Scriven, H. Suschitzky, R.R. Thomas, Tetrahedron Lett. 1977, 18, 3175 – 8.

[172] A.K. Schrock, G.B. Schuster, J. Am. Chem. Soc. 1984, 106, 5228 – 34.

[173] T. - Y. Liang, G.B. Schuster, J. Am. Chem. Soc. 1986, 108, 546 – 8.

[174] Smith, P. A. S. In Nitrenes; Lwowski, W., Ed.; Interscience: 1970; p.120.

[175] Huisgen, R.; Vassius, D.; Appl. M. Chem. Ber. 1958,91, 1. Huisgen, R.: ADDI. M. Ibid. 1958. 1. 12.

[176] Sundberg, R. J.; Brenner, M.; Suter, S. R., Das, B. P. Tetrahedron Lett 1970 271 5.

[177] Crow, W. D.; Wentrup, C. Tetrahedron Lett 1968, 6149.

[178] Chapman, 0. L.; LeRoux, J.-P. J. Am Chem. SOC. 1978, 100, 282.

[179] P.A.S. Smith, in Azides and Nitrenes – Reactivity and Utility; E.F.V. Scriven, ed.; Academic Press, New York, 1984.

[180] E. Leyva , M.S. Platz , G. Persy , J. Wirz , J. Am. Chem. Soc. 1986 , 108 , 3783 – 90

[181] T. Yamaoka, H. Kashiwagi, S. Nagakura, Bull. Chem. Soc. Japan 1972, 45, 361 – 5

[182] Y.Z. Li , J.P. Kirby , M.W. George , M. Poliakoff, G.B. Schuster, J. Am. Chem. Soc. 1988, 110, 8092 – 8 .

[183] R.J. Sundberg , S.R. Suter , M. Brenner, J. Am. Chem. Soc. 1972, 94, 513 – 20 . (b) B.A. De Graff , D.W. Gillespie , R.J. Sundberg , J. Am. Chem. Soc. 1974, 96, 7491 – 6.

[184] Dunkin, I. R.; Thomson, P. C. P. J. Chem. SOC., Chem. Commun. 1980, 499.

[185] Donelly, T.; Dunkin, I. R.; Norwood, D. S. D.; Prentice, A.; Shields, C. J. ; Thompson, P. C. P. J. Chem. SOC., Perkin Trans. 2 1985, 307

[186] Leyva, E.; Platz, M. S. Tetrahedron Lett. 1985, 26, 2147.

[187] Nina Gritsan and Matthew Platz, Photochemistry of Azides: The Azide/Nitrene Interface, Organic Azides: Syntheses and Applications, edited by Stefan Bräse and Klaus Banert © 2010 John Wiley & Sons, Ltd. ISBN: 978-0-470-51998-1.

[188] N.P. Gritsan, E.A. Pritchina, Russ. Chem. Rev. (Uspekhi Khimii) 1992, 61 , 910 – 39.

[189] E.A. Pritchina, N.P. Gritsan, J. Photochem. Photobiol. A: Chemistry, 1988, 43, 165 – 82.

[190] N.P. Gritsan, E.A. Pritchina, J. Inf. Rec. Mat. 1989, 17 , 391 – 404.

[191] J. M. Eisenhart , A. B. Ellis, J. Org. Chem. 1985, 50 , 4108 – 4113 .

[192] Hwang CM, Sant S, Masaeli M, Kachouie NN, Zamanian B, Lee SH, et al. Fabrication of three-dimensional porous cell-laden hydrogel for tissue engineering. Biofabrication 2010;2:035003.

[193] Zhu J, Marchant RE. Design properties of hydrogel tissue-engineering scaffolds. Expert Rev. Med. Devices 8(5), 607–626 (2011).

[194] Torgersen J, Ovsianikov A, Mironov V et al. Photo-sensitive hydrogels for three-dimensional laser micro-fabrication in the presence of whole organisms. J. Biomed. Opt. (2012) (In Press).

[195] Ovsianikov A et al, Unpublished Data.

[196] Ovsianikov A, Deiwick A, Van Vlierberghe S et al. Laser fabrication of three-dimensional CAD scaffolds from photosensitive gelatin for applications in tissue engineering. Biomacromolecules 12(4), 851–858 (2011).

[197] Ovsianikov A, Deiwick A, Van Vlierberghe S et al. Laser fabrication of 3D gelatin scaffolds for the generation of bioartificial tissues. Materials 4(1), 288–299 (2011).

[198] Fedorovich NE, Oudshoorn MH, van Geemen D, Hennink WE, Alblas J, Dhert WJA. The effect of photopolymerization on stem cells embedded in hydrogels. Biomaterials 30(3), 344–353 (2009).

[199] Bryant SJ, Bender RJ, Durand KL, Anseth KS. Encapsulating chondrocytes in degrading PEG hydrogels with high modulus: engineering gel structural changes to facilitate cartilaginous tissue production. Biotechnol. Bioeng. 86(7), 747–755 (2004).

[200] Boontheekul T, Hill EE, Kong H-J, Mooney DJ. Regulating myoblast phenotype through controlled gel stiffness and degradation. Tissue Eng. 13(7), 1431–1442 (2007).

[201] Van Den Bulcke, A. I.; Bogdanov, B.; De Rooze, N.; Schacht, E. H.; Cornelissen, M.; Berghmans, H. Biomacromolecules 2000, 1, 31–38.

[202] Van Vlierberghe, S.; Dubruel, P.; Lippens, E.; Cornelissen, M.;Schacht, E. J. Biomater. Sci., Polym. Ed. 2009, 20, 1417–1438.

[203] Nichol, J. W.; Koshy, S. T.; Bae, H.; Hwang, C. M.; Yamanlar, S.; Khademhosseini, A. Biomaterials 2010, 31, 5536–5544.

[204] Djabourov, M. Contemp. Phys. 1988, 29, 273–297.

[205] The Science and Technology of Gelatin; Ward, A. G., Courts, A., Eds.; Food Science and Technology Series; Academic Press: New York, 1977.

[206] Chung, L.; Dinakarpandian, D.; Yoshida, N.; Lauer-Fields, J. L.; Fields, G. B.; Visse, R.; Nagase, H. EMBO J. 2004, 23, 3020–3030.

[207] Benton, J. A.; DeForest, C. A.; Vivekanandan, V.; Anseth, K. S. Tissue Eng., Part A 2010, 15, 3221–3230.

[208] Schuurman W, Levett PA, Pot MW, van Weeren PR, Dhert WJA, Hutmacher DW, et al. Gelatin-methacrylamide hydrogels as potential biomaterials for fabrication of tissue-engineered cartilage constructs. Macromol Biosci 2013;13: 551-61.

[209] Nichol JW, Koshy ST, Bae H, Hwang CM, Yamanlar S, Khademhosseini A. Cellladen microengineered gelatin methacrylate hydrogels. Biomaterials 2010; 31: 5536-44.

[210] Aubin H, Nichol JW, Hutson CB, Bae H, Sieminski AL, Cropek DM, et al. Directed 3d cell alignment and elongation in microengineered hydrogels. Biomaterials 2010; 31: 6941-51.

[211] Du YA, Lo E, Ali S, Khademhosseini A. Directed assembly of cell-laden microgels for fabrication of 3d tissue constructs. Proc Natl Acad Sci USA 2008;105:9522-7.

[212] Van Den Bulcke, A. I.; Bogdanov, B.; De Rooze, N.; Schacht, E. H.; Cornelissen, M.; Berghmans, H. Biomacromolecules 2000, 1, 31–38.

[213] Buchanan, Cara F., Elizabeth E. Voigt, Christopher S. Szot, Joseph W. Freeman, Pavlos P. Vlachos, Marissa Nichole Rylander"Three-Dimensional Microfluidic Collagen Hydrogels for Investigating Flow-Mediated Tumor-Endothelial Signaling and Vascular Organization" Tissue Engineering Part C: Methods (2014) 20: 64-75

[214] Piao, Zheng-Gang, Jae-Sung Kim, Jun-Sik Son, Sook-Young Lee, Xian-Hao Fang, Ji-Su Oh, Jae-Seek You, Su-Gwan Kim"Osteogenic Evaluation of Collagen Membrane Containing Drug-Loaded Polymeric Microparticles in a Rat Calvarial Defect Model" Tissue Engineering Part A (2014) 20: 3322-3331

[215] Kolluru, Pavan V., Justin Lipner, Wenying Liu, Younan Xia, Stavros Thomopoulos, Guy M. Genin, Ioannis Chasiotis "Strong and tough mineralized PLGA nanofibers for tendon-to-bone scaffolds" Acta Biomaterialia (2013) 9: 9442-9450

[216] Valence, Sarra de, Jean-Christophe Tille, Chiraz Chaabane, Robert Gurny, Marie-Luce Bochaton-Piallat, Beat H. Walpoth, Michael Muller "Plasma treatment for improving cell biocompatibility of a biodegradable polymer scaffold for vascular graft applications" European Journal of Pharmaceutics and Biopharmaceutics (2013) 85: 78-86

[217] George, A., A.W. Maijenburg, M.G. Maas, D.H.A. Blank, J.E. ten Elshof "Patterning Functional Materials Using Channel Diffused Plasma-Etched Self-Assembled Monolayer Templates" Langmuir (2011) 27 (19): 12235-12242

[218] Hsu, C.Y., J.W. Huang, K.J. Lin "High sensitivity and selectivity of human antibody attachment at the interstices between substrate-bound gold nanoparticles" Chemical Communications (2011) 47 (3): 872—874

[219] Lee, W., J. Son, S.-S. Yoo, J.-K. Park "Facile and Biocompatible Fabrication of Chemically Sol-Gel Transitional Hydrogel Free-Standing Microarchitectures" Biomacromolecules (2011) 12 (1): 14-18

[220] Muller, Mathias, Ulrich Jung, Viktoria Gusak, Sandra Ulrich, Michelle Holz, Rainer Herges, Christoph Langhammer, Olaf Magnussen "Localized Surface Plasmon Resonance Investigations of Photoswitching in Azobenzene-Functionalized Self-Assembled Monolayers on Au" Langmuir (2013) 29: 10693-10699

[221] Borg, Lisa, Anna L. Domanski, Rudiger Berger, Rudolf Zentel "Photoinduced Charge Separation of Self-Organized Semiconducting Superstructures Composed of a Functional Polymer-TiO_2 Hybrid" Macromol. Chem. Phys. (2013) 214: 975-984

[222] Xu, H., J. Wu, C.-C. Chu, M. Shuler "Development of disposable PDMS micro cell culture analog devices with photopolymerizable hydrogel encapsulating living cells" Biomedical Microdevices (2012) 14: 409-418

[223] Chen, Q., S.C. Bae, S. Granick "Directed self-assembly of a colloidal kagome lattice" Nature (2011) 469 (7330): 381-384

[224] Hamid, Qudus, Chengyang Wang, Jessica Snyder, Wei Sun "Surface modification of SU-8 for enhanced cell attachment and proliferation within microfluidic chips" Journal of Biomedical Materials Research Part B: Applied Biomaterials (2014) 00B: 1-12

[225] Li, Y, H W Ng, B D Gates, C Menon "Material versatility using replica molding for large-scale fabrication of high aspect-ratio, high density arrays of nano-pillars" Nanotechnology (2014) 25: 285303

[226] Lycans, Rebecca M, Catherine B Higgins, Michael S Tanner, Eric R Blough, B Scott Day "Plasma treatment of PDMS for applications of in vitro motility assays" Colloids and Surfaces B: Biointerfaces (2014) 116: 687-694

[227] Srinivasan, N.R., P.A. Shankar, Rajdip Bandyopadhyaya "Plasma treated activated carbon impregnated with silver nanoparticles for improved antibacterial effect in water disinfection" Carbon (2013) 57: 1-10

[228] Zhang, Jianfu, Dongdong Chen, Yang Li, Junqi Sun "Layer-by-layer assembled highly adhesive microgel films" Polymer (2013) 54: 4220-4226

[229] Shahal, T., B. Geiger, I. Dunlop, J. Spatz "Regulation of Integrin Adhesions by Varying the Density of Substrate-Bound Epidermal Growth Factor" Biointerphases (2012) 7 (1-4): 1-11.

[230] Ovsianikov A, Malinauskas M, Schlie S et al. Three-dimensional laser micro- and nano-structuring of acrylated poly(ethylene glycol) materials and evaluation of their cytoxicity for tissue engineering applications. Acta Biomaterialia 7(3), 967–974 (2011).

[231] Stephan Benedikt, Jieping Wang, Marica Markovic, Norbert Moszner, Kurt Dietliker, Aleksandr Ovsianikov, Hansjorg Grutzmacher, Robert Liska. Highly Efficient Water-Soluble Visible Light Photoinitiators, Journal of polymer science, Part A: Polymer Chemistry 2015.